Level Density Studies in ^{49}V

Jianying Li

Triangle Universities Nuclear Laboratory

Department of Physics

Duke University

1990

LEVEL DENSITY STUDIES IN ^{49}V

by

Jianying Li

This research was performed at Triangle Universities Nuclear Laboratory as a part of a joint collaboration between TUNL and Fudan University

Date: May 1, 1990

Approved:

E.G. Bilpuch, Supervisor, Duke University

G.E.Mitchell, Supervisor, North Carolina State University

Fujia Yang, Supervisor, Fudan University

Wenlong Shen

Guangjun Ni

Qin Xi-Jun

Dissertation submitted in partial fulfillment of the requirements for the degree of Doctor of Philosophy in the Department of Nuclear Science in the Graduate School of Fudan University

1990

Abstract

The differential cross sections for the ^{48}Ti(p,p) and ^{48}Ti(p,p') reactions have been measured from E_p = 3.08 to 3.86 MeV at laboratory angles θ = 90°, 108°, 127°, 145°, 150° and 165°. Data were taken with the Triangle Universities Nuclear Laboratory KN Van de Graaff accelerator and associated high resolution system. The overall energy resolution was about 350 eV.

Resonances observed in the excitation functions were analyzed with a multilevel, multichannel R-matrix program. Resonance energies, spins, parities, total widths and partial widths were determined for a total of 716 resonances.

Six analog states were identified, five of which were fragmented. The Coulomb energy differences between analog states and parent states were determined; these showed good agreement with Janecke's semi-empirical predictions. Spectroscopic factors were determined for the analog states and compared with those of the parent states. Reasonable agreement was found between the spectroscopic factors for the parent and analog states.

Statistical properties of the resonances in ^{49}V were examined. The observed resonances were used to determined the level densities for the various level sequences. Two methods (iterative and bootstrap) were used to calculate the fraction of missing levels. Values obtained from the two methods were consistent. Level sequences were compared with the Wigner and Porter-Thomas distributions and reasonable agreement found. The average values of the proton strength functions were determined from the reduced widths of the non-analog levels. The level densities of the $1/2^+$ and $1/2^-$ states are approximately the same. Bethe's J-dependent level density formula was used to calculate the ratios of

the level densities for $J > 1/2$ to the $J = 1/2$ density. After correcting for missing levels, the J dependence of the experimental level densities is in good agreement with the theoretical prediction.

Acknowledgements

I would like to thank my advisor, Dr. E. G. Bilpuch, for his support and encouragement during this research. I would like to thank my advisor, Dr. F. J. Yang, for his encouragement during my graduate studies. I am also very grateful to my advisor, Dr. G. E. Mitchell, for his guidance through the course of these experiments, and especially for his assistance in the preparation of this dissertation.

I owe special thanks to C. R. Westerfeldt for his invaluable assistance and support as well as his maintenance of the accelerator and computer systems. I am greatly indebted to Dr. B. W. Smith for his many helpful discussions and suggestions, and for his assistance in performing the experiments. The kindness and understanding of Dr. Smith and his wife Paige is especially appreciated. I also wish to thank Dr. J. S. Bull for help in performing the experiments. Additional thanks go to Dr. J. F. Shriner, Dr. L. James, C. Jackson, S. Frankle, C. Coburn, B. Winn, J. Drake, K. Keeter and C. Frankle for their help in various stages of these experiments. Special thanks are due K. Mitchell, for her help in the preparation of this dissertation.

The assistance and instruction of S. E. Edwards, R. Rummel, P. Carter, and P. Mulkey in maintenance of the electronics and accelerator system is greatly acknowledged. The excellent work of the machine shop, led by A. W. Lovette, is also greatly appreciated.

To my family I offer my sincere appreciation for their support and guidance through my life. Most of all, I thank my wife, Yan, for her love, patience and encouragement in the past years. Without her encouragement and help, this dissertation would not have been possible.

This work was supported in part by the United States Department of Energy.

Table of Contents

List of Figures

List of Tables

Chapter I Introduction

The measurement of nuclear resonances has been closely associated with statistical theories of nuclear reactions and spectra since the discovery of neutron resonances by Moon and Tillman (1936) and Rasetti et al. (1936). Nuclear level densities play a central role in any statistical analysis of nuclear reactions. Recently studies of symmetry breaking in the compound nuclear system have promoted renewed interest in nuclear level densities. The predicted enhancement of fundamental symmetry violation in a complex system is critically dependent on the value of the level density. It has been suggested that the average properties of the nuclear system are determined by the nuclear dynamics and that the fluctuations are generic and consistent with random matrix theory. Thus both average and fluctuation properties of the nuclear system are quite interesting to study. In this dissertation, the average properties are emphasized.

Soon after the observation of neutron resonances, Bethe (1936,1937) published landmark papers on nuclear level densities. Since that time there have been major efforts both to measure and to model nuclear level densities. Almost all of the level density theories for nuclei have been based on phenomenological models. These models gave parametric descriptions of the level densities. Parameters were extracted from the existing data in order to calculate level densities for nuclei for which no experimental information was available. These parameters are dependent on (and also limited by) the available data. It is thus desirable to increase the data base used in determining the level density parameters. Average s-wave neutron resonance spacings have long been one of the major sources of nuclear level density information. Neutron resonances provided the basis for a phenomenological description of global properties such as average level density and

strength function. However, it is difficult to study the dependence of the level density on total angular momentum (J) and parity (π) with neutron resonance data, since in most cases only s-wave resonances are observed and analyzed reliably. Measurements of proton resonances should extend the present data base of neutron resonance data and provide interesting tests for the existing level density models. The proton measurements also have advantages over the neutron measurements. The major advantage is the ability to study resonances of different J and π. Historically there were problems with the quality of the proton resonance data: poor overall experimental resolution, resonance analysis complications arising from Coulomb interference effects, contributions from several orbital angular momenta, and the requirement of a multilevel, multichannel analysis.

The development of the High Resolution Laboratory (HRL) at the Triangle Universities Nuclear Laboratory (TUNL) in the 1960's made possible improved proton resonance data. A feedback system with two beams is utilized and an overall experimental resolution of 300-400 eV is achieved for incident proton beams of 1-4 MeV. In the HRL a large amount of high-resolution proton resonance data has been accumulated which is useful in a variety of nuclear studies. Recently these data were systematically analyzed in terms of average resonance spacings, with the average s-wave resonance spacings from proton and neutron resonances compared by Vonach et al. (1988). The proton data were then analyzed with two current phenomenological level density models and compared with the results obtained using neutron data in the models. There is general agreement between the results from the neutron and proton data, indicating that the high resolution proton resonance data can be used to determine nuclear level densities with about equal accuracy as that achieved in modern neutron resonance experiments.

We therefore sought to obtain more high quality, high density level sequences to examine both the angular momentum dependence and the parity dependence of the level density. A level sequence is defined as a set of energy levels all of which have the same good quantum numbers J and π. The ^{49}V system was chosen for study because of its

high level density . The proton resonance data were analyzed using the multilevel and multichannel R-matrix formalism. The s-, p-, d-and f-wave level sequences were extracted from the data, and these sequences used to examine the dependence of the level density on J and π.

A brief survey of relevant theoretical topics is contained in Chapter II. Chapter III describes the experimental equipment and target preparation. Chapter IV discusses the data analysis and the determination of level sequences. The results of the experiments are presented and discussed in Chapter V.

Chapter II Theoretical Background

A. R--Matrix Theory

1. Introduction

Slow neutron reactions have played an important role in nuclear physics since their discovery in 1935. Although the survey of slow neutron cross sections by Fermi's group (Amaldi et al. 1935) promoted the single-particle model of nuclear reactions (Bethe 1935), this model could not explain neutron resonances. Bohr (1936) resolved this crisis by proposing the compound nucleus mechanism. He showed that very long-lived states (as compared to nuclear transit times) could occur in the region where the energy was sufficient for particle emission. This is due to the rapid sharing of the energy of the incoming nucleon among the other nucleons. Once this sharing has occurred in a system of many nucleons, it is very unlikely that a large amount of energy will be concentrated on one particle; thus the system will last a long time, executing a large number of collisions and energy exchanges before decaying by particle emission or electromagnetic radiation.

Following Bohr's proposal many quantitative descriptions of nuclear reactions in terms of the compound nucleus mechanism were published. Breit and Wigner (1936) were the first to use time-dependent perturbation theory adapted from the atomic system to describe the cross section. Although the expressions of the Breit-Wigner formula for cross sections were reasonable in *form*, there were important differences between atomic and nuclear reactions. In the atomic case the excitation energy is concentrated on a sin-

gle particle (an electron) and the long life is due to the *weakness* of the coupling of this particle to the radiation field. In the nuclear case the *strength* of the nuclear forces leads to a sharing of the available energy by all particles (nucleons) and the long life is due to the small probability of the energy being concentrated on a single particle. In addition the appropriate nuclear potential was completely unknown .

The unsatisfactory reliance on perturbation theory was removed in 1938 by Kapur and Peierls (1938) and later by Wigner and Eisenbud (1947), who formulated a rigorous theory of nuclear reactions which has come to be known as R-matrix theory. The R-matrix theory allows the determination of the scattering cross section without knowledge of either the nuclear potential or the nuclear wave function. The basic idea of R-matrix theory is as follows: a complete set of formal states (of all particles) can be defined in a volume of nuclear size by the imposition of certain fixed boundary conditions on the surface of the volume, and the wave function for the internal region Ψ_{JM} corresponding to definite angular momenta J and components M can be formally expanded in the internal region in terms of this set of states. Here the formal states are the compound nuclear states; references to the internal region are replaced with adjustable parameters. In the R-matrix theory, first expounded by Wigner and Eisenbud, these parameters were emphasized. Wigner and Eisenbud exploited the fact that particular choices of these parameters have simple physical significance and therefore enabled the convenient introduction of physical information into the general theory. One therefore fits the experimental cross sections in terms of the parameters of R-matrix theory, and attempts to explain the values of these parameters on the basis of some nuclear theory. The R-matrix theory is discussed below, following the conventions and definitions of Lane and Thomas (1958). The details of the derivations will be omitted. For more detailed information refer to the comprehensive review of Lane and Thomas or to Vogt (1962).

2. R-Matrix Theory

2.1 Definitions

Consider a projectile α_1 (with mass $M\alpha_1$, electric charge $Z\alpha_1$) hitting a target α_2 (mass $M\alpha_2$, charge $Z\alpha_2$) to form a compound nucleus which then decays into two parts α_1', α_2', as shown in Figure 2.1. The relative orbital angular momentum of the two particles is l and its component is m. The fragments α_1 and α_2 have spins I_1 and I_2, which are combined vectorially into the channel spin s (with projection ν) as shown schematically: $s = I_1 + I_2$.

We define a pair c (or channel) in terms of a set of quantum numbers $c = \{\alpha(I_1I_2)s\nu, lm\}$, where α is written for the pair $\alpha_1\ \alpha_2$. One can also combine the channel spin s and the relative orbital angular momentum l into a total spin quantum number $J = S + L$ and its component M. In this case c implies the set $\{\alpha\ (I_1I_2)sl,JM\}$. The transformation between these two schemes is simple.

For each particle pair $\{\alpha_1\ \alpha_2\}$, there is a set of interaction radii a_c. The radius a_c is the minimum radial distance of separation of the pair at which the nuclei experience no polarizing force from each other. This set of radii divides the configuration space of all A nucleons into an "internal" region, in which all the nucleons are close together in a volume of nuclear dimensions in physical space, and an "external" region (Breit 1940), in which the nucleons are separated into two groups, A_1 and A_2, in physical space beyond the distance a_c. The values a_c depends only on α, and

$$r_c \equiv a_c = r_o\,(A_1^{\frac{1}{3}} + A_2^{\frac{1}{3}}),$$

where r_o is independent of A_1 and A_2. In addition to A_1, A_2 (or α_1, α_2), the quantities that specify a channel are $\{(I_1I_2)s\nu, lm\}$ or $\{(I_1I_2)\,sl, JM\}$; this set of quantities is usually denoted as c.

There is no interaction between channels. This means that a given channel can not

Figure 2.1 Schematic of compound nucleus process.

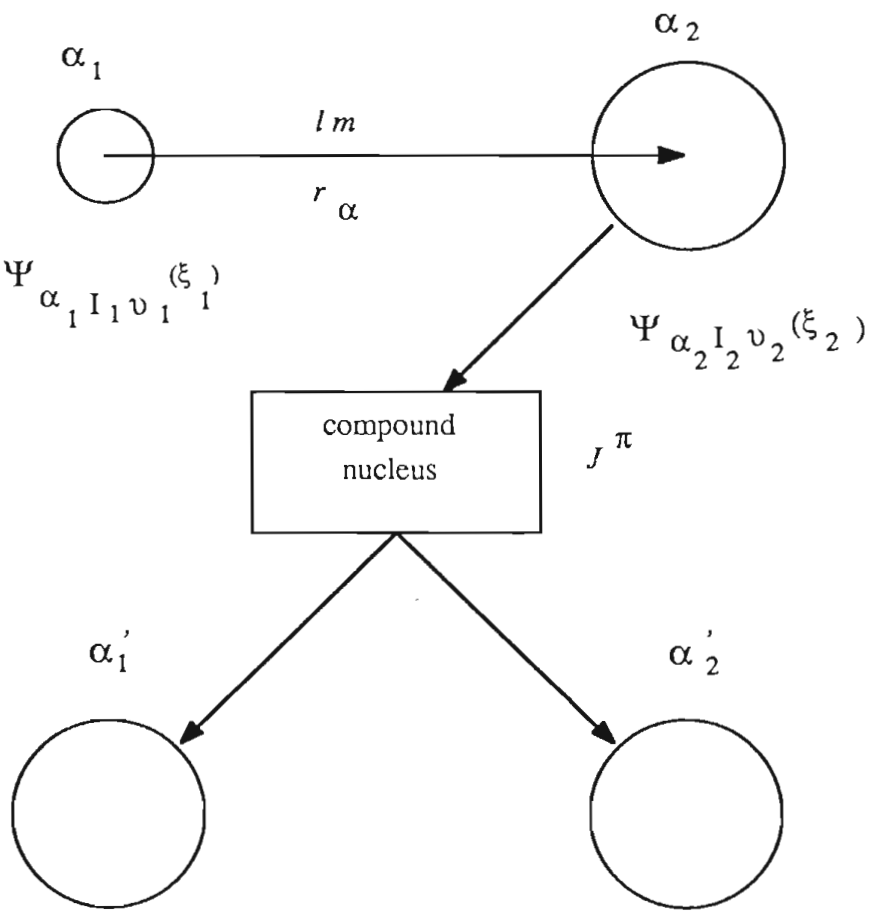
α_1
α_2
$l\,m$
r_α
$\Psi_{\alpha_1 I_1 \upsilon_1}(\xi_1)$
$\Psi_{\alpha_2 I_2 \upsilon_2}(\xi_2)$
compound nucleus
J^π
α_1'
α_2'

change directly into another channel, although channel-channel correlations have been observed (Shriner 1987, Mitchell 1985). Such a change can only take place indirectly via the internal region. This internal region is bounded by the "channel surface" S_c. The surface which divides the whole space into interior and exterior regions is the sum of S_c.

$$\mathcal{S} = \sum_c \mathcal{S}_c$$

For convenience we list the following additional channel characterizations:

$E_c \equiv E_\alpha$, the energy of relative motion of the particles of the pair c;

$M_c \equiv M_\alpha = (M\alpha_1 \cdot M\alpha_2) / (M\alpha_1 + M\alpha_2)$, the reduced mass;

$k_c \equiv k_\alpha = (2M_\alpha |E_\alpha| / \hbar^2)^{\frac{1}{2}}$, the wave number;

$v_c \equiv v_\alpha = \hbar k_\alpha / M_\alpha$, the relative velocity;

$\eta_c \equiv \eta_{\alpha l} = (Z\alpha_1 \cdot Z\alpha_2 e^2) / \hbar v_\alpha$, the Coulomb field parameter;

$\sigma_c \equiv \sigma_{\alpha l} = \arg\Gamma(1 + l_c + i\eta_c)$, the Coulomb phase shift;

$\rho_c \equiv \rho_\alpha = k_\alpha r_\alpha$.

2.2 Wave Functions for the External Region

Throughout configuration space the nonrelativistic Schrodinger equation will be used:

$$H\Psi = E\Psi,$$

where H is the sum of the kinetic energy operator and the potential energy operator. From the definition of external, (only non polarizing forces), the only potential which must be considered is the Coulomb interaction, $V_c(r_\alpha)$. We do not consider the centroid motion. Therefore the wave function Ψ in the channel c may be taken as the product of three parts

$$\Psi = \chi(\mathbf{r}_\alpha)\, \Psi_{\alpha_1}(\xi_{\alpha_1}) \Psi_{\alpha_2}(\xi_{\alpha_2}),$$

where $\chi(\mathbf{r}_\alpha)$ describes the relative motion of α_1 and α_2 and $\psi_{\alpha_1}(\xi_{\alpha_1})\psi_{\alpha_2}(\xi_{\alpha_2})$ describe the internal states of α_1 and α_2.

a Channel Spin Wave Functions

In this region only the Coulomb interaction is considered. The wave functions of the individual α_1 and α_2 are combined to construct a channel spin wavefunction $\psi_{\alpha s v}$.

$$\psi_{\alpha s v} = \sum_{v=i_1+i_2} (I_1 I_2 i_1 i_2 | s v)\psi_{\alpha_1 I_1 i_1}\psi_{\alpha_2 I_2 i_2}, \tag{2.2.1}$$

where $\mathbf{s} = \mathbf{I}_1 + \mathbf{I}_2$, is the channel spin, v is the projection of s and the coefficients $(I_1 I_2 i_1 i_2 | s v)$ are Clebsch-Gordan coefficients.

The channel spin wave functions are mutually orthogonal and normalized :

$$\int \psi^*_{\alpha s v}\psi_{\alpha' s' v'} ds = 4\pi a_\alpha^2 \delta_{\alpha s v, \alpha' s' v'}, \tag{2.2.2}$$

where the integral is taken over the totality of channel surface

$$S = \sum_c S_c .$$

b. Wave Function of Relative Motion

The complete wave function of relative motion in the channel consists of two parts : radial and angular

$$\chi = r_\alpha^{-1} u_{\alpha s l}(r_\alpha)(i^l Y_m^{(l)}(\Omega_\alpha)), \tag{2.2.3}$$

where $Y_m^{(l)}(\Omega_\alpha)$ are the usual spherical harmonics and $u_{\alpha s l}(r_\alpha)$ are solutions to the radial Schrodinger equation

$$\left[\frac{d^2}{dr_\alpha^2} - \frac{l(l+1)}{r_\alpha^2} - \left(\frac{2\pi}{h}\right)^2 2M_\alpha\left(\frac{Z_{\alpha_1} Z_{\alpha_2} e^2}{r_\alpha} - E_\alpha\right)\right] u_{\alpha s l}(r_\alpha) = 0 , \tag{2.2.4}$$

or

$$u''_{\alpha l}(\rho_\alpha) - [\, l(l+1)\,\rho^{-2}_\alpha + 2\eta_\alpha \rho^{-1}_\alpha - 1]\, u_{\alpha l}(\rho_\alpha) = 0\,, \tag{2.2.5}$$

where a prime denotes differentiation with respect to ρ_α.

This equation has been studied in depth by Bloch et al. (1950, 1951). The regular and irregular solutions of this equation have the asymptotic forms:

$$F_c \equiv F_{\alpha l} \sim sin\,(\rho_\alpha - \eta_\alpha log 2\rho_\alpha - \tfrac{1}{2} l\pi + \sigma_{\alpha l}) \tag{2.2.6a}$$

$$G_c \equiv G_{\alpha l} \sim cos\,(\rho_\alpha - \eta_\alpha log 2\rho_\alpha - \tfrac{1}{2} l\pi + \sigma_{\alpha l}). \tag{2.2.6b}$$

The solutions can also be chosen to represent incoming (I) and outgoing (O) waves. Convenient asymptotic forms are

$$I_c \equiv I_{\alpha l} \sim \exp\,[\,-i\,(\rho_\alpha - \eta_\alpha log 2\rho_\alpha - \tfrac{1}{2} l\pi + \sigma_{\alpha 0})] \tag{2.2.7a}$$

$$O_c \equiv O_{\alpha l} \sim \exp\,[+i\,(\rho_\alpha - \eta_\alpha log 2\rho_\alpha - \tfrac{1}{2} l\pi + \sigma_{\alpha 0})]\,. \tag{2.2.7b}$$

The relations between the two sets are

$$I_c = (G_c - i F_c)\exp(i\omega_c)$$

$$O_c = (G_c + i F_c)\exp(-i\omega_c),$$

where $\omega_c \equiv \omega_{\alpha l} = \sigma_{\alpha l} - \sigma_{\alpha o} = \sum_{n=1}^{l} tan^{-1}(\eta_\alpha / n)$. (2.2.7c)

c Complete Channel Wave Functions

Complete wave functions for the external region can now be written in the $(\alpha slvm)$ scheme corresponding to incoming and outgoing waves of unit flux crossing any sphere centered at the origin.

$$\mathcal{I}_c \equiv \mathcal{I}_{\alpha slvm} = (I_{\alpha l} / v_\alpha^{1/2})\, r_\alpha^{-1}\, \psi_{\alpha sv}(\, i^l Y^{(l)}_m) \tag{2.2.8a}$$

$$\mathcal{O}_c \equiv \mathcal{O}_{\alpha slvm} = (O_{\alpha l} / v_\alpha^{1/2})\, r_\alpha^{-1}\, \psi_{\alpha sv}(\, i^l Y^{(l)}_m) \tag{2.2.8b}$$

and

$$\Psi(\text{general}) = \Sigma_c (x_c \mathcal{O}_c + y_c \mathcal{I}_c). \tag{2.2.9}$$

The y_c are the amplitudes of the incoming wave $\mathcal{I}_c$ in the various channels c while the x_c are the amplitudes of outgoing wave $\mathcal{O}_c$.

It is convenient to introduce the surface functions

$$\varphi_{\alpha slvm} = r_\alpha^{-1} \psi_{\alpha sv}(i^l Y_m^{(l)}). \tag{2.2.10}$$

According to Eq. (2.2.2) , we have

$$\int \varphi^*_{\alpha slvm} \varphi_{\alpha' s' l' v' m'} dS = \delta_{\alpha slvm,\alpha' s' l' v' m'} . \tag{2.2.11}$$

The complete channel wave function can also be expressed as

$$\Psi = \varphi_c u_c(r). \tag{2.2.12}$$

Multiplying both sides of equation (2.2.12) by φ^*_c and integrating over the surface S:

$$u_c(a_c) = \int \varphi^* \Psi dS . \tag{2.2.13}$$

Now introduce the value quantity on the boundary surface

$$V_c = (\hbar^2 / 2M_c a_c)^{1/2} u_c(a_c) = (\hbar^2 / 2M_c a_c)^{1/2} \int \varphi^* \Psi dS, \tag{2.2.14a}$$

and the derivative quantity on the boundary surface

$$D_c = (a_c \hbar^2 / 2M_c)^{1/2} \left[du_c / dr_c \right]_{r_c = a_c}$$

$$= V_c + (a_c \hbar^2 / 2M_c)^{1/2} \int \varphi^* gran_n \Psi dS, \tag{2.2.14b}$$

where Ψ is the complete wave function of the system and $gran_n$ is the gradient normal to S. These quantities, which are expressed as surface integrals, are useful to match the internal and external functions.

The expansions on S for Ψ and its normal gradient in terms of the assumed complete set of surface function φ_c are therefore

$$\Psi = \Sigma_c (2M_c a_c / \hbar^2)^{1/2} V_c \varphi_c \tag{2.2.15a}$$

$$gran_n(r_c \Psi) = \Sigma_c (2M_c a_c / \hbar^2)^{1/2} D_c \varphi_c$$

$$gran_n \Psi = \Sigma_c (2M_c / a_c \hbar^2)^{1/2} (D_c - V_c)\varphi_c. \tag{2.2.15b}$$

Some frequently occurring combinations of the surface values and derivatives of incoming waves I and outgoing waves O are useful:

$$L_c \equiv \left(\rho_c O'_c / O_c \right)_{r_c = a_c} = S_c + iP_c \tag{2.2.16a}$$

$$\Omega_c = \left(I_c / O_c \right)^{1/2}_{r_c = a_c} = \exp i(\omega_c - \Phi_c) . \tag{2.216b}$$

The quantities S_c , P_c and Φ_c are referred to as the shift factor, penetrability factor and hard-sphere scattering phase shift, respectively.

According to Eq. (2.2.7), we have

$$S_c = \left[\rho_c (F_c F_c' + G_c G_c') / \left(F_c^2 + G_c^2\right)\right]_{r_c = a_c} \tag{2.2.17a}$$

$$P_c = \left[\rho_c / \left(F_c^2 + G_c^2\right)\right]_{r_c = a_c} \tag{2.2.17b}$$

$$\Phi_c \equiv \Phi_{\alpha l} = \tan^{-1}\left(F_c / G_c\right)_{r_c = a_c} . \tag{2.217c}$$

2.3 Wave Function For the Internal Region and R-matrix

In the internal region the total wave function Ψ is composed of various wave functions Ψ_{JM} corresponding to definite angular momenta J and components M. These wave functions satisfy the wave equation:

$$H \Psi_{JM} = E \Psi_{JM} . \tag{2.3.1}$$

This equation is too complicated to be solved since the exact form of the nuclear potential is unknown. But as shown in section 2.1, Ψ_{JM} can be formally expanded in the internal region in terms of a complete set of mutually orthogonal eigenfunctions $X_{\lambda JM}$ of that region,

$$\Psi_{JM} = \Sigma_\lambda A_{\lambda J} X_{\lambda JM} . \tag{2.3.2}$$

As in Eq. (2.2.14) we can define the value and derivative quantities for the internal eigenfunction

$$\gamma_{\lambda c} \equiv V_{\lambda c} = (\hbar^2 / 2M_c a_c)^{1/2} \int \varphi^* X_{\lambda JM} \, dS \tag{2.3.3a}$$

$$\delta_{\lambda c} \equiv D_{\lambda c} = \gamma_{\lambda c} + (a_c \hbar^2 / 2M_c)^{1/2} \int \varphi^* \, gran_n \, X_{\lambda JM} \, dS . \tag{2.3.3b}$$

The $\gamma_{\lambda c}$ are very important parameters; $\gamma^2_{\lambda c}$ has the dimension of energy and is referred to as the *reduced level width.*

We now specify the general boundary conditions to be satisfied by the complete set of states $X_{\lambda JM}$ on the surface S_c. Their conditions are taken to have the form

$$D_{\lambda c} / V_{\lambda c} \; (\equiv \; \delta_{\lambda c} / \gamma_{\lambda c}) = B_c \,, \tag{2.3.4}$$

where B_c are independent of λ.

Now we establish the fundamental R-matrix relation. Consider the general solutions for the wave equation at two energies:

$$H\Psi_1 = E_1 \Psi_1 \qquad H\Psi_2 = E_2 \Psi_2. \tag{2.3.5}$$

Green's theorem gives

$$(E_2 - E_1) \int_\tau \Psi_2^* \Psi_1 \, d\tau = \int_s (\hbar^2 / 2M_c)(\Psi_2^* \, gran_n \Psi_1 - \Psi_1 \, gran_n \Psi_2^*) dS \,. \tag{2.3.6}$$

By substituting (2.2.15) into this equation, we obtain

$$\int_\tau \Psi_2^* \Psi_1 \, d\tau = [1/(E_2 - E_1)] \Sigma_c \; (V^*_{2c} D_{1c} - V_{1c} D^*_{2c}). \tag{2.3.7}$$

From Eq. (2.3.2) the expansion coefficients A_λ can be expressed as

$$A_{\lambda J} = \int_\tau X^*_{\lambda JM} \Psi \, d\tau. \tag{2.3.8}$$

Letting $\Psi_2 = X_{\lambda JM}$, $E_2 = E_\lambda$ and $\Psi_1 = \Psi$, $E_1 = E$, we have

$$A_{\lambda J} = [1/(E_\lambda - E)] \Sigma_c \; (V^*_{\lambda c} D_c - V_c D^*_{\lambda c}). \tag{2.3.9}$$

Because $V_{\lambda c}$ and $D_{\lambda c}$ are real and $D_{\lambda c} = B_c V_{\lambda c}$,

$$A_{\lambda J} = [1/(E_\lambda - E)] \Sigma_c \, D^o_c \gamma_{\lambda c} \tag{2.3.10a}$$

and

$$D^o_c = D_c - B_c V_c \,. \tag{2.3.10b}$$

Substituting for $\gamma_{\lambda c}$ using definition 2.3.3., expansion (2.3.2) now becomes

$$\Psi_{JM} = \sum_c [\sum_\lambda \frac{X_{\lambda JM} \gamma_{\lambda c}}{E_\lambda - E}] D^o_c. \tag{2.3.11}$$

Operating on Eq. (2.3.11) with $\int_s \varphi^*_{c'} dS$ and using Eqs. (2.2.14) and (2.3.3), we obtain the fundamental R-matrix relation

$$V_{c'} = \Sigma_c \, R_{c'c} \, D^o_c \tag{2.3.12}$$

where

$$R_{c'c} = \sum_\lambda \frac{\gamma_{\lambda c'} \gamma_{\lambda c}}{E_\lambda - E} \,. \tag{2.3.13}$$

Here the subscript λ refers to a complete set of states and the quantities $\gamma_{\lambda c}$, $\gamma_{\lambda c'}$ and E_λ are energy-independent but depend on a_c, B_c. The $\gamma_{\lambda c}$ are called "reduced width amplitudes". For each state λ, one $\gamma_{\lambda c}$ is defined for each channel c. The E_λ are the energy eigenvalues of the state λ.

2.4 Collision Matrix and Cross Section

Recall Eq. (2.2.9)

$$\Psi \text{ (general)} = \Sigma_c \, (x_c \mathcal{O}_c + y_c \mathcal{I}_c), \tag{2.4.1}$$

where y_c and x_c represent the amplitudes of incoming and outgoing waves. For a given y_c, the numbers x_c are determined by the properties of the system. The role of the collision matrix is simply to express the x_c in terms of the y_c as follows:

$$x_{c'} = -\Sigma_c U_{c',c} y_c , \tag{2.4.2}$$

where $U_{c',c}$ is the collision matrix. As mentioned before, there are two possible channel designation schemes $\{\alpha slvm\}$and $\{\alpha slJM\}$ in which U can be defined, the connection between the collision matrix in these two representations is

$$U_{\alpha' s' l' v' m', \alpha slvm} = \Sigma_{JM} \, (slvm \,|\, JM) \, U^{J}_{\alpha' s' l', \alpha sl} \, (s' l' v' m' \,|\, JM). \tag{2.4.3}$$

Substituting Eq. (2.4.2) into Eq. (2.4.1) we have:

$$\Psi \text{ (general)} = \Sigma_c \, (\delta_{cc'} \mathcal{I}_c - U_{c',c} \mathcal{O}_c) \, y_c. \tag{2.4.4}$$

The normalized plane wave moving along the +z axis is

$$\frac{1}{v^{\frac{1}{2}}} e^{ikZ} \psi_{\alpha sv} = \sum_{l=0}^{\infty} \frac{1}{v^{\frac{1}{2}}} (2l+1) i^l j_l(kr) P_l(\cos\theta) \psi_{\alpha sv}$$

$$= \sum_{l=0}^{\infty} \frac{1}{v^{\frac{1}{2}}} (2l+1) \frac{i^l}{kr} F_l(r) P_l(\cos\theta) \psi_{\alpha sv}$$

$$= \sum_{l=0}^{\infty} \frac{2l+1}{v^{1/2}kr} i^l P_l(\cos\theta)\left[\frac{i}{2}e^{-i\omega_c}\left(I_c - O_c e^{2i\omega_c}\right)\right]\psi_{\alpha sv}$$

$$= \sum_{l=0}^{\infty} \frac{i\sqrt{2l+1}\sqrt{\pi}}{k} e^{-i\omega_c}\left\{\frac{i^l\sqrt{2l+1}}{\sqrt{4\pi}} P_l(\cos\theta)\left[\frac{1}{v^{1/2}r}\left(I_c - O_c e^{2i\omega_c}\right)\psi_{\alpha sv}\right]\right\}, \tag{2.4.5a}$$

Note that

$$Y_0^{(l)}(\Omega) = \frac{\sqrt{2l+1}}{\sqrt{4\pi}} P_l(\cos\theta),$$

and (2.4.5a) now becomes

$$= \sum_{l=0}^{\infty} \frac{i\sqrt{2l+1}\sqrt{\pi}}{k} e^{-i\omega_c}\left\{\frac{i^l}{v^{\frac{1}{2}}r} Y_0^{(l)}(\Omega) I_c \psi_{\alpha sv} - \frac{i^l}{v^{\frac{1}{2}}r} Y_0^{(l)}(\Omega) O_c \psi_{\alpha sv} e^{2i\omega_c}\right\}$$

$$= \sum_{\ell=0}^{\infty} \frac{i\sqrt{2\ell+1}\sqrt{\pi}}{k} e^{-i\omega_c}\left\{\mathcal{I}_{\alpha s\ell v0} - \mathcal{O}_{\alpha s\ell v0} e^{2i\omega_c}\right\}. \tag{2.4.5b}$$

The wave function Ψ' represents an incident wave of particles of type α, channel spin s and component v, moving along the z axis and disturbed only by the Coulomb field:

$$\Psi' = \sum_{cc'}(\delta_{cc'}\mathcal{I}_c - e^{2i\omega_c}\delta_{cc'}\mathcal{O}_{cc'})y_c, \tag{2.4.6}$$

with

$$y_c \equiv y_{\alpha slv0} = \frac{i\pi^{1/2}}{k_\alpha}(2l+1)^{1/2}. \tag{2.4.7}$$

Adding Ψ' to the right side of Eq. (2.4.4) and then subtracting it from the right side of Eq. (2.4.4) gives

$$\Psi = \Psi' + \Sigma_{cc'}\,(\,e^{2i\omega_c}\,\delta_{cc'} - U_{cc'})\mathcal{O}_{c'}y_c. \tag{2.4.8}$$

According to Schiff (1949), the asymptotic form of Ψ' is

$$\Psi'_{\alpha sv} \sim \frac{\psi_{\alpha sv}}{\sqrt{v_\alpha}} \left\{ \left(1 - \frac{\eta_\alpha^2}{ik_\alpha (r_\alpha - Z_\alpha)} \right) \exp i\{k_\alpha Z_\alpha - \eta_\alpha \log k_\alpha (r_\alpha - Z_\alpha) - \sigma_{\alpha 0}\} \right.$$

$$\left. - \frac{\pi^{1/2}}{r_\alpha k_\alpha} C_\alpha(\theta_\alpha) \exp i\{\rho_\alpha - \eta_\alpha \log 2\rho_\alpha + \sigma_{\alpha 0}\} \right\}, \qquad (2.4.9)$$

where

$$C_\alpha(\theta_\alpha) = (4\pi)^{-1/2} \eta_\alpha \cos ec^2\left(\frac{\theta_\alpha}{2}\right) \exp\left\{ -2i\eta_\alpha \log \sin\left(\frac{\theta_\alpha}{2}\right) \right\}. \qquad (2.4.10)$$

Note that the second part of Eq. (2.4.9) corresponds to a Coulomb scattering wave with coefficient $C_\alpha(\theta_\alpha)$.

With y_c from Eq. (2.4.7), the asymptotic form of Eq. (2.4.8) becomes

$$\Psi \sim \frac{1}{\sqrt{v_\alpha}} \psi_{\alpha sv} \left\{ \left(1 - \frac{\eta_\alpha^2}{ik_\alpha (r_\alpha - Z_\alpha)} \right) \exp i\{k_\alpha Z_\alpha - \eta_\alpha \log k_\alpha (r_\alpha - Z_\alpha) - \sigma_{\alpha 0}\} \right.$$

$$\left. - \sum_{\alpha' s' v'} \frac{\pi^{\frac{1}{2}}}{r_{\alpha'} k_{\alpha'}} C_{\alpha'}(\theta_{\alpha'}) \exp i\{\rho_{\alpha'} - \eta_{\alpha'} \log 2\rho_{\alpha'} + \sigma_{\alpha' 0}\} \right\} \delta_{\alpha' s' v', \alpha sv}$$

$$+ \frac{i\pi^{1/2}}{k_\alpha} \sum_{\alpha' s' l' v' m', l} (2l+1)^{1/2} \left[e^{2i\omega_{\alpha' l'}} \delta_{\alpha' s' l' v' m', \alpha slv0} - U_{\alpha' s' l' v' m', \alpha slv0} \right]$$

$$\cdot \frac{1}{\sqrt{v_{\alpha'}} r_{\alpha'}} \exp i[\rho_{\alpha'} - \eta_{\alpha'} \log 2\rho_{\alpha'} + \sigma_{\alpha' 0}] (-i)^l (i)^{l'} Y_{m'}^{(l')}(\Omega_{\alpha'}) \psi_{\alpha' s' v'} \qquad (2.4.10)$$

$$\sim \frac{1}{\sqrt{v_\alpha}} \psi_{\alpha sv} \left\{ \left(1 - \frac{\eta_\alpha^2}{ik_\alpha (r_\alpha - Z_\alpha)} \right) \exp i\{k_\alpha Z_\alpha - \eta_\alpha \log k_\alpha (r_\alpha - Z_\alpha) - \sigma_{\alpha 0}\} \right.$$

$$+ \sum_{\alpha' s' v'} \frac{\pi^{\frac{1}{2}}}{k_{\alpha'}} \left\{ -C_{\alpha'}(\theta_{\alpha'}) \delta_{\alpha' s' v' \alpha sv} + i \sum_{l' m' l} (2l+1)^{\frac{1}{2}} \left[e^{2i\omega_{\alpha' l'}} \delta_{\alpha' s' l' v' m', \alpha slv0} \right. \right.$$

$$\left. \left. - U_{\alpha' s' l' v' m', \alpha slv0} \right] Y_{m'}^{(l')}(\Omega_{\alpha'}) \right\} \frac{1}{v_{\alpha'}^{1/2} r_{\alpha'}} \exp i\{\rho_{\alpha'} - \eta_{\alpha'} \log 2\rho_{\alpha'} + \sigma_{\alpha' 0}\} \psi_{\alpha' s' v'}$$

$$\sim \frac{1}{\sqrt{v_\alpha}}\psi_{\alpha sv}\left\{\left(1-\frac{\eta_\alpha^2}{ik_\alpha(r_\alpha - Z_\alpha)}\right)\exp i\left\{k_\alpha Z_\alpha - \eta_\alpha \log k_\alpha(r_\alpha - Z_\alpha) - \sigma_{\alpha 0}\right\}\right.$$

$$\left. + \sum_{\alpha' s' v'} A_{\alpha' s' v', \alpha sv}(\Omega_{\alpha'}) \frac{1}{v_{\alpha'}^{1/2} r_{\alpha'}} \exp i\left\{\rho_{\alpha'} - \eta_{\alpha'} \log 2\rho_{\alpha'} + \sigma_{\alpha' 0}\right\}\psi_{\alpha' s' v'}\right. \quad (2.4.11)$$

where

$$A_{\alpha' s' v', \alpha sv}(\Omega_{\alpha'}) = \frac{\pi^{\frac{1}{2}}}{k_\alpha}\left\{-C_{\alpha'}(\theta_{\alpha'})\delta_{\alpha' s' v', \alpha sv} + i\sum_{l' m' l}(2l+1)^{\frac{1}{2}}\right.$$

$$\left. \cdot \left[e^{2i\omega_{\alpha' l'}}\delta_{\alpha' s' l' v' m', \alpha slv0} - U_{\alpha' s' l' v' m', \alpha slv0}\right]Y_m^{(l)}\Omega(\alpha')\right\}. \quad (2.4.12)$$

$A_{\alpha' s' v', \alpha sv}$ are the amplitudes of the outgoing waves of type α's'v' at infinity. The differential cross sections are by definition given by

$$d\sigma_{\alpha sv, \alpha' s' v'} = \left|A_{\alpha' s' v', \alpha sv}(\Omega_{\alpha'})\right|^2 d\Omega_{\alpha'}. \quad (2.4.13)$$

Thus far we have used the $\{\alpha slvm\}$ scheme to describe the collision matrix U. For the compound nucleus, it is often more convenient to use the $\{\alpha slJM\}$ scheme. To change U from the $\{\alpha slvm\}$ to the $\{\alpha slJM\}$ scheme, we substitute the transformation (2.4.3) into the amplitude expression (2.4.12):

$$A_{\alpha' s' v', \alpha sv}(\Omega_{\alpha'}) = \frac{\pi^{\frac{1}{2}}}{k_\alpha}\left[-C_{\alpha'}(\theta_{\alpha'})\delta_{\alpha' s' v', \alpha sv} + i\sum_{JMl'm'}(2l+1)^{\frac{1}{2}}\right.$$

$$\left. \cdot (slv0|JM)(s'l'v'm'|JM)T^J_{\alpha' s' l', \alpha sl} Y_{m'}^{(l')}(\Omega_{\alpha'})\right] \quad (2.4.14)$$

where

$$T^J_{\alpha' s' l', \alpha sl} = e^{2i\omega_{\alpha' l'}}\delta_{\alpha' s' l', \alpha sl} - U^J_{\alpha' s' l', \alpha sl}. \quad (2.4.15)$$

For unpolarized incident and target particles, the cross section (2.4.13) may be summed over v' and averaged with respect to v:

$$d\sigma_{\alpha s,\alpha' s'} = (2s+1)^{-1}\sum_{\nu\nu'}\left|A_{\alpha' s'\nu',\alpha s\nu}(\Omega_{\alpha'})\right|^2 d\Omega_{\alpha'}, \tag{2.4.16}$$

and the absolute squaring operation can be performed by using two sets of summing integers

$$\{J_1 M_1 l_1 l'_1 m'_1\} \text{ and } \{J_2 M_2 l_2 l'_2 m'_2\}.$$

We determine the final result

$$\begin{aligned} d\sigma_{\alpha s,\alpha' s'}/d\Omega_{\alpha'} &= \pi k_\alpha^{-2}\left|C_{\alpha'}(\theta_{\alpha'})\right|^2\delta_{\alpha' s',\alpha s} \\ &+\left[k_\alpha^2(2s+1)\right]^{-1}\sum_L B_L(\alpha' s',\alpha s)P_L(\cos\theta_{\alpha'}) + \sqrt{\pi}\left[k_\alpha^2(2s+1)\right]^{-1} \\ &\cdot\sum_{Jl}(2J+1)\delta_{\alpha' s' l',\alpha s l}\,\mathrm{Re}\left[iT^{J*}_{\alpha' s' l',\alpha s l}C_{\alpha'}(\theta_{\alpha'})P_l(\cos\theta_{\alpha'})\right] \end{aligned} \tag{2.4.17}$$

where

$$\begin{aligned} B_L(\alpha' s',\alpha s) = \frac{1}{4}(-1)^{s-s'} &\sum_{J_1 J_2 l_1 l_2 l'_1 l'_2}\overline{Z}(l_1 J_1 l_2 J_2, sL)\overline{Z}(l'_1 J_1 l'_2 J_2, s'L) \\ &\cdot\left(T^{J_1}_{\alpha' s' l'_1,\alpha s l_1}\right)\left(T^{J_2}_{\alpha' s' l'_2,\alpha s l_2}\right)^*. \end{aligned} \tag{2.4.18}$$

The first term of expression (2.4.17) may be identified as pure Coulomb scattering, the second as resonance scattering and reaction, and the last as interference between the Coulomb scattering and resonance scattering. The last term generates different shapes at different angles for elastic scattering of different orbital angular momentum *l*.

2.5 Relation Between the R-Matrix and the Collision Matrix

We now complete the final link, the connection between the R-matrix and the collision matrix U. Since the R-matrix specifies the form of the wave function on the surface S and the U-matrix specifies the form at infinity, the connection between the two is established by joining these regions.

From section 2.2.c, any solution Ψ in the external region can be expressed as

$$\Psi = \sum_c (x_c \mathcal{G}_c + y_c \mathcal{J}_c) \tag{2.2.9}$$

and the expressions of the surface "value" and "derivative" are

$$V_c = (\hbar^2 / 2M_c a_c)^{1/2} u_c(a_c) = (\hbar^2 / 2M_c a_c)^{1/2} \int \varphi^* \Psi \, dS \tag{2.2.14a}$$

$$D_c = (a_c \hbar^2 / 2M_c)^{1/2} \left[du_c / dr_c \right]_{r_c = a_c}$$

$$= V_c + (a_c \hbar^2 / 2M_c)^{1/2} \int \varphi^* \, gran_n \Psi \, dS, \tag{2.2.14b}$$

Substituting Eq. (2.2.8) and Eq. (2.2.9) into these equations and using Eq. (2.2.11), we have

$$V_c = (\tfrac{1}{2}\hbar)^{\frac{1}{2}} (\rho_c^{-\frac{1}{2}} O_c x_c + \rho_c^{-\frac{1}{2}} I_c y_c) \tag{2.4.19a}$$

$$D_c = (\tfrac{1}{2}\hbar)^{\frac{1}{2}} (\rho_c^{\frac{1}{2}} O_c' x_c + \rho_c^{\frac{1}{2}} I_c' y_c). \tag{2.4.19b}$$

Since these must satisfy the fundamental R-matrix relation (2.3.12), one finds, in matrix notation, that

$$(\rho^{-\frac{1}{2}}\mathbf{O}\boldsymbol{x} + \rho^{-\frac{1}{2}}\mathbf{I}\boldsymbol{y}) = \mathbf{R}[(\rho^{\frac{1}{2}}\mathbf{O}'\boldsymbol{x} + \rho^{\frac{1}{2}}\mathbf{I}'\boldsymbol{y}) - \mathbf{B}(\rho^{-\frac{1}{2}}\mathbf{O}\boldsymbol{x} + \rho^{-\frac{1}{2}}\mathbf{I}\boldsymbol{y})], \tag{2.4.20a}$$

or

$$[\rho^{-\frac{1}{2}}\mathbf{O} - \mathbf{R}\rho^{\frac{1}{2}}(\mathbf{O}' - \rho^{-1}\mathbf{B}\mathbf{O})]\boldsymbol{x} = -[\rho^{-\frac{1}{2}}\mathbf{I} - \mathbf{R}\rho^{\frac{1}{2}}(\mathbf{I}' - \rho^{-1}\mathbf{B}\mathbf{I})]\boldsymbol{y}\,, \tag{2.4.20b}$$

Comparing with $\boldsymbol{x} = -\mathbf{U}\boldsymbol{y}$ gives the relation between the U and R matrices

$$\mathbf{U} = \boldsymbol{\Omega}\mathbf{P}^{\frac{1}{2}}[\mathbf{1} - \mathbf{R}(\mathbf{L} - \mathbf{B})]^{-1}[\mathbf{1} - \mathbf{R}(\mathbf{L}^* - \mathbf{B})]\mathbf{P}^{-\frac{1}{2}}\boldsymbol{\Omega}\,, \tag{2.4.21}$$

where $\mathbf{L}$, $\boldsymbol{\Omega}$, $\mathbf{P}$ and $\mathbf{B}$ are diagonal matrices whose elements are defined by Eqs. (2.2.16a), (2.216b), (2.2.17) and (2.3.4).

With this relation all needed information for the calculation of the cross section has been obtained. In other words, the properties of the compound nucleus can be determined by fitting the experimental cross section. The calculation of the cross section has been coded for use in data analysis in the FORTRAN code MULTI6.

B. Statistical Properties

The R-matrix theory has proven very useful in the analysis of compound nuclear resonance data, and will be used to analyze the excitation functions. Our purpose, however, is to study the statistical properties of the resonances, such as the average level density, strength function, spectrum fluctuations and strength fluctuations. In this section we review the relevant statistical theories.

1. Average Level Density

Nuclear level densities play a central role in any statistical analysis of nuclear reactions. Soon after the observation of neutron resonances. Bethe (1936,1937) published seminal papers on level densities in nuclear systems. Since then a large amount of work has been performed both to measure and to model nuclear level densities.

Bethe considered two quite different models for nuclear level densities. In the Fermi gas model, the interaction between the particles was small, nucleons were considered free and the total energy of the nucleus was equal to the sum of the energies of the individual particles. The other model was based on the liquid drop model, where the interaction was large, compared to the kinetic energy of the particles, and the total energy was the sum of the interaction potential and the kinetic energies of the particles.

In both cases, the nuclear problem was considered from a statistical approach, and classical ideas were used: The entropy of the nucleus was obtained from the relation between energy and temperature using ordinary thermodynamic relations; the entropy S is then by definition related to the number of states of the nucleus by $\rho \sim e^{S}$. Thus the number of states (per energy interval) can be expressed in terms of the excitation energy of the nucleus.

Bethe derived a general expression for the average spacing of the nuclear levels

$$D(U) = \frac{1}{\rho(U)} = (2\pi)^{\frac{1}{2}} \tau \left(\frac{dU}{d\tau}\right)^{\frac{1}{2}} e^{-S}$$

$$= (2\pi n)^{\frac{1}{2}} \left(\frac{U^{n+1}}{a}\right)^{\frac{1}{2n}} \exp\left(-\frac{n}{n-1}\sqrt[n]{aU^{n-1}}\right),$$

where U is the excitation energy, τ is nuclear temperature, and "a" is called the level density parameter. The assumed relation between U and τ is

$$U = a\tau^n,$$

In the Fermi gas model n=2. Bethe obtained

$$D(U) = 2\frac{U^{\frac{3}{4}}}{a^{\frac{1}{4}}}\sqrt{\pi}\exp\left(-2\sqrt{aU}\right), \qquad \rho(U) = \frac{a^{\frac{1}{4}}}{2\sqrt{\pi}U^{\frac{3}{4}}}\exp\left(2\sqrt{aU}\right).$$

Bethe also noted that the spacing would be dependent on the angular momentum of the nucleus; a certain value J was most probable. He introduced J- dependence in the form

$$\rho(J) \propto \left[\frac{2J+1}{2\sigma^2}\right]\exp\left[-\frac{\left(J+\frac{1}{2}\right)^2}{2\sigma^2}\right],$$

where the parameter σ is known as the spin cutoff parameter.

Bethe's expression could be used to calculate level densities based on the parameters obtained from the existing data. However, as the data base increased, Bethe's expression was found to be inadequate. The expanded data base indicated that the level density depended not only upon the excitation energy and angular momentum of the levels, but also on shell effects, and on the atomic mass A. Many efforts were made to include these effects. Gilbert and Cameron (1965) for example, developed parameterizations which corrected for both odd-even pairing effects and shell effects.

Gilbert and Cameron adopted Bethe's level-density formula at high excitation energies

$$\rho(U,J) = \frac{\sqrt{\pi}}{12}\frac{\exp\left(2\sqrt{aU}\right)}{a^{\frac{1}{4}}U^{\frac{5}{4}}}\left[\frac{2J+1}{2\sqrt{2\pi}\,\sigma^3}\right]\exp\left[-\frac{\left(J+\frac{1}{2}\right)^2}{2\sigma^2}\right],$$

where $\rho(U,J)$ is the density (in MeV^{-1}) of levels of given angular momentum J at an energy U. For the spin-dependence parameter σ they found

$$\sigma^2 = 0.0888\, a\tau A^{\frac{2}{3}} = 0.0888\sqrt{aU}\, A^{\frac{2}{3}},$$

where τ is the nuclear temperature.

Gilbert and Cameron pointed out that if those equations were used to fit the neutron resonance data, there would be systematic differences in the values of "a" for even-even, odd-A, and odd-odd nuclei. They followed the approach of Newton (1956) and introduced a "pairing energy" *P(Z)* or *P(N)*. U is now defined by

$$U = E - P(N) - P(Z),$$

where E is the total excitation energy, while *P(Z)* and *P(N)* are zero for odd values of N or Z.

In Bethe's theory, a/A is constant. However, there were obvious shell effects present in "a". Gilbert and Cameron found a simple connection between a/A and S, the shell correction. They found that for the spherical nuclei, there was a good linear correlation

$$a / A = 0.00917S + 0.142,$$

while for deformed nuclei

$$a / A = 0.00917S + 0.120,$$

where S = S(N)+S(Z) is the total shell correction in MeV.

Gilbert and Cameron also demonstrated that at low excitation energies a "constant nuclear temperature" representation of nuclear-level densities could be used. The level densities were then

$$\rho \sim \exp(E/T),$$

(where T is the nuclear temperature, a constant) instead of

$$\rho \sim \exp[2\,(aE)^{\frac{1}{2}}]$$

as in Bethe's theory. Gilbert and Cameron's expression gave a better fit than Bethe's to the experimental data over the first 10 MeV or so of excitation energy.

The results of Gilbert and Cameron continue to be very useful. However, in Gilbert and Cameron's expression, the level density parameter was independent of the excitation energy, meaning that shell effects continue to manifest themselves in the level density at arbitrarily high excitation energies. This prediction is not true; the parameter "a" is dependent on energy; as the excitation energy increases the shell effects on the level density weaken and at high enough excitation energies (~100 MeV) the mass dependence of "a" tends to the simple quasiclassical limit $a = \text{const} \cdot A$ (Ignatyuk 1970). Based on the new data and analysis, Ignatyuk et al. (1975) and Kataria et al. (1978) separately proposed new semi-empirical nuclear level density formulas. The forms of the Ignatyuk model (known as the IST model) and the Kataria model (known as the KRK model) are different, but both take into account the influence of nuclear shell structure on level densities and the excitation energy dependence of shell effects. Both models not only proved to be very successful in fitting the experimental data on neutron resonance spacings, but also provided a reliable extrapolation to higher excitation energies.

All of the models mentioned above are phenomenological models----the parameters are dependent on (as well as limited by) the available data. It is thus desirable to increase the data base used in determining the parameters. For a long time average s-wave neutron resonance spacings have been a primary source of nuclear level density information. TUNL started to acquire high quality proton resonance data in the late 60's with the development of the high resolution technique. Since then a large amount of high-resolution proton resonance data has been accumulated. Recently these data were reanalyzed systematically. The average s-wave resonance spacings from proton and neutron resonances were compared by Vonach et al. (1988). In this comparison s-wave resonance

spacings from both proton and neutron data were carefully reanalyzed and the bootstrap method (see Chapter IV for details) was used to correct for missing levels. Because of the variation in excitation energies of the nuclei involved, the level densities were converted to a standard excitation energy. After these corrections, the A dependence of the level density was determined to be similar for both protons and neutrons, indicating that the proton data are suitable for inclusion in the nuclear data base. Vonach et al. also determined the atomic mass dependence of the level density parameter "a" for both proton and neutron data using the two recently developed models by Ignatyuk et al. (IST model) and by Kataria et al. (KRK model). A linear dependence of the parameter "a" on the mass number A was found in both models and the agreement between the values obtained for the proton and neutron data was also good. The conclusion from the comparison was that high-resolution proton resonance data can be used to determine nuclear level densities with an accuracy about equal to that achieved in modern neutron resonance experiments.

However, the greatest advantage of using proton resonances is the ability to study both the angular momentum dependence and the parity dependence of the level density. The study of J and π dependence is much more difficult with neutron resonance data, since in most cases only s-wave resonances were observed and analyzed reliably. Thus one of the motivations of this experiment was to determine level densities for higher angular momentum states.

2. Wigner Distribution

The nearest neighbor level spacings are expected to obey a distribution of the form

$$P(x) = \frac{\pi}{2} x \exp\left[-\frac{\pi x^2}{4}\right] dx$$

for $x = D / < D >$, where D is the spacing between nearest states of the same spin and

parity, and <D> is the average spacing. This distribution, known as the Wigner distribution, was first proposed by Wigner in 1957 under the assumption that the distribution should be proportional to D for small D; i.e., the "repulsion" between levels is linear (as later derived by Porter and Rosenzweig (1960) from random matrix theory). The repulsion is essentially a result of the fact that the system (of levels having the same J^{π}) is not degenerate in energy (the Pauli exclusion principle). The Wigner distribution is valuable in providing an estimate of the purity of a level sequence. Usually the comparison is between binned data and a smooth curve, as shown in Figure 5.13a. There is an inherent problem in this type of comparison, since the binned data are based on an arbitrary selection of bin widths. By selecting appropriate bin widths it is possible to make the data compare more or less favorably with the Wigner distribution. This arbitrariness of bin width selection has been partially eliminated in this study by using bin widths of equal probability. However, even in this case changing the number of equally probable bins leads to data plots which appear somewhat different. This arbitrariness can be removed by using a cumulative Wigner distribution, as shown in Figure 5.13b.

The cumulative number of levels N(x) is

$$N(x_i) = i, \quad \text{where } x_i = D_i / \langle D \rangle,$$

and the theoretical distribution

$$N(x') = N_0 \int_0^{x'} P(x)\,dx,$$

where P(x) is the Wigner distribution and N_0 is the total number of levels in the sequence.

3. Porter--Thomas Distribution

For a given sequence of nuclear levels the reduced widths follow a Porter-Thomas distribution

$$P(y)\,dy = \frac{1}{\sqrt{2\pi y}}\exp\left(-\frac{y}{2}\right)dy \quad ,$$

where

$$y = \gamma^2_{\lambda} / \gamma^2_{average},$$

where γ_{λ}^2 is the reduced width for level λ, and $\gamma^2_{\text{average}}$ is the averaged reduced width. This distribution was first proposed by Porter and Thomas in 1956 and was later obtained from random matrix theory by Porter (1965).

The Porter-Thomas distribution can also be used as a test for sequence selection. As with the Wigner distribution the problem of the selection of bin width is also encountered with the binned data. Again, we use a cumulative plot to remove the subjectivity. The data are plotted according to

$$N(y_i) = i, \text{ where } y_i = \gamma^2_{\lambda} / \gamma^2_{average},$$

with the theoretical distribution plotted as

$$N(y_i) = N_0 \int_0^{y'} P(y)\,dy \quad ,$$

where $P(y)$ is the Porter-Thomas distribution.

C. Analog States

It is well known that if the nuclear force is charge independent, then the proton and neutron may be considered as two states of one particle--the nucleon. States in different nuclei with the same mass form isobaric multiplets, which have a common quantum number, the isospin T. These two states differ only in the value of the third component of isospin $T_3 = (N - Z) / 2$. For many years it was assumed that the large Coulomb forces would destroy isobaric correspondence in heavier nuclei. It was felt that the Coulomb force would sufficiently "mix" the analog state with the normal "background states" (those having the same spin and parity as the analog state) to spread the analog strength over a large energy range (~ a few MeV) and cause the identity of the analog state to be destroyed. Evidence for Isobaric Analog Resonances (IAR) in heavier nuclei was provided by Anderson and Wong (1961). Three years later Fox et al. (1964) observed IAR in the compound nucleus in ^{88}Sr (p,n) and ^{89}Y(p,n) excitation functions. The first evidence for fine structure in analog states was provided by Richard et al. (1964) in the reaction ^{92}Mo (p,p). Fine structure was conclusively established by Keyworth et al. (1966, 1968). The fine structure was explained by Robson (1965) in terms of mixing of the analog and background states in the external region.

Following the description of analog states given by Robson, and later extended by Mello (1967) to include the many channel case, many different theoretical approaches were used to describe the features of analog states. For a more complete list of references see Wilkinson (1969).

In the following section only a brief description which follows Robson and Mello will be given. Consider two systems : (proton + target) and (neutron + target), the states of which we denote by $|pC\rangle$ and $|nC\rangle$, respectively. It is reasonable to assume (Lane 1961, 1962) that the target system C has pure isospin $T_o = T_{oz}$. $|nC\rangle$ is a single particle state in the parent nucleus and can be expanded in terms of states of total isospin T ,

$$| nC > = \; | 1/2\ 1/2 > | T_o\ T_o > = | T_o{+}1/2\ T_o{+}1/2 >,$$

Similarly we can expand $| pC >$ as

$$| pC > = \; | 1/2\ -1/2 > | T_o\ T_o >$$

$$= (2T_o{+}1)^{-1/2} [| T_o{+}1/2\ T_o{-}1/2 > + (2T_o)^{1/2} | T_o{-}1/2\ T_o{-}1/2 >]$$

$$= (2T_o{+}1)^{-1/2} [| T_> > + (2T_o)^{1/2} | T_< >],$$

where $| T_> > = | T_o{+}1/2\ T_o{-}1/2 >$ and $| T_< > = | T_o{-}1/2\ T_o{-}1/2 >$.

We find $| T_> >$ by applying T^- (the isospin lowering operator) to $| nC >$,

$$T^- | T_o{+}1/2\ T_o{+}1/2 > = (2T_o{+}1)^{1/2} | T_o{+}1/2\ T_o{-}1/2 >$$

$$= (2T_o{+}1)^{1/2} | T_> >.$$

$| T_> >$ are the isobaric analog states of $| nC >$ states and $| T_< >$ have the same isospin as the ground states of the nucleus (p+ C).

The analog of the parent state is formed by exchanging a neutron for a proton without changing any quantum numbers (except T_3). The energy difference between these two states will be the sum of the Coulomb energy of the extra proton and the neutron-proton mass difference. The energy relation between these two states is shown in Figure 2.2.

From the $| pC >$ expression (Eq. 2.2.2) we see that the p + C channel does not form states of pure isospin. Because Coulomb forces mix the two components $T_>$, $T_<$, total isobaric spin T is not a good quantum number for the $| pC >$ system. According to Robson (1965), however, there is a *restricted* region of radial space in which T may be relatively pure.

We can rewrite $| T_> >$ by applying T^- directly to $| 1/2\ 1/2 > | T_o\ T_o >$

$$| T_> > = (2T_o + 1)^{-1/2} [T^- | 1/2\ 1/2 > | T_o\ T_o >]$$

$$= (2T_o{+}1)^{-1/2} [| 1/2\ -1/2 > | T_o\ T_o > + (2T_o)^{1/2} | 1/2\ -1/2 > | T_o\ T_o{-}1 >]$$

$$= (2T_o{+}1)^{-1/2} [| pC > + (2T_o)^{1/2} | nA >,$$

where $| nA >$ is a 2 particle-1 hole configuration and represents a neutron coupled to the analog of the ground state of the target

$$| A > = | T_o\ T_o{-}1 > = (2T_o)^{-1/2}\ T^- | T_o\ T_o >.$$

Figure 2.2 Analog state energy schematic for ^{49}Ti and ^{49}V system.

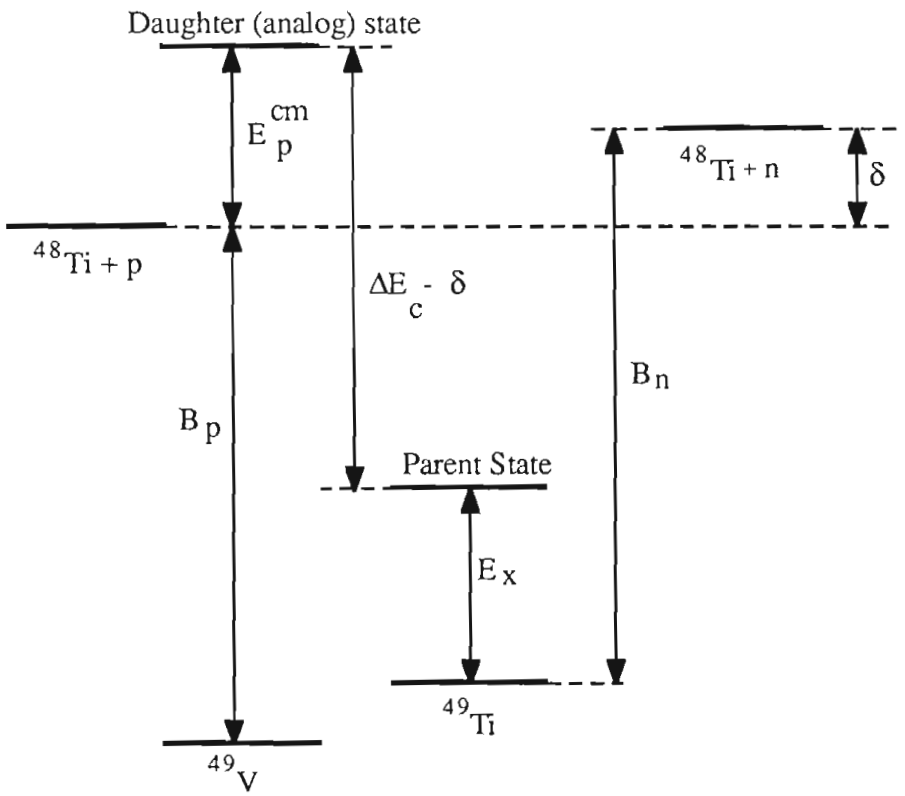

B_p = Binding energy of the proton = 6.758 MeV (J. K. Tuli 1985)

B_n = Binding energy of the neutron = 8.142 MeV (J. K. Tuli 1985)

δ = p-n mass difference

ΔE_c = Coulomb energy difference = 7.793 MeV (Janecke 1969)

Figure 2.3 Particle-hole picture of the analog state.

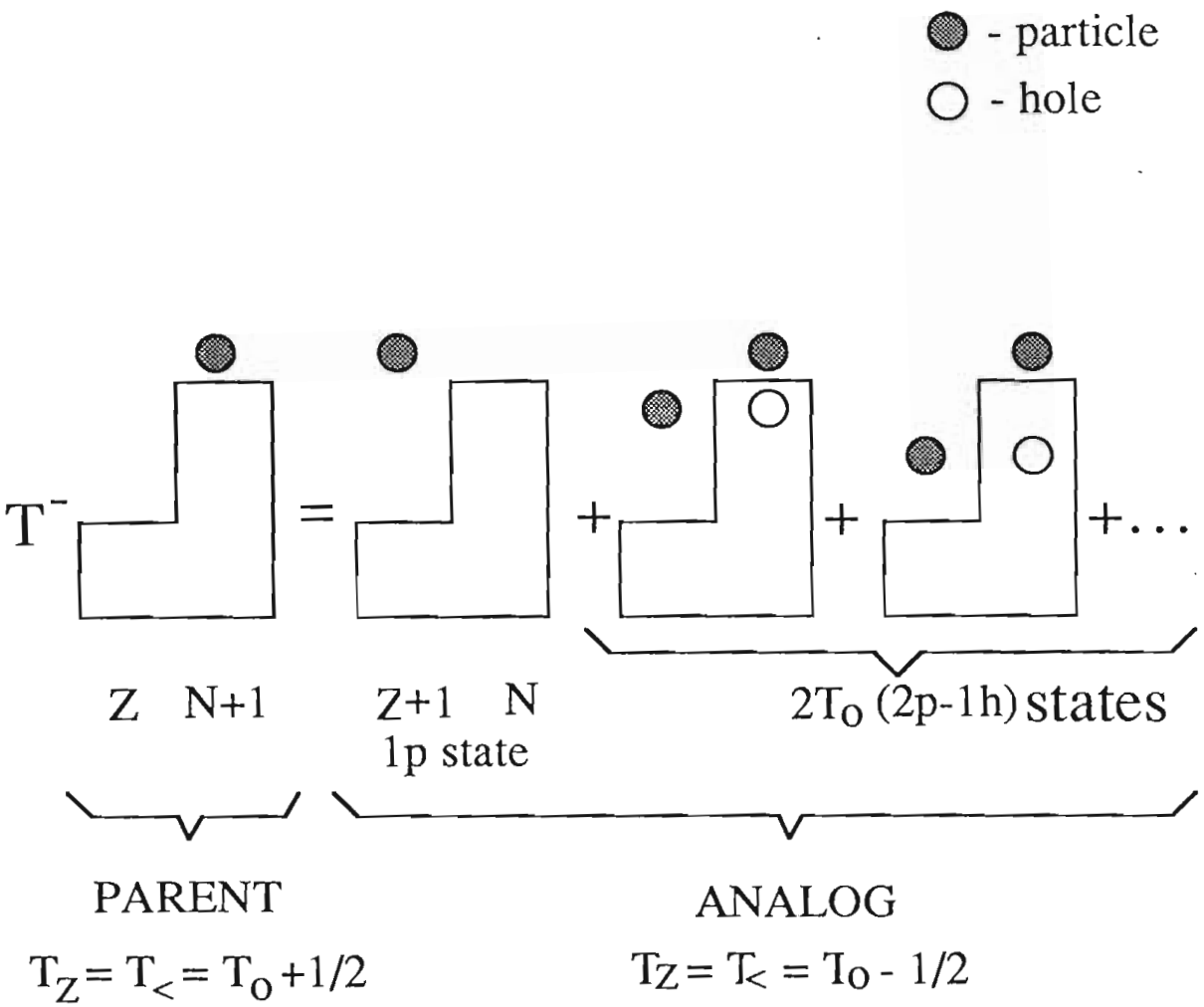
● - particle
○ - hole
T⁻
=
+
+
+...
Z N+1
Z+1 N
1p state
2T₀ (2p-1h) states
PARENT
ANALOG
T_Z = T_< = T₀ +1/2
T_Z = T_< = T₀ - 1/2

The coefficients for these configurations are a result of the Pauli exclusion principle: only $2T_o$ excess neutrons in the core can be exchanged for protons having the same quantum numbers. There are thus $2T_o$ possible ways to form $| nA >$. This is shown in Figure 2.3.

If the analog state is excited by a proton bombarding the core, then $| pC >$ represents that part of the analog state which resonates in the proton elastic scattering (p,p) reaction. The $| nA >$ is that part of the analog state which resonates in the charge exchange (p,n) reaction. It is obvious from the expression (2.2.4) that the probability of $| T_> >$ decaying through $| pC >$ is $[1 / (2T_o + 1)]$. In our experiment the energy is well below the threshold of n + A; in other words, the $| nA >$ channel is a closed channel and does not contribute to the width of the analog resonances observed in our experiment (^{49}V). Thus the width of an analog resonance observed in the experiment is multiplied by $(2T_o + 1)$ to give the single particle reduced widths of the analog state at this energy:

$$\gamma^2_{\lambda.s.p} = (2T_o + 1) \gamma^2_{Ap},$$

where γ^2_{Ap} are the reduced widths of the analog resonance observed. $\gamma^2_{\lambda.s.p}$ are the single particle reduced widths of the analog state.

We now consider the single particle spectroscopic factors. Single particle states can be defined as the configuration which occurs when the residual two body interaction between the particle (neutron or proton) and the nucleons in the core is zero. In reality, of course, the residual two body interaction does not vanish and it causes the single particle state to mix with the background states of the same spin and parity. Because the mixing here is caused by nuclear forces, the single particle strength can spread over a much wider range, on the order of several MeV. The single particle state is then fragmented and the distribution of fine structure widths has a Lorentzian shape about the original single particle energy in the intermediate model given by Lane et al. (1955). This is the so called giant resonance in the single particle strength function. We have:

$$\Sigma_\lambda \gamma^2_{\lambda.s.p.} = \gamma^2_{s.p.} ,$$

where $\gamma^2_{\lambda.s.p.}$ are now defined as the single particle reduced widths of the fine structure fragments λ of the distribution. The prime means summation only over those states of a particular giant resonance.

The single particle spectroscopic factor can now be defined as the fraction of the total single particle strength which is contained in any single fragment λ:

$$S_\lambda \equiv \gamma^2_{\lambda.s.p.} / \gamma^2_{s.p.}$$

The spectroscopic factor for a bound state in the parent nucleus (with reduced widths $\gamma^2_{\lambda n}$) can be measured through a (d, p) reaction on (${}_Z A_N$), and

$$S_{dp} = \gamma^2_{\lambda n} / \gamma^2_{s.p.}$$

For an analog state

$$\gamma^2_{\lambda.s.p.} = \gamma^2_{\lambda n} = (2T_o + 1)\gamma^2_{Ap}.$$

The spectroscopic factor of the parent state is then

$$S_{dp} = (2T_o + 1)\gamma^2_{Ap} / \gamma^2_{s.p.} = (2T_o + 1)\Gamma_{Ap} / \Gamma_{s.p},$$

with the penetrability canceling. $\Gamma_{S.P.}$ is the single particle width of the p + C state and can be calculated theoretically. The spectroscopic factor thus provides a direct comparison of the (p,p) and (d, p) experimental results. Together with the energy relation between parent and analog states, this strength relation will be used in the identification of analog states.

Chapter III Experimental Equipment

1. Accelerator, Control System and Electrostatic Analyzer System

This experiment was performed with the Triangle Universities Nuclear Laboratory (TUNL) KN model Van de Graaff accelerator and associated high resolution feedback system. Originally the KN Van de Graaff accelerator was designed for operation up to 3MV on terminal; its voltage was limited mainly by sputtering effects due to an aluminum electrode accelerator tube. In 1982 an accelerator tube with stainless steel electrodes was installed and the accelerator was upgraded to reach higher energy (up to 4 MV terminal potential). The high resolution feedback system, consisting of an electrostatic analyzer and associated electronics, was originally developed by Park et al. (Park, 1958). In recent years the system has been upgraded to allow computer control, which enables the accumulation of excitation function data over a wide energy range without operator intervention and has resulted in increased reliability and ease of data acquisition (Westerfeldt 1988).

A schematic of the High Resolution Laboratory and control system is shown in Fig 3.1. A 100 Mhz radio frequency (RF) ion source inside the dome produces both protons and molecular HH^{+} ions by RF dissociation of the low pressure hydrogen gas within the source bottle. Both species are extracted from the ion source plasma by the positively biased "probe" electrode and focused by a negatively biased "focus" electrode. After extraction both ion species are accelerated through the tube and enter an analyzing magnet, where the proton (H^{+}) beam is bent 25° into a series of focusing and steering

Figure 3.1 Schematic of the High Resolution Laboratory and control system.

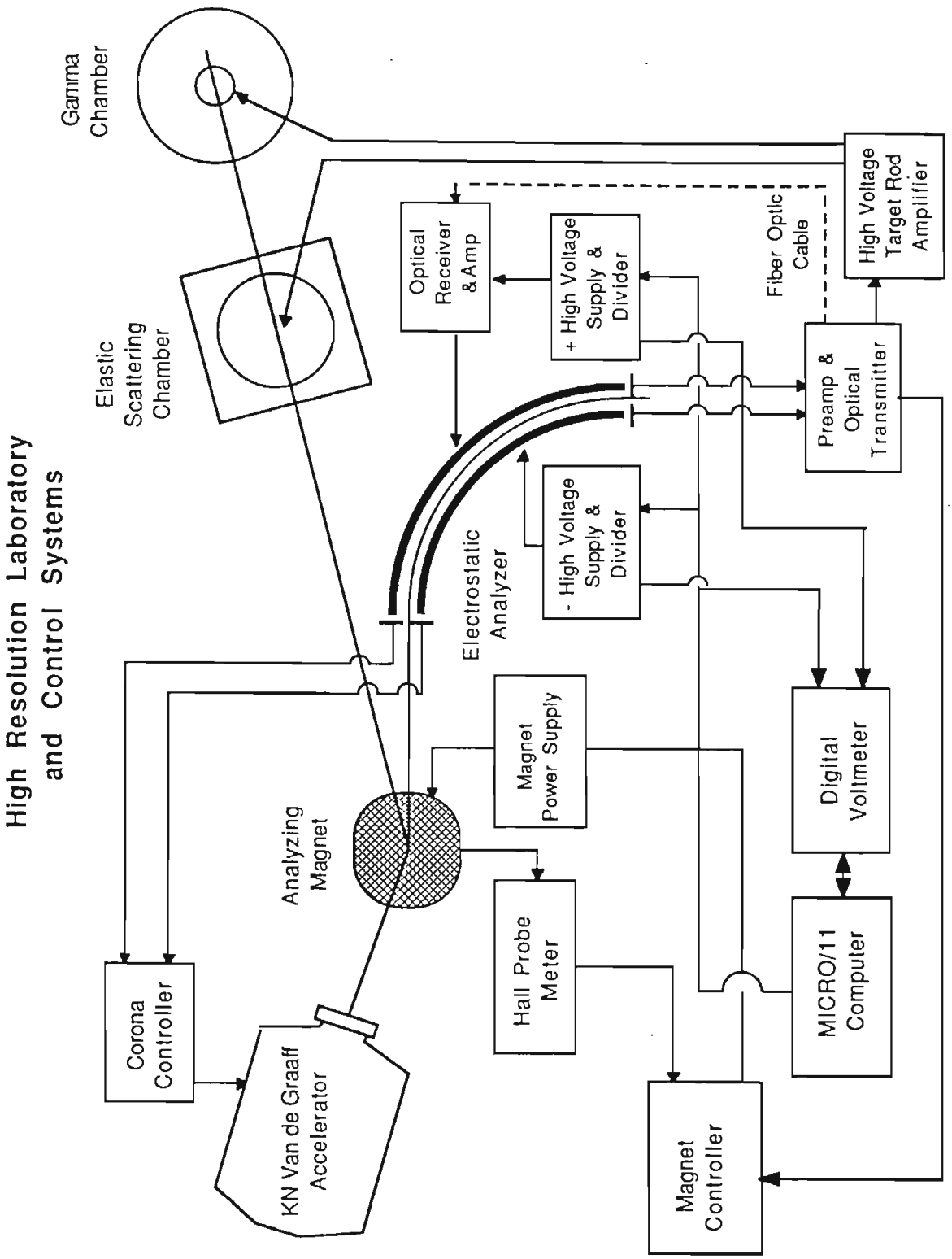
High Resolution Laboratory
and Control Systems
Gamma
Chamber
Elastic
Scattering
Chamber
Optical
Receiver
&Amp
+ High Voltage
Supply &
Divider
Fiber Optic
Cable
High Voltage
Target Rod
Amplifier
Preamp &
Optical
Transmitter
- High Voltage
Supply &
Divider
Electrostatic
Analyzer
Magnet
Power Supply
Digital
Voltmeter
Analyzing
Magnet
Hall Probe
Meter
MICRO/11
Computer
Corona
Controller
KN Van de Graaff
Accelerator
Magnet
Controller

magnets before entering the scattering chamber, while the molecular (HH^+) beam is deflected 17° towards the electrostatic analyzer. In front of the analyzer are located a pair of vertical slits which monitor the position of the HH^+ beam. Accelerator voltage fluctuations cause a change in the deflection angle of the beam in the magnet, and thus change the position of the beam spot on the slits. This results in a difference in the amount of beam current intercepted by each slit. In order to stabilize the terminal potential, the energy correction signal derived from this difference is fed back to the terminal, through several sharp corona needles located in the pressure tank just above the voltage dome. Because of the slow drift time of the ions from the needle to the terminal, this system provides correction only for large, slow (~10Hz) terminal voltage fluctuations, reducing the magnitude of these fluctuations to about 1 keV.

After passing through the corona slits (which are also the object slits of the analyzer), the HH^+ beam enters the electrostatic analyzer, a central component in the high resolution system. The analyzer consists of two metal plates curved in 90° arcs with a gap separation of 4.5 mm. These plates are biased with equal and opposite high voltages provided by a pair of programmable Bertan power supplies. These power supplies are controlled by a Fluke digital voltmeter which is in turn controlled by a PDP-11 microprocessor. Controlling the voltage on the two plates allows a beam with the proper energy (proportional to the plate voltage) to pass completely through the analyzer. The proportionality constant, determined by the geometry, for this analyzer gives a 1 volt to 111 eV ratio. A beam with the proper energy follows a trajectory through the ESA, emerges from the analyzer and strikes another pair of slits. If the energy of the beam changes, then the radius of the ion trajectory in the analyzer also changes, causing the HH^+ beam to move back and forth across the exit slits. Since the electrostatic field in the analyzer is perpendicular to the HH^+ beam trajectory, the analyzer does not change the beam energy and the proton energy fluctuations have the same time dependence as the molecular beam. Monitoring the difference signal from the exit slits therefore provides a very accu-

rate measurement of the energy fluctuations of the proton beam which is used to perform experiments. This difference signal is amplified by 111 and then sent to the target rod, which is biased to 3 KV DC to decelerate or accelerate the protons (depending on the sign of the signal) before they interact with the target nucleus. This signal is also fed back to the outer plate of the analyzer to keep the beam centered in the analyzer. Finally, the signal is sent back to the magnet controller through a low pass filter to achieve automatic control of the magnetic field and (via the corona feedback circuit), the accelerator voltage. This system produces a nearly monoenergetic proton beam on target. For thin film targets the system is capable of an overall resolution of 300-400 eV, with a long term energy drift of about 30 eV/ hour at $E_p = 2.045$ MeV .

3.2. Scattering Chamber and Detectors

A top view of the scattering chamber and detector placement is shown in Figure 3.2. The proton beam enters the chamber after being focused to a diameter of approximately 0.125 inch by a combination of collimators and steering and focusing elements in the beam line. After the beam hits the target, located in the center of the chamber, the majority of the protons pass through the target without interacting before they are collected by a Faraday cup placed at the end of the chamber. In front of the Faraday cup a plate biased at -90 V DC is positioned to prevent secondary electron emission from the cup. The targets are mounted on a sliding rod which holds up to four targets and a tuning ring. Since the high voltage signal from the analyzer is applied to the target rod during data acquisition, the target rod is electrically isolated from all grounds. Typical beam currents are 4-5 μA with less than 20 nA on the tuning ring. The chamber is also electrically isolated from the beam line and is connected to a clean ground. To maintain a vacuum of 1 μTorr during the experiment, the chamber is equipped with a diffusion pump and freon baffle. A cold trap surrounding the target rod above the beam is filled with liquid nitro-

gen to reduce the pressure locally and to trap hydrocarbons backstreaming from the diffusion pump.

Six surface barrier silicon detectors were used to observe the protons. These detectors were placed at 90°, 108°, 127°, 145°, 150°, and 165° relative to the beam direction. A collimation assembly was mounted in front of each detector to limit the number of counts from secondary scattering. The collimation and location of each detector was adjusted such that each detector counted approximately the same number of particles from Rutherford scattering. The solid angles for the detectors were 90° -- 1.19 msr, 108°-- 2.00 msr, 127° -- 3.00 msr, 145° -- 3.88 msr, 150° -- 4.06 msr, 165° -- 4.23 msr. The target was rotated 25° with respect to the beam to enable all of the detectors to view the target surface.

3.3. Electronics, Data Acquisition and XSYS

The electronic data acquisition system consists of several standard NIM and Computer Automated Measurements and Control (CAMAC) modules, a microprogrammable Branch Driver (MBD) and a VAX 11/750 computer, and is supported by a data acquisition and processing software system XSYS developed at TUNL (King 1981). Figure 3.3 shows the block diagram of the electronics.

A charged particle scattered from the target is detected by a surface barrier detector. A pulse is generated which is proportional to the energy of the particle. This pulse is sent through a preamplifier and a linear amplifier to form two well-shaped signals, the bipolar and unipolar signals. The bipolar signal is used to discriminate against carbon scattering events, which if left in the spectrum cause pileup peaks and broaden the peaks of interest, as well as increase the dead time of the data acquisition system. The bipolar signal is split into two signals. One of these signals is sent to a TSCA, the output of which is connected to the gate of gated SCA. The TSCA is operated in window mode with a window

Figure 3.2 Top view of the HRL charged particle scattering chamber.

Charged Particle Scattering Chamber

(Top View)

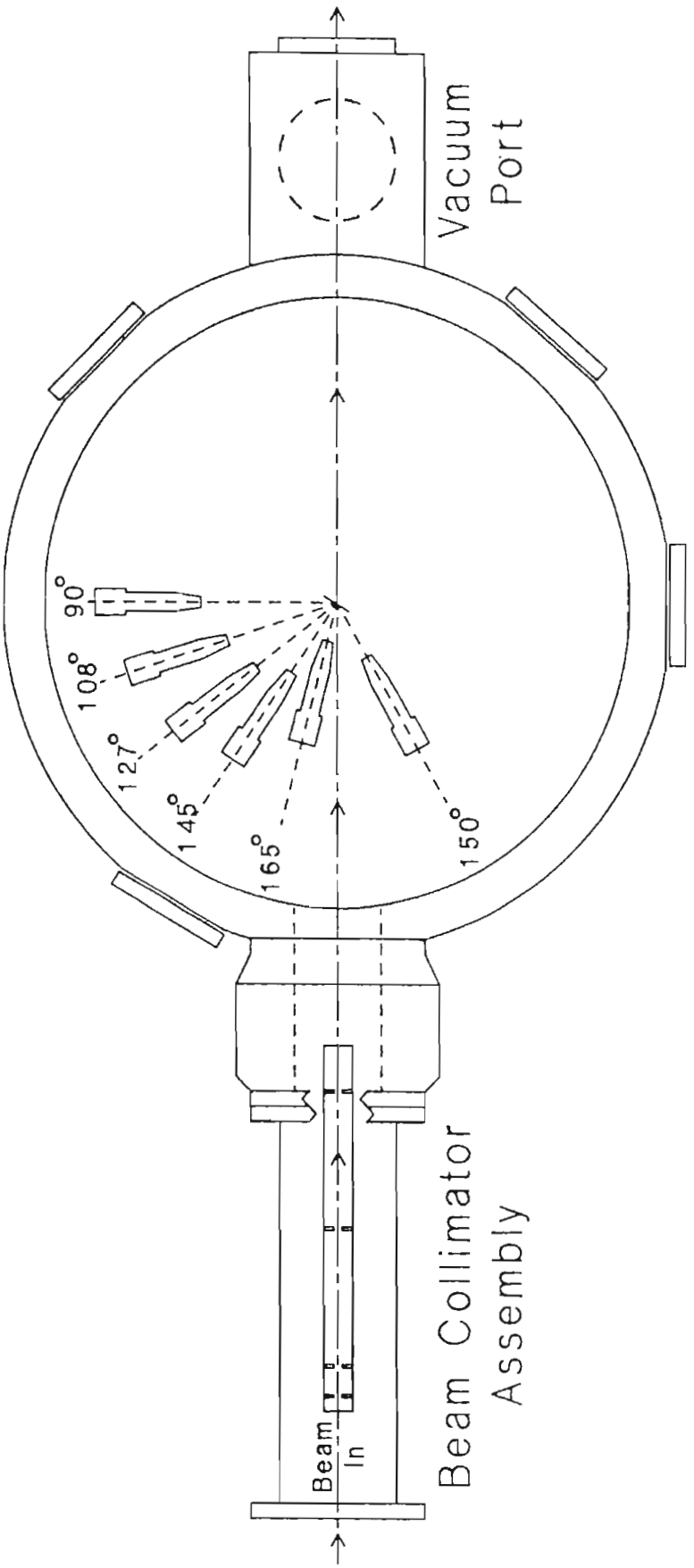

Figure 3.3 Block diagram of HRL data acquation electronics.

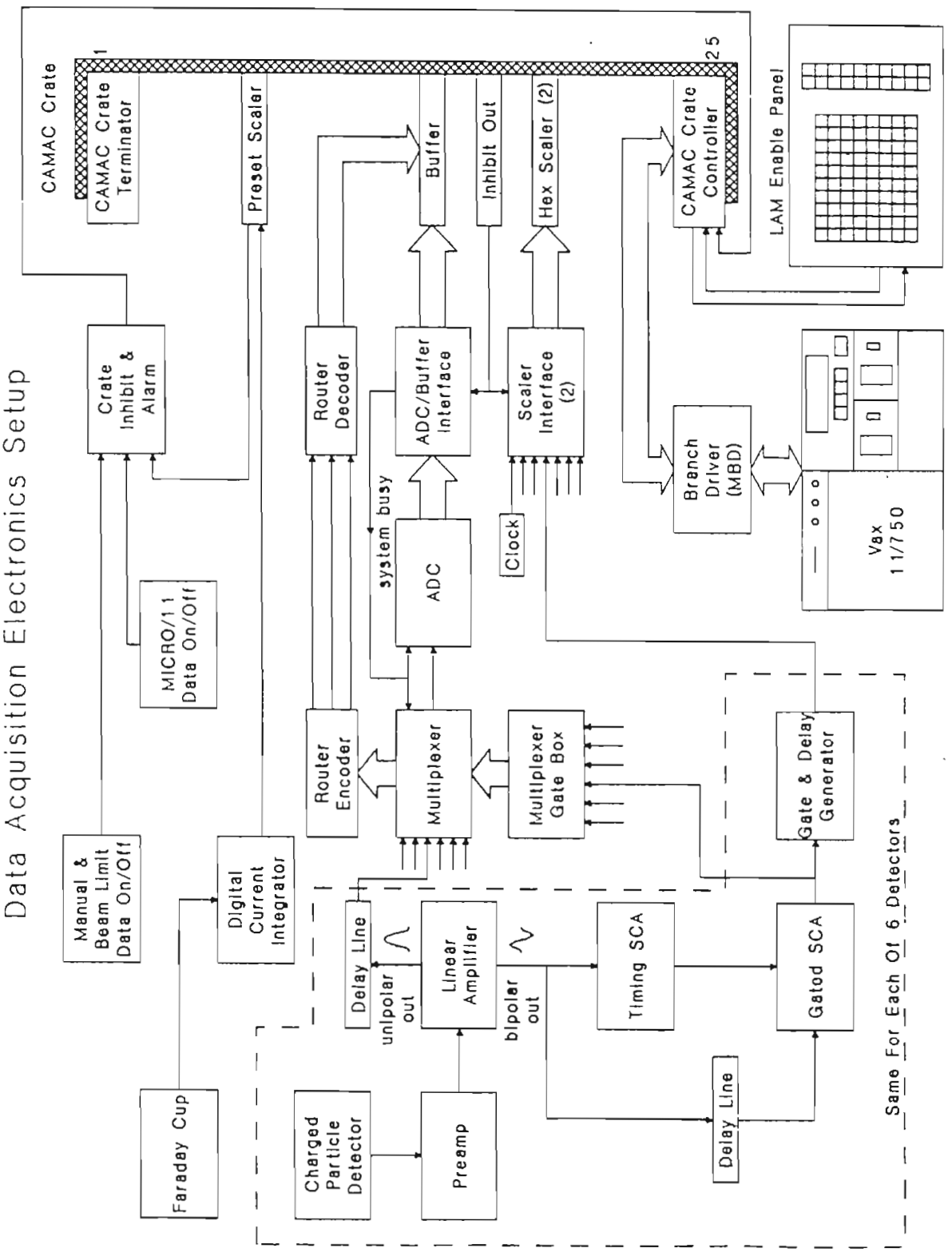
Data Acquisition Electronics Setup
CAMAC Crate
CAMAC Crate Terminator
1
25
Preset Scaler
Buffer
Inhibit Out
Hex Scaler (2)
CAMAC Crate Controller
LAM Enable Panel
Crate Inhibit & Alarm
Router Decoder
ADC/Buffer Interface
Scaler Interface (2)
Branch Driver (MBD)
Vax 11/750
MICRO/11 Data On/Off
system busy
ADC
Clock
Manual & Beam Limit Data On/Off
Digital Current Integrator
Router Encoder
Multiplexer
Multiplexer Gate Box
Gate & Delay Generator
Delay Line
unipolar out
Linear Amplifier
bipolar out
Timing SCA
Gated SCA
Faraday Cup
Charged Particle Detector
Preamp
Delay Line
Same For Each Of 6 Detectors

set on the carbon peak to allow only carbon pulses to pass through. The other bipolar signal, after a 900 ns delay, is routed to the gated SCA, which is then connected to the gate of the multiplexer. The gated SCA is operated in integral and anticoincidence mode; if a carbon event is determined to have taken place then the TSCA inhibits the gated SCA, and no signal is sent to the multiplexer (thus inhibiting the multiplexer). If the event is a non-carbon event (no output from the TSCA), then the gated SCA will generate a short pulse which enables the multiplexer (allowing the processing of the unipolar signal). This pulse is also sent to a gate and delay generator which produces a short logic pulse. These signals are counted by a CAMAC scaler. The dead time of the data acquisition system can be computed by comparing the counts in the spectrum with the scaler counts.

The unipolar signal is delayed 900 ns, allowing the processing of the bipolar signal which is sent to multiplexer. When activated, the multiplexer processes the unipolar signal, and this output is sent to the ADC to be digitized. The routing address, which indicates from which detector the signal originates, is encoded by the multiplexer into a 3-bit signal and is sent along with the output from the multiplexer.

After conversion by the ADC the converted signal and the decoded routing word are accumulated in a CAMAC Borer Buffer Module, where they are encoded again into a 16-bit word to await transfer to the MBD and finally to the VAX. There are two buffers (512-words each) in the Borer Buffer Module. When one of the buffers is full the module provides a Look-at-Me (LAM) signal to the Crate Controller (CC) for data transferring. Meanwhile, incoming signals from the ADC are stored in the other buffer, allowing continuous data processing. In this way very high counting rates can be processed.

Data collection is controlled by the preset scaler. After passing through the target the proton beam is stopped in a Faraday cup, which is connected to a current integrator. The output of the integrator is connected to a preset scaler which, when the amount of charge reaches the preset value, inhibits the data acquisition and signals to the VAX that the data run is finished. Several other inhibiter circuits are used to ensure that the system

is operating under acceptable conditions. The output of the current integrator is also connected to a current meter with lower and upper limit switches. Data acquisition is halted if the beam current is outside the lower and upper limits. The beam energy is monitored using Digital Voltmeter (DVM) by the microprocessor, which is connected to the analyzer plates. If the voltage changes on the analyzer plates corresponds to an energy variation of more than 10 eV (0.09V) from the selected energy, then the microprocessor inhibits the data collection.

XSYS is the TUNL data acquisition and analysis system for VAX computers. It was developed at TUNL in 1981 (King 1981); Roberson and Gould provided the latest overview of XSYS (Roberson, 1985). The data acquisition programs and procedures developed for the High Resolution Laboratory (HRL) are discussed in detail by Bull (1989). In this dissertation XSYS will be discussed only briefly.

Before beginning an experiment, the data acquisition system must first be initialized. This is performed by executing the command file HIRES, which contains all the commands necessary to set up the data acquisition system and to start data accumulation. HIRES first clears all the XSYS flags and deallocates the old data areas before choosing the new data areas. Data areas include areas for detector spectra, yield curves and areas for run numbers and beam energies. HIRES also defines 19 gates for each spectrum data area, enabling the yield to be determined on-line.

After establishing the data areas and gates, the HIRES executes another command procedure, HIRESON, to begin data acquisition. HIRESON first allocates the VAX port TTa4. This connects the microprocessor (which controls the voltage of the analyzer plates) to the VAX, enabling the VAX to communicate the desired energy to the PDP. HIRESON then down loads the General Data Acquisition Program (GDAP) into the MBD. GDAP is a collection of routines, written in the MBD's assembly language, which run on the MBD. This program handles all CAMAC functions. Next HIRESON installs a data acquisition subprocess using Buff.DAP as input, a scaler subprocess using

Sclr.DAP as input, and sets hibernating subprocesses and controls which will be started when preset is reached. Finally, before exiting, HIRESON executes command file BOXFILL to label all the boxes.

In addition to the experimenter's process, four subprocesses are used by the VAX for data acquisition, as shown in Figure 3.4. XSORT is a program written in FORTRAN which runs as a subprocess on the VAX. This process sorts the data from the ADC buffers and distributes them into the appropriate data areas. XSORT first opens a .DAP file (Buff.DAP) which has been installed by the HIRESON command file and reads in Event Analysis Language (EVAL) program name and the MBD channel number, which are needed by the EVAL compiler. The size of the VAX buffers, which is needed to determine the size and location of several areas within the buffer in VAX memory, is read next, followed by the initialization CNAF commands, each of which is sent to GDAP in the MBD to be executed immediately upon being read. The acronym CNAF stands for Crate number, module number, subaddress of the module and function code. These commands are executed by the MBD. Following these the BUF and LAM CNAFs are read. These latter commands are stored in the Channel Buffer instead of being executed immediately.

The second major part of XSORT consists of the Data Sort Loop. The MBD always remains in HALT unless a channel is activated. Either a LAM or a signal from the VAX can activate a channel. As mentioned before, the Borer Buffer Module connected to the ADC has two buffers. When one of the buffers is full it generates a LAM signal, which activates the MBD. In turn, the MBD interrupts the XSORT process, indicating that a buffer is ready to be sorted. For each LAM that occurs each of the internally stored CNAFs for the MBD channel is executed, and data are written to the VAX data buffer as requested by CNAFs. XSORT restarts the MBD, filling the other buffer in Borer Buffer Module, then calls the EVAL program to sort the full buffer (buffer 1). Finally XSORT resets buffer status and clears buffer word count, and this buffer is now ready for filling.

Figure 3.4 Block diagram of the data acquisition processes.

HRL Data Acquisition Processes

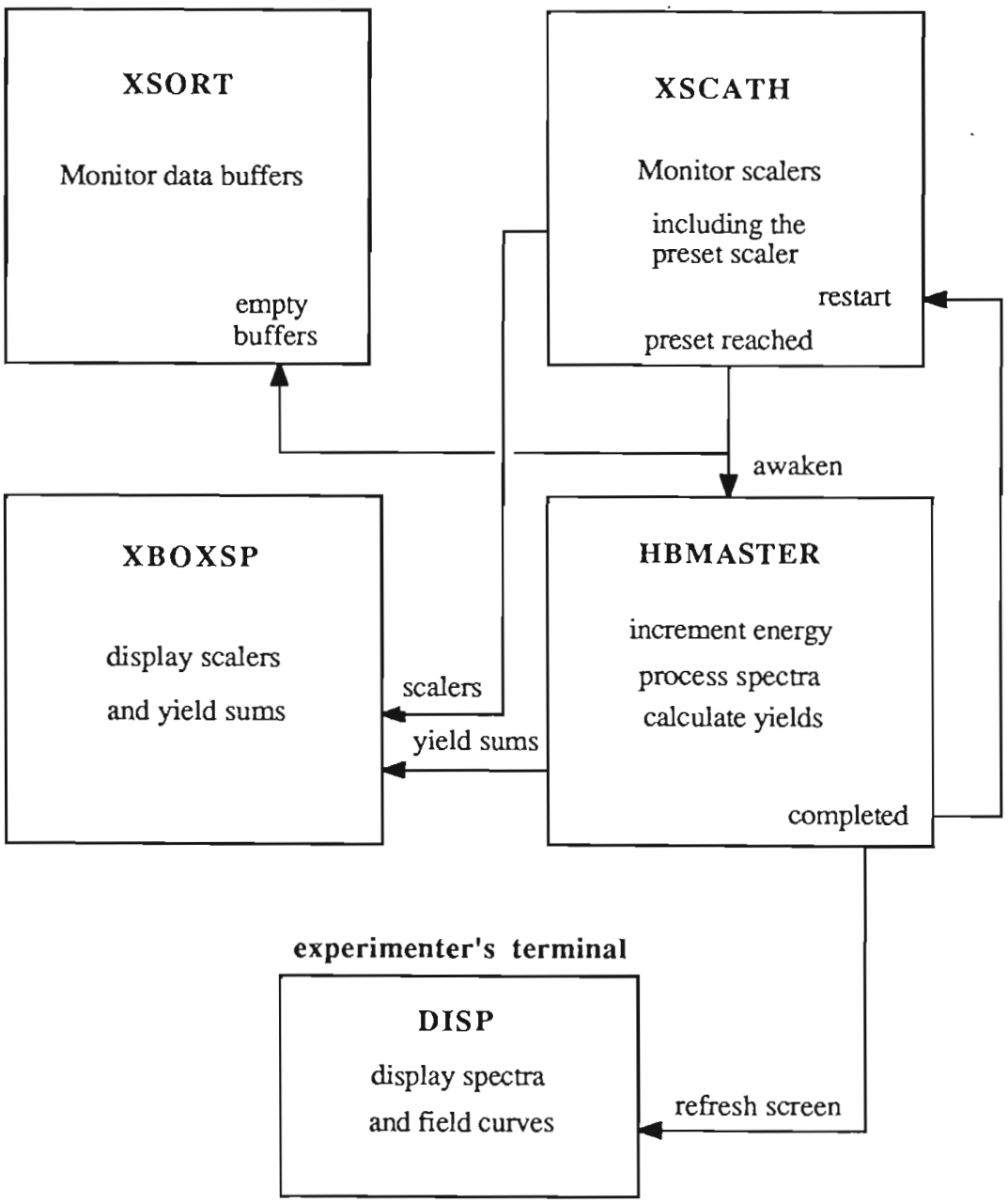

This loop is continuous until the run is stopped either by HAlt or by XSCAT. In that case XSORT instructs the MBD to flush the currently active buffer. XSORT then calls the EVAL to sort the flushed data and goes to sleep until the run has been started again.

XSCAT is another data acquisition subprocess. This subprocess monitors the CAMAC scaler modules and administers the scaler information on the VAX. In this experiment the preset scaler is connected to the current integrator. When this scaler reaches a predetermined value, XSCAT ends the data run by first inhibiting the CAMAC crate so that no more data is taken. XSCAT then signals XSORT through MBD to process the data still stored in the ADC buffer. XSCAT also notifies the VAX that the run has been completed and awakens an existing process (master process) from a hibernating state. When awakened, the master process first instructs the PDP to increase the energy of the proton beam by Estep by incrementing the analyzer plate voltage. Next the spectra, scalers and other information are dumped to tape to be processed during the off-line analysis. All of the windows are then checked to determine whether they should be shifted. For the purpose of online display the process also sums windows and, by calculating the dead time correction and subtracting background, calculates and stores the yield sums in the appropriate data area, along with the beam energy and run number. Finally, all the spectra and scalers are cleared and the data acquisition is restarted.

The fourth subprocess created for data acquisition is XBOXSP. This program displays current proton energy, run number, values of scalers, yield sums and dead time factors. XSYS also provides a graphic DISPlay package to display spectra and yield curves on the online display terminal.

3.4. Targets

Thin film targets prepared at TUNL with the vapor deposition method, using a high vacuum high current evaporator system, were used in this experiment. Commercially

available 5 $\mu g / cm^2$ carbon foils were floated on the target rings to serve as target support. The enriched isotope (99.1 %) ^{48}Ti was available as an oxide compound. First this compound was reduced using hydrogen as the reducing agent.

The white $^{48}TiO_2$ powder was placed in an open Molybdenum boat coated with Aluminum Oxide. The boat was put into a chamber which was evacuated and then filled with hydrogen gas up to about 250 Torr. The Mo boat was then heated slowly. In principle, the higher the temperature, the more efficient the reduction process. However, because at high temperatures the powder has a tendency to jump out of the boat and because the temperature should remain below the melting point of the compound, the temperature was very carefully controlled. After the boat was heated for 20 minutes, the gas was pumped out and fresh hydrogen introduced. This procedure was repeated several times until the powder became black, indicating that it has been reduced to titanium.

The reduced isotope was then placed in an open Tantalum boat, which had been baked at a high temperature for 20-30 minutes to reduce the moisture content, and the titanium was evaporated onto target rings placed above the boat. Again the temperature was carefully controlled. A typical thickness for ^{48}Ti was 1.5 $\mu g / cm^2$. The thickness monitor inside the evaporation chamber was used during the evaporation procedure to provide an estimate of the thickness. The Rutherford cross section was also used to determine both the thickness of the ^{48}Ti and the thicknesses of all contaminants. Figure 3.5 shows a sample spectrum at 165° with the carbon peak electronically removed.

Figure 3.5 Charged particle spectrum from Ti target at 165°. The carbon scattering has been electronically removed.

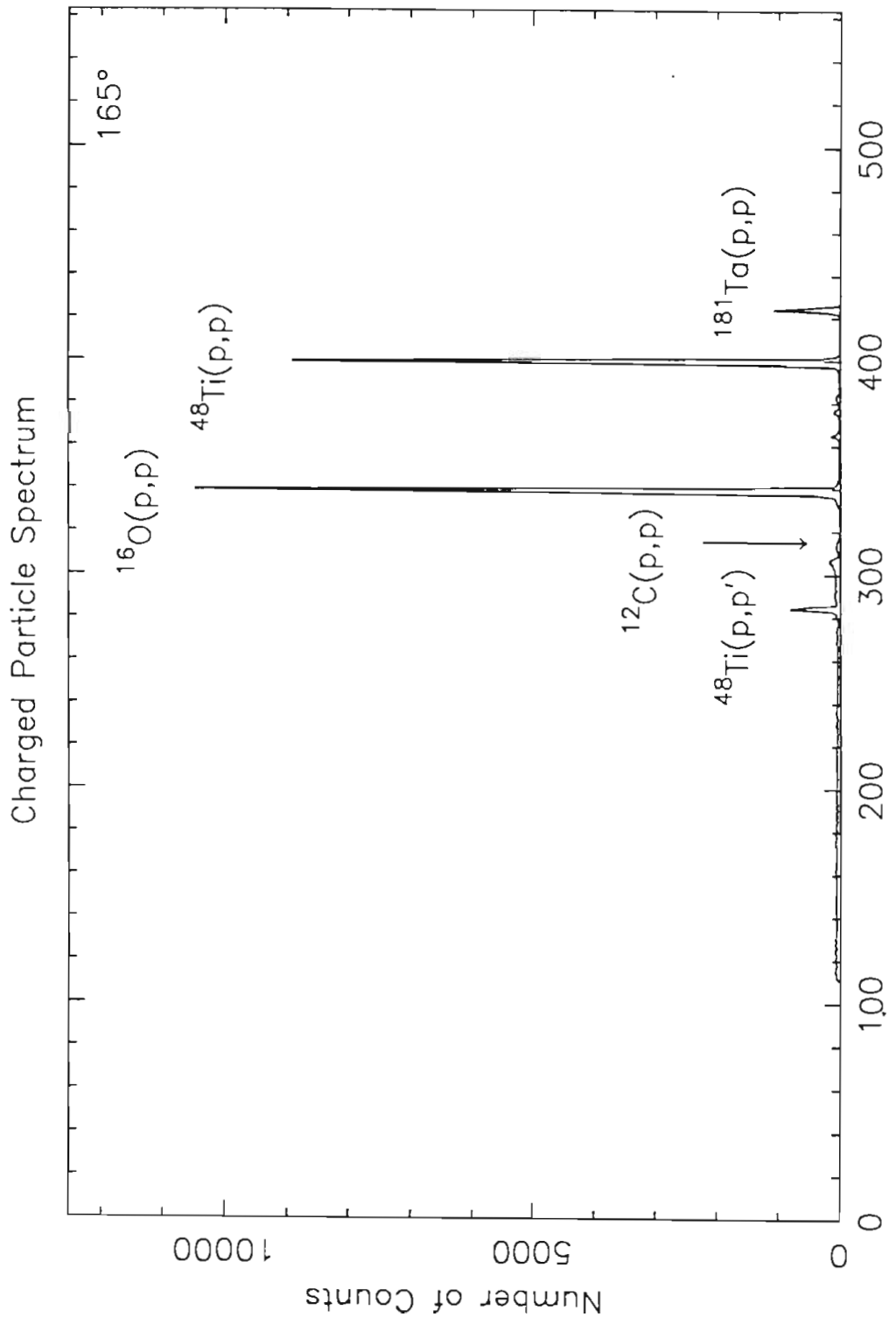
Charged Particle Spectrum
165°
^{16}O(p,p)
^{48}Ti(p,p)
^{12}C(p,p)
^{48}Ti(p,p')
^{181}Ta(p,p)
Number of Counts
0
5000
10000
0
100
200
300
400
500
Channel Number

Chapter IV Experimental Procedure

1. Data Acquisition

Excitation functions were measured in the energy range from E_p = 3.08 to 3.86 MeV. The reactions ^{48}Ti(p,p) and ^{48}Ti(p,p') were measured at six angles. The energy step was normally set to 100 eV to ensure observation of small resonances. An accumulated charge of 200 μC of protons on targets containing 1-2 μg/cm^2 of Ti, typically resulted in about 5,000 - 10,000 counts in the elastic peak in each of the spectra, or < 2 % counting statistics. The gain of each amplifier was adjusted to give the elastic peak an appropriate amplitude and to separate the inelastic peak from the carbon peak. The window of the TSCA was set to gate the carbon peak out of the spectrum. The spectrum was calibrated using two known peaks in the spectrum, and the windows for the yield determination were defined.

Before data were measured, all electronics were warmed up for several hours. The voltage of the accelerator was increased slowly and carefully to reach the initial energy. The energy of the accelerator was calibrated using a secondary standard ^{56} Fe (p,p) resonance at E_p= 3.2387 MeV.

Before the beam was tuned into the electrostatic analyzer, the analyzer plates were set to the correct voltage. This was accomplished by first connecting the computer terminal in the laboratory to the PDP and executing the command file SETUP on the PDP. This file zeroed the DACs which control the plate voltage, initialized the Fluke Digital Voltmeter and regulated the analyzer plate voltage to steer the beam with the desired energy through the analyzer. Once the analyzer plates were at the desired voltage the terminal was switched back to the VAX, which also connected the PDP to the VAX, enabling

the VAX to communicate with the PDP.

The data were collected and stored on magnetic tape. Excitation functions were generated at all six angles for the entire energy range E_p= 3.08 to 3.86 MeV for both ^{48}Ti(p,p) and ^{48}Ti(p,p'). The yields were obtained by summing the number of counts contained in the elastic and inelastic scattering peaks in the spectra, and were listed in a file suitable for the R-matrix program MULTI6.

2. Data Analysis

The data were analyzed with the multilevel, multichannel R-matrix formalism. The R-matrix theory was first coded in FORTRAN for computer usage by Sellin (1969) and has been extended and revised over the years. The latest version was described by Nelson (1983). Search procedures are impractical for the multilevel problem with the available computing facilities. Therefore a systematic trial and error procedure was adopted to fit the experimental data. Because the spin of the target is zero in this experiment, there is only one entrance channel, but there are several exit channels (this is shown in Figure 4.1). A set of parameters for each of the energy levels is needed as the input of MULTI6. These parameters are: resonance energy E_λ, total angular momentum of the compound state J and its parity π, exit channel spin s', exit orbital angular momentum l' and laboratory width Γ. As will be discussed later, for well separated and fairly strong resonances, the l-value and thus the parity are normally apparent by inspection. Values for J, $\Gamma(\Gamma_p,\Gamma_{p'},...)$ are assumed. The laboratory width Γ assumed is converted to a reduced width $\gamma_p^2 = \Gamma_p / 2P$, where P is the Coulomb penetrability $P=kr / (F^2 + G^2) \mid_r$ evaluated at $r = r_o(1 + A^{\frac{1}{3}})\, fm$ with r_o= 1.25 fm. After each execution of a MULTI6 calculation the computed theoretical cross sections are compared visually with the experimental yield curves (which have been normalized to the theoretical cross sections), and adjustments are made in the resonance parameters. The process is repeated until a satis-

Figure 4.1 Angular momentum coupling scheme for the ^{48}Ti(p,p) and ^{48}Ti(p,p') reactions in the channel spin representation.

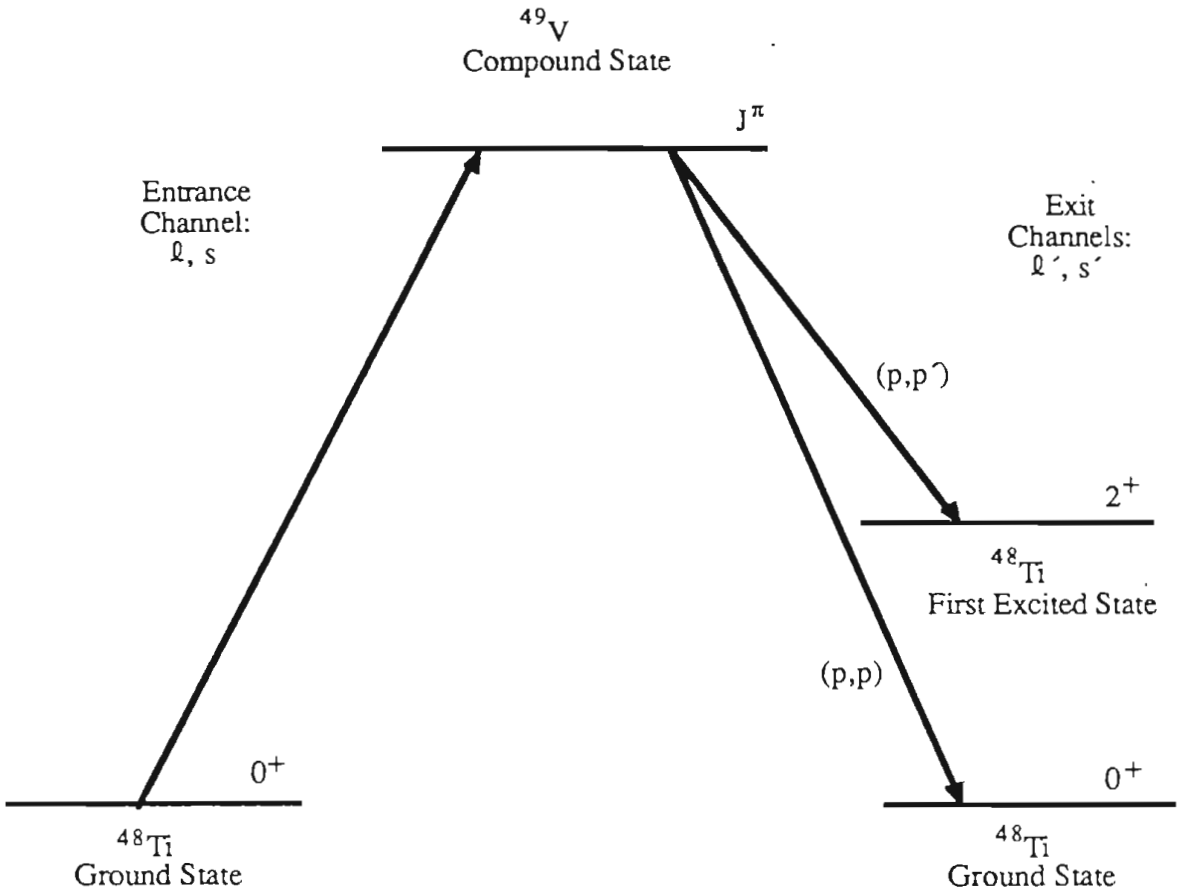

$$J = \ell' \oplus s'$$

$$\pi = (-1)^{\ell}$$

Elastic Exit Channel Spin: $s_p' = 0 \oplus \frac{1}{2} = \frac{1}{2}$

Inelastic Exit Channel Spin: $s_p' = 2 \oplus \frac{1}{2} = \frac{3}{2}, \frac{5}{2}$

Exit Orbital Angular Momentum $\ell' = 0, 1, 2, \ldots$

factory visua fit is obtained. The final resonance parameters are then used to construct level sequences.

As discussed in chapter II, the boundary condition must be fixed in order to obtain a complete set of formal states in the internal region. Throughout our analysis, the boundary condition is set equal to the shift function at the resonance energy. The penetrability is another factor which must be considered. As shown in Figure 4.2, the penetrability decreases rapidly with l. In general the limit of observability due to penetrability effects is approximately 1%; thus the viable incident energy range is above 3.5 MeV for $l' = 3$ (f-wave resonances). In practice only resonances with $l' < 4$ need be considered.

3. Selection of Sequences

One of the primary motivations of this study was the determination of level densities for all of the observed level sequences in the ^{49}V system. A level sequence is a set of energy levels all of which have the same good quantum numbers: the angular momentum J and parity π. In the selection of a level sequence there are some physical and experimental features which must be considered to ensure a meaningful and accurate level density determination.

3.1 Spin Assignments

A key factor for successful analysis of elastic scattering data is that the bombarding energy be well below the top of the Coulomb barrier; this condition was satisfied in the present experiment. The strong Coulomb effect permits easy identification of l-values and makes detailed analysis feasible; it also leads to rather sharp, narrow resonances. The expression for the differential cross section (Eq. 2.4.17) contains three terms, one of which is the interference between resonance scattering and Coulomb scattering. This in-

Figure 4.2 Exit penetrability versus energy for the ^{48}Ti(p,p) reaction.

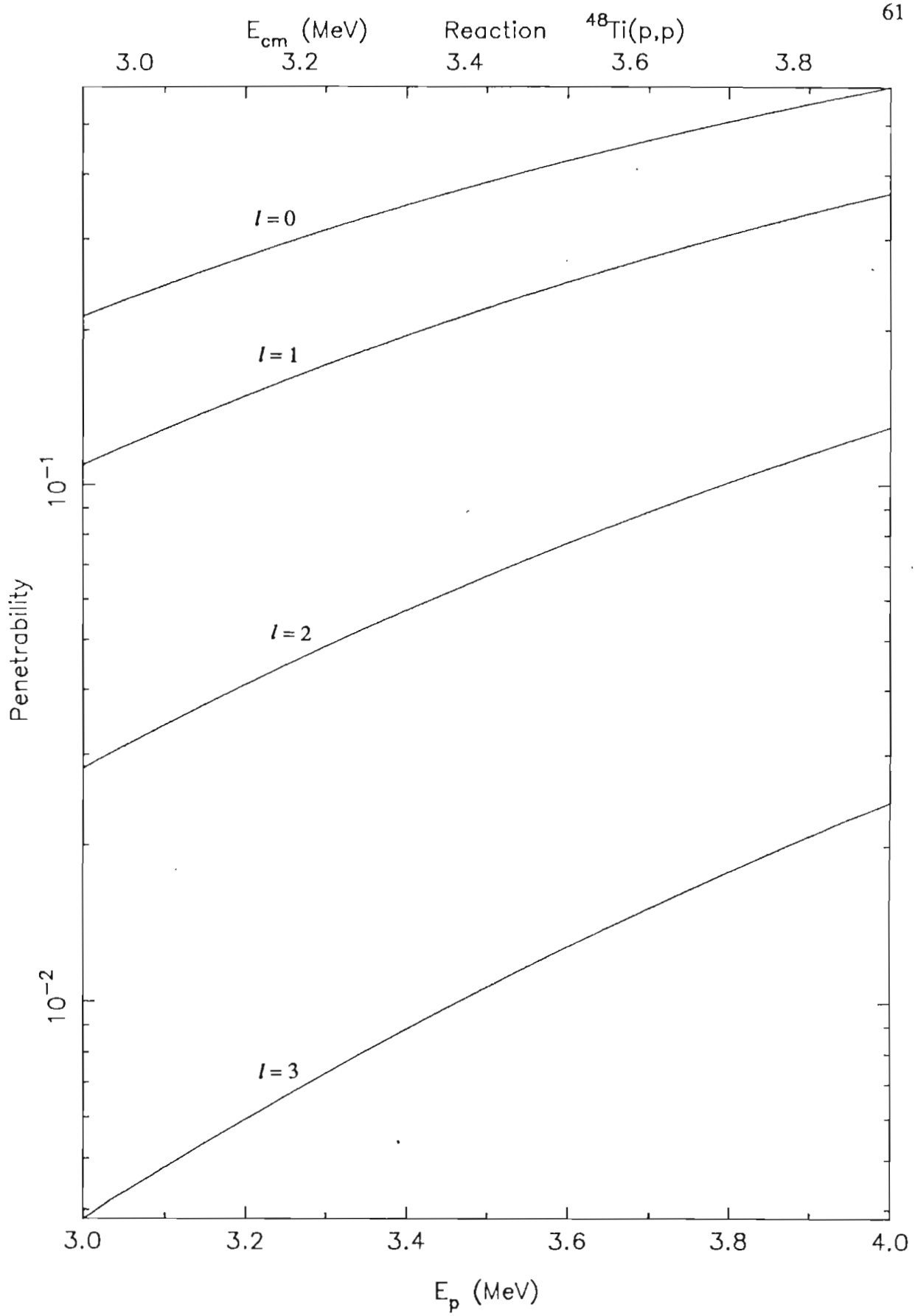
E_cm (MeV)
Reaction ⁴⁸Ti(p,p)
3.0
3.2
3.4
3.6
3.8
l = 0
l = 1
l = 2
l = 3
Penetrability
10⁻¹
10⁻²
3.0
3.2
3.4
3.6
3.8
4.0
E_p (MeV)

terference leads to quite different characteristic shapes at different angles for resonances of different l-values. These shapes can be used to determine the l-value by inspection. In Figure 4.3 resonance shapes are shown for resonances of different J^{π} at various scattering angles (with $\Gamma_p=\Gamma$ = 50 eV and energy resolution Δ =350 eV). At 90° all positive parity states (l = even) show a downward trend, while all negative parity states (l = odd) have an upward trend. The states with l = 0 are easily distinguished from those of l = 1 or 2. Assignments are almost always unambiguous for $s_{1/2}$ resonances. However, there is often a serious problem in distinguishing between the J-value l+1/2 and l -1/2 for narrow resonances. Since this distinction is crucial for determination of the level density, efforts have been made to remove or at least reduce the ambiguity. It is apparent from Figure 4.3 that for fairly strong resonances, there are some differences between $p_{1/2}$ and $p_{3/2}$ or between $d_{3/2}$ and $d_{5/2}$ states. The differences in the shapes for $p_{1/2}$ and $p_{3/2}$ resonances are greater at $\theta = 105^{\circ}$ and $\theta = 165^{\circ}$. The heights of the $d_{3/2}$ and $d_{5/2}$ resonances can be used to distinguish between J = 3/2 and 5/2. For example, if one assigns a $d_{5/2}$ state as $d_{3/2}$ and fits the data well at 90°, the fit will be too low at 165°. Thus careful comparison between the fit and the data helps to remove many of the ambiguities. However, in practice, this difference is small for relatively weak resonances. In this case the inelastic scattering data play an important role in the assignments. The inelastic angular distributions for the various outgoing l'-values and channel spins are shown in Figure 4.4. The angular distribution for $p_{3/2}$ is anisotropic, while the angular distribution for $p_{1/2}$ (not shown in the figure) is isotropic. Thus if the p-wave resonance has an anisotropic angular distribution, the resonance can be uniquely assigned J = 3/2. In the d-wave resonance case, the situation is more complicated, but the angular distributions are still helpful in removing some of the uncertainties in J assignments.

Another factor which may prevent an accurate determination of J is level-level interference. The high level density in ^{49}V makes it suitable for statistical study, but this high level density also causes interference between levels, which can change the reso-

Figure 4.3 J^{π} resonance shapes for various scattering angles.

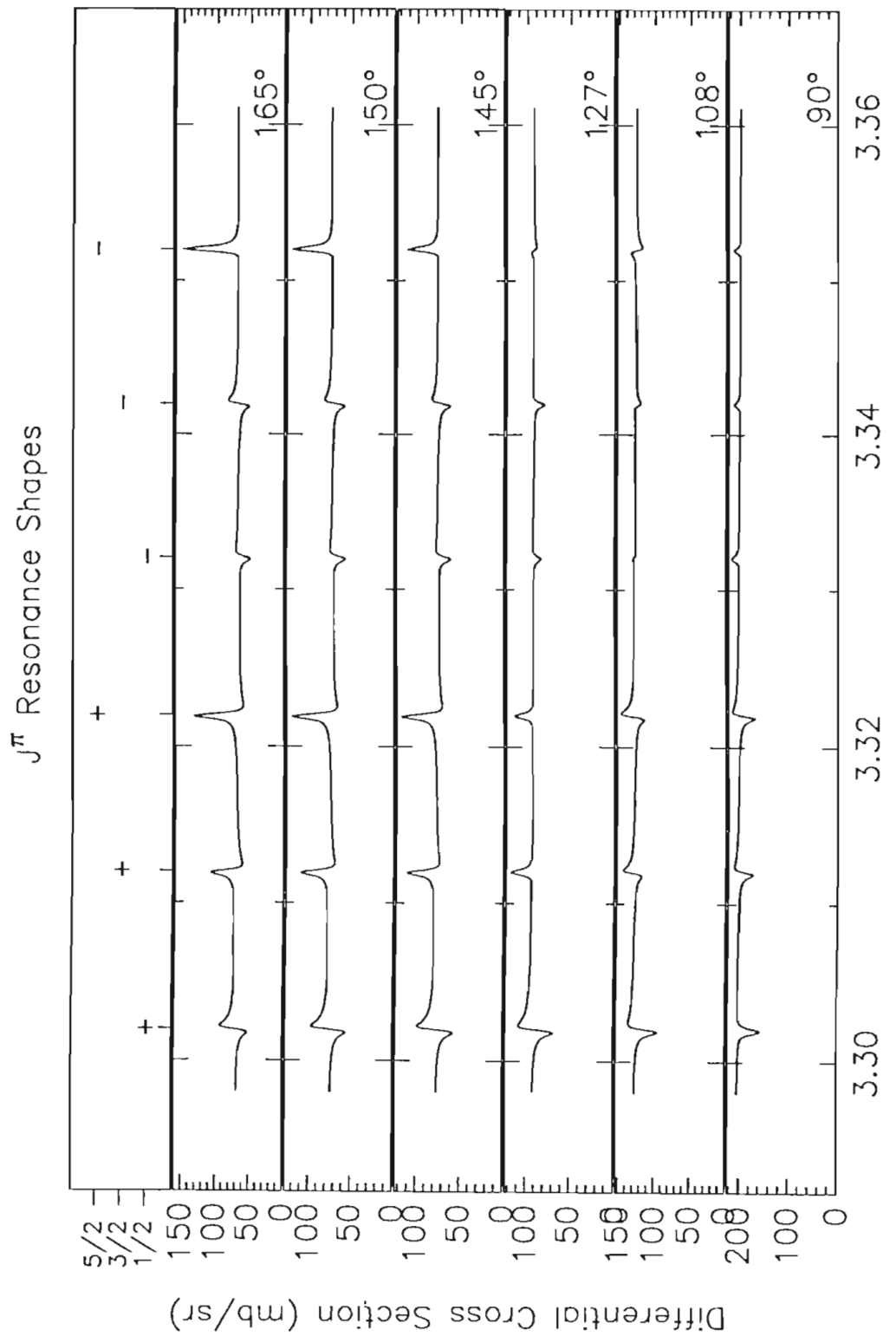
J^{π} Resonance Shapes
5/2
3/2
1/2
+
+
−
+
−
−
165°
150°
145°
127°
108°
90°
Differential Cross Section (mb/sr)
Incident Proton Energy (MeV)
3.30
3.32
3.34
3.36

Figure 4.4 Angular distributions for inelastically scattered protons.

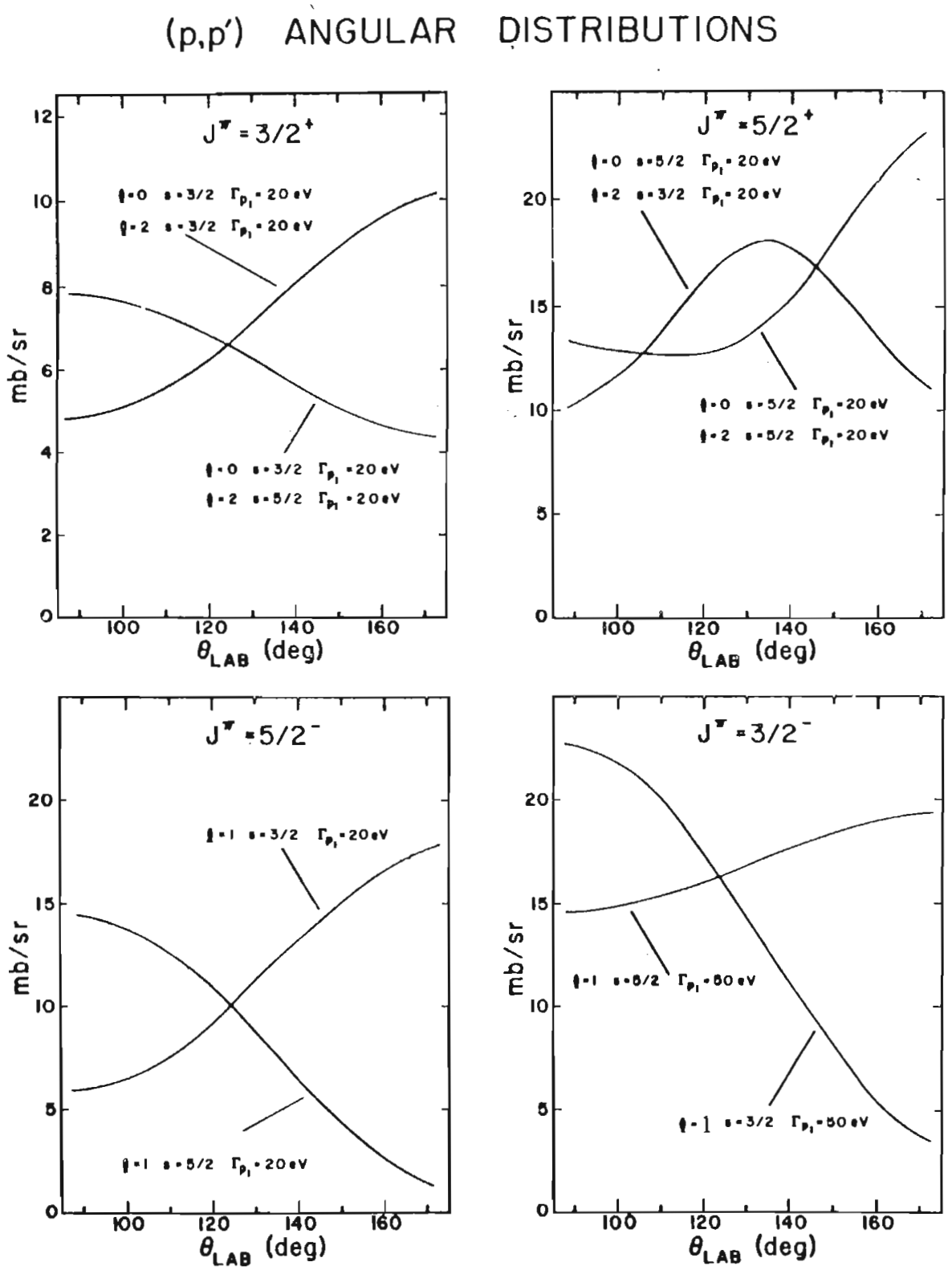
(p,p') ANGULAR DISTRIBUTIONS
J^π = 3/2^+
ℓ=0 s=3/2 Γ_p1 = 20 eV
ℓ=2 s=3/2 Γ_p1 = 20 eV
ℓ=0 s=3/2 Γ_p1 = 20 eV
ℓ=2 s=5/2 Γ_p1 = 20 eV
J^π = 5/2^+
ℓ=0 s=5/2 Γ_p1 = 20 eV
ℓ=2 s=3/2 Γ_p1 = 20 eV
ℓ=0 s=5/2 Γ_p1 = 20 eV
ℓ=2 s=5/2 Γ_p1 = 20 eV
J^π = 5/2^-
ℓ=1 s=3/2 Γ_p1 = 20 eV
ℓ=1 s=5/2 Γ_p1 = 20 eV
J^π = 3/2^-
ℓ=1 s=5/2 Γ_p1 = 50 eV
ℓ=1 s=3/2 Γ_p1 = 50 eV
mb/sr
θ_LAB (deg)

nance shapes. Figure 4.5 shows an example of how the interference effects change the resonance shapes.

In summary, there are many factors which may cause ambiguities in the determination of the J-values for p- and d- wave resonances. However, one can minimize the ambiguity in the spin assignments by fitting both elastic and inelastic scattering. The most accurate way to determine the J-value is with the (p,p'γ) reaction.

3.2. Experimental Concerns

In an ideal sequence one would observe all of the resonances. In practice, because the energy resolution is finite, the weakest resonances may not be observed. With 350 eV resolution, we observe resonances with laboratory widths as small as 5 eV. This can be understood as follows: consider a Breit-Wigner resonance with resonance width Γ and Gaussian resolution function (with FWHM Δ). Following the results of Feld(1951), the ratio Γ/Δ can be plotted as a function of the maximum experimental cross section $\sigma_m^{\,e}$ (neglecting interference effects) divided by the maximum theoretical cross section $\sigma_m^{\,t}$. For small Γ/Δ, $\sigma_m^{\,e} \approx 1.5\,(\Gamma/\Delta)\,\sigma_m^{\,t}$. The unbound resonance cross section $\sigma_m^{\,t}$ at 3.5 MeV is

$$\frac{\lambda^2}{(2\pi)^2} = \frac{1}{k^2} = \left(\frac{\hbar}{2\pi}\right)^2 \frac{1}{2ME} \approx \left(\frac{\hbar c}{2\pi}\right)^2 \frac{1}{2m_p c^2 E} = \frac{(197.3)^2}{2 \times 937 \times 3.5} \approx 60\, mb/sr$$

which gives

$$\sigma_m^{\,e} = 90\ (\Gamma/\Delta)\ mb/sr$$

The Coulomb cross section at this energy, on the other hand, is about 90 *mb/sr* at 165° (see Figure 4.3). Thus the ratio of the resonance term to the Coulomb term is roughly Γ/Δ. For 5 eV resonance width and 350 eV resolution width this effect is of order one percent effect. Since the point scatter in the data is only ~1%, it is reasonable to observe such weak resonances.

Figure 4.5 Interference effects on resonance shapes for $3/2^+$ and $1/2^+$ states. The values of the energy separation for the $3/2^+$ (Γ_{lab} = 25 eV) resonance relative to the $1/2^+$ (Γ_{lab} = 100 eV) resonance are: -400, -200, -100, 100, 200, 400 eV respectively from left to right.

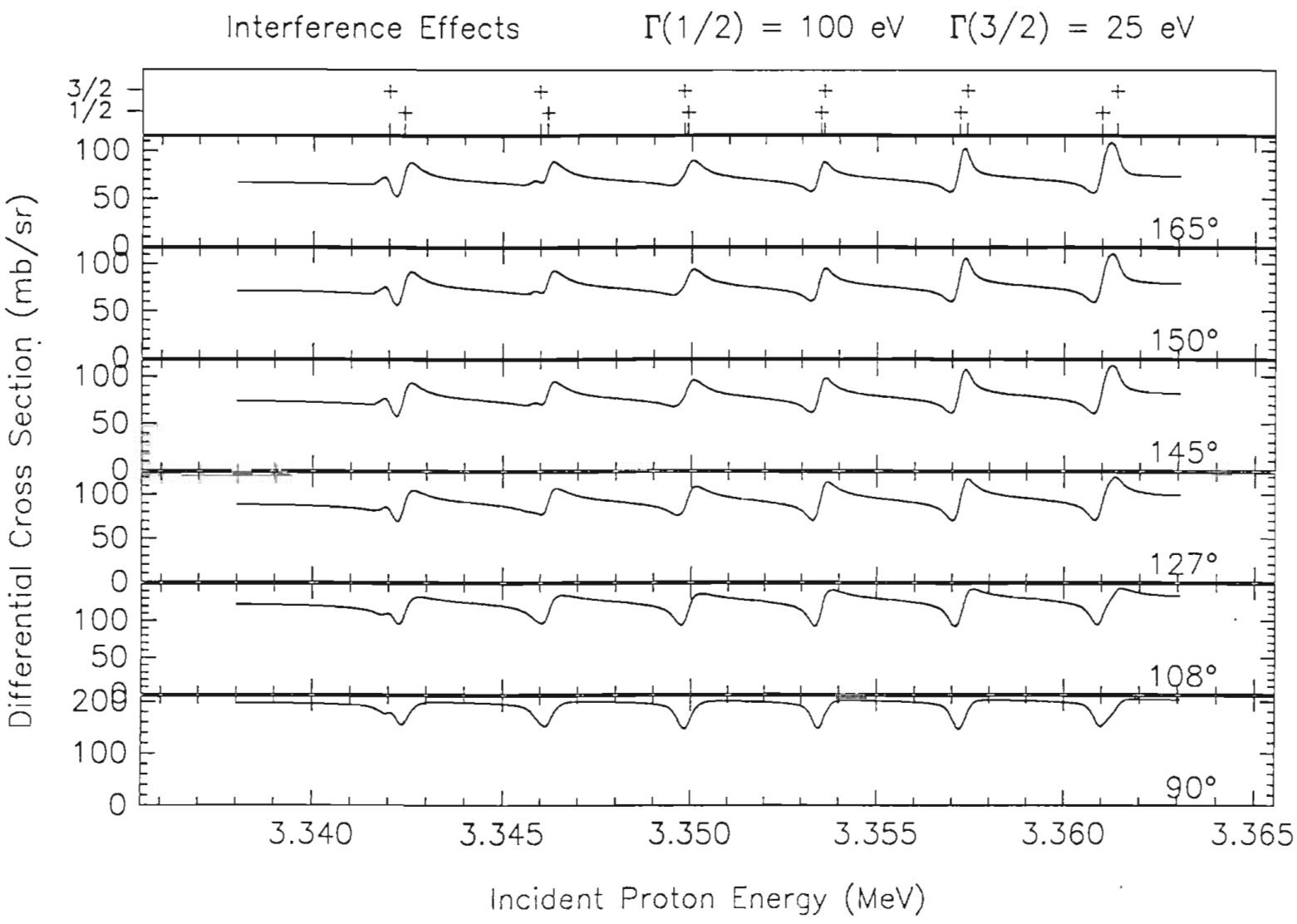
Interference Effects
Γ(1/2) = 100 eV
Γ(3/2) = 25 eV
3/2
1/2
165°
150°
145°
127°
108°
90°
Differential Cross Section (mb/sr)
Incident Proton Energy (MeV)
3.340
3.345
3.350
3.355
3.360
3.365

4. Level Density Determination

The level density for a sequence is equal to the number of levels in this sequence divided by the energy range of the sequence. It is clear from the discussion above that due to the finite energy resolution not all resonances are actually observed. In order to obtain an accurate level density, an estimate is needed of the number of missing levels. In the following section two improved methods for determining the missing fraction will be given.

4.1. Iterative Method

From chapter II we know that the reduced widths follow the Porter-Thomas distribution

$$P(y) = \sqrt{\frac{1}{2\pi y}} \exp\left(-\frac{y}{2}\right),$$

where

$$y = \frac{\gamma^2}{\gamma^2_{average}}.$$

The distribution of reduced widths can provide a quantitative means to determine the number of missed levels in a sequence. From the experimental observed widths, a minimum reduced width can be obtained

$$\gamma^2_{\min} = \min\left\{\frac{\Gamma_i}{2P_i(E)}\right\},$$

where $P_i(E)$ is the penetrability which depends on the energy. We assume that levels with reduced widths below the minimum reduced width are not observed, while all of the levels with reduced widths larger than the minimum value are observed. With this assumption the percentage of missing resonances for a given sequence is

$$M.F. = \int_0^{y_{cutoff}} P(y)dy,$$

where

$$y_{cutoff} = \frac{\gamma^2_{\min}}{\gamma^2_{average}}.$$

This in turn allows the determination of the theoretical number of levels in the sequence

$$N_{theoretical} = N_{observed}\left(\frac{1}{1 - M.F.}\right)$$

Using the theoretical number of levels a new $\gamma^2_{\text{average}}$ can be calculated

$$\gamma^2_{average} = \frac{\sum \gamma_i^2}{N_{theoretical}}.$$

This new average reduced width can be used to calculate a new y_{cutoff}; which in turn, will be used to calculate a new M.F. With a cyclical algorithm a constant value for the missing fraction is obtained after a few iterations. This value is used to determine the level density ρ, or average level spacing <D>,

$$\rho = \frac{1}{\langle D \rangle} = \frac{N_{theoretical}}{E_{\max} - E_{\min}}.$$

This method usually works well, but its disadvantage is obvious: the value for the cutoff is given by the value of the smallest reduced width. Due to experimental problems, the width and J^π values of smaller levels are always questionable. Therefore we also use another method which determines the missing fraction from the entire sequence.

4.2. Bootstrap Method

The bootstrap, a relatively new method, uses the entire sequence to determine the missing fraction, and thus allows more confidence in the spacing or density determination. The bootstrap method first samples with replacement the levels from the original set of $N_{observed}$ levels; this method of sampling means that any level may be in the sample more than once or not at all. Once this selection is performed the minimum reduced width of this new sequence is determined along with the average reduced width. A y_{cutoff}

is calculated and the missing fraction is determined using the method described in section 4.1. The process of randomly sampling and determining the corresponding missing fraction is repeated many times, typically 1,000-10,000. The resulting set of missing fractions is used to generate a missing fraction distribution. From this distribution the mean missing fraction is found and is used to calculate the $N_{observed}$ for the sequence. The bootstrap method has been proven superior to the iterative method, since the whole sequence is used in the missing fraction determination. Both the iterative and bootstrap methods will be used to determine the level density in this dissertation.

Figure 4.6 shows the missing fraction distribution for the ^{48}Ti(p,p) $\frac{1}{2}^+$ sequence, with the mean value bin marked. The central 68% of the distribution is also determined and used to provide error estimates. For a normal distribution this error corresponds to one standard deviation. These limits are also shown in Figure 4.6.

Figure 4.6 Missing fraction distribution for $1/2^+$ levels generated by the bootstrap method.

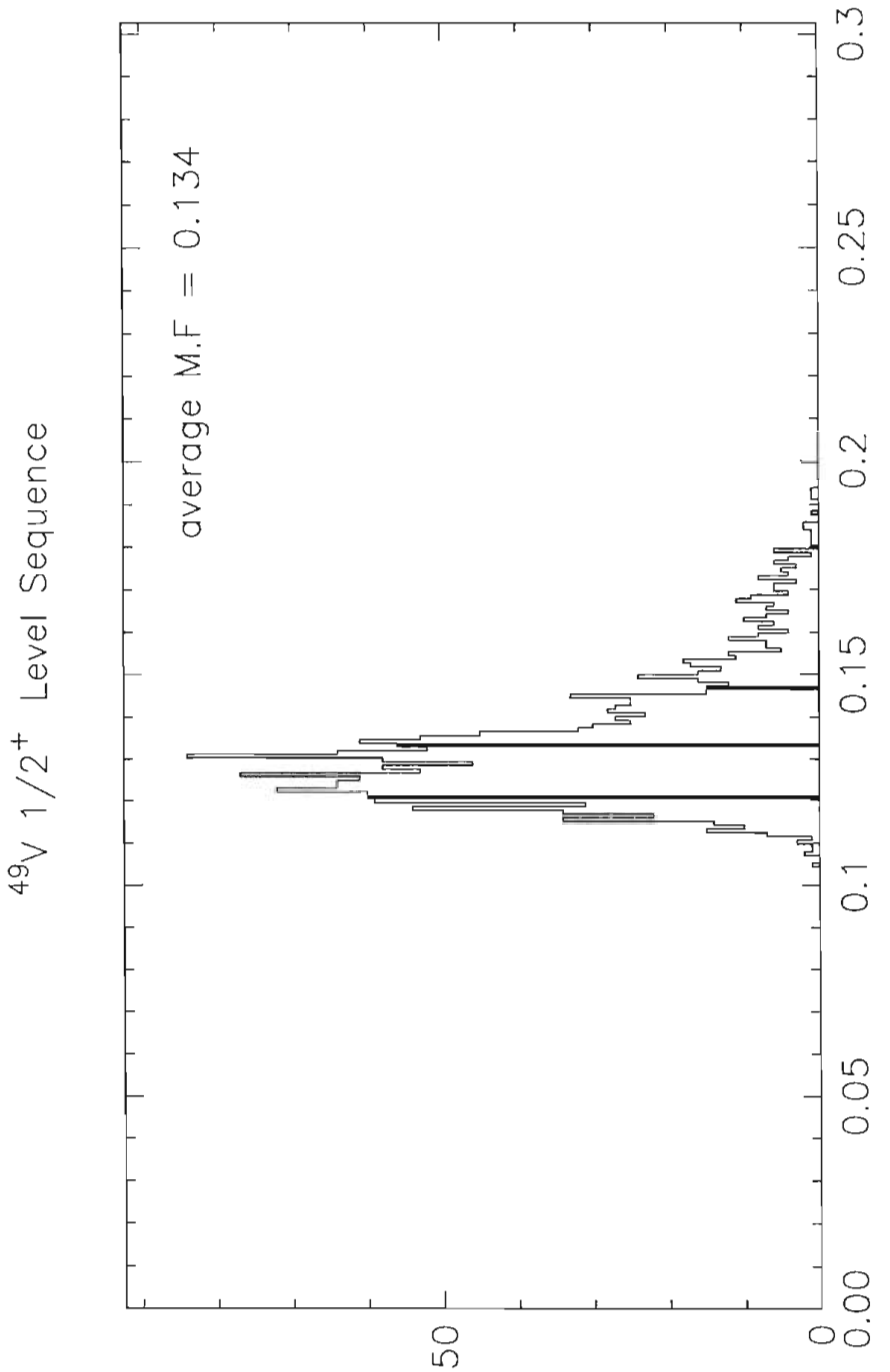
^{49}V 1/2^{+} Level Sequence
average M.F = 0.134
0
50
0.00
0.05
0.1
0.15
0.2
0.25
0.3

Chapter V Results and Discussions

A. Data Summary

In this experiment excitation functions were measured in the energy range E_p=3.08 to 3.86 MeV. The data were analyzed with the program MULTI6 following an iterative process described in Chapter IV. For the energy range studied, 716 resonances were observed with $J^\pi = 1/2^+$ (s-wave), $1/2^-$ and $3/2^-$ (p-wave), $3/2^+$ and $5/2^+$ (d-wave) and $5/2^-$ (f-wave). All of the $5/2^-$ states are fragments of analog states. States with angular momentum $l > 3$ were not expected to be observed due to penetrability effects. The resulting data and fits are presented in Figures 5.1 to 5.5 for the ^{48}Ti (p,p) and ^{48}Ti (p,p') reaction cross sections at 165°.

The overall fitting is satisfactory, except in the region around E_p =3.5 MeV. Here the observed level density is higher, due to two analog states, which cause very strong level-level interference. Typically, the uncertainties in the resonance widths are about 10%. For very small resonances the uncertainties could be as large as 20%. There are some ambiguities in the J assignment for p- and d-wave resonances. Misassignments certainly exist, especially when the level density is so high that resonances strongly overlap. In this experiment the excitation energy range in the compound nucleus $E_x(^{49}V)$ is from 9.77 to 10.54 MeV. These data overlap with that of Prochnow (1971) in the lower energy region. There is good agreement for the resonance parameters obtained in the two experiments in the overlap region. At higher energy, only one energy level from Gales et al. (1976) was known. That energy level was studied in the (^{3}He, pd) reaction and was determined to be the analog of the $5/2^-$ state at 3.844 MeV in ^{49}Ti. The excitation energy of this level was determined to be 10.230 MeV. In this experiment the level was found

Figure 5.1 Data and fit for the Ti(p,p) and Ti(p,p') reactions at 165° for incident proton energies of 3.08 to 3.24 MeV.

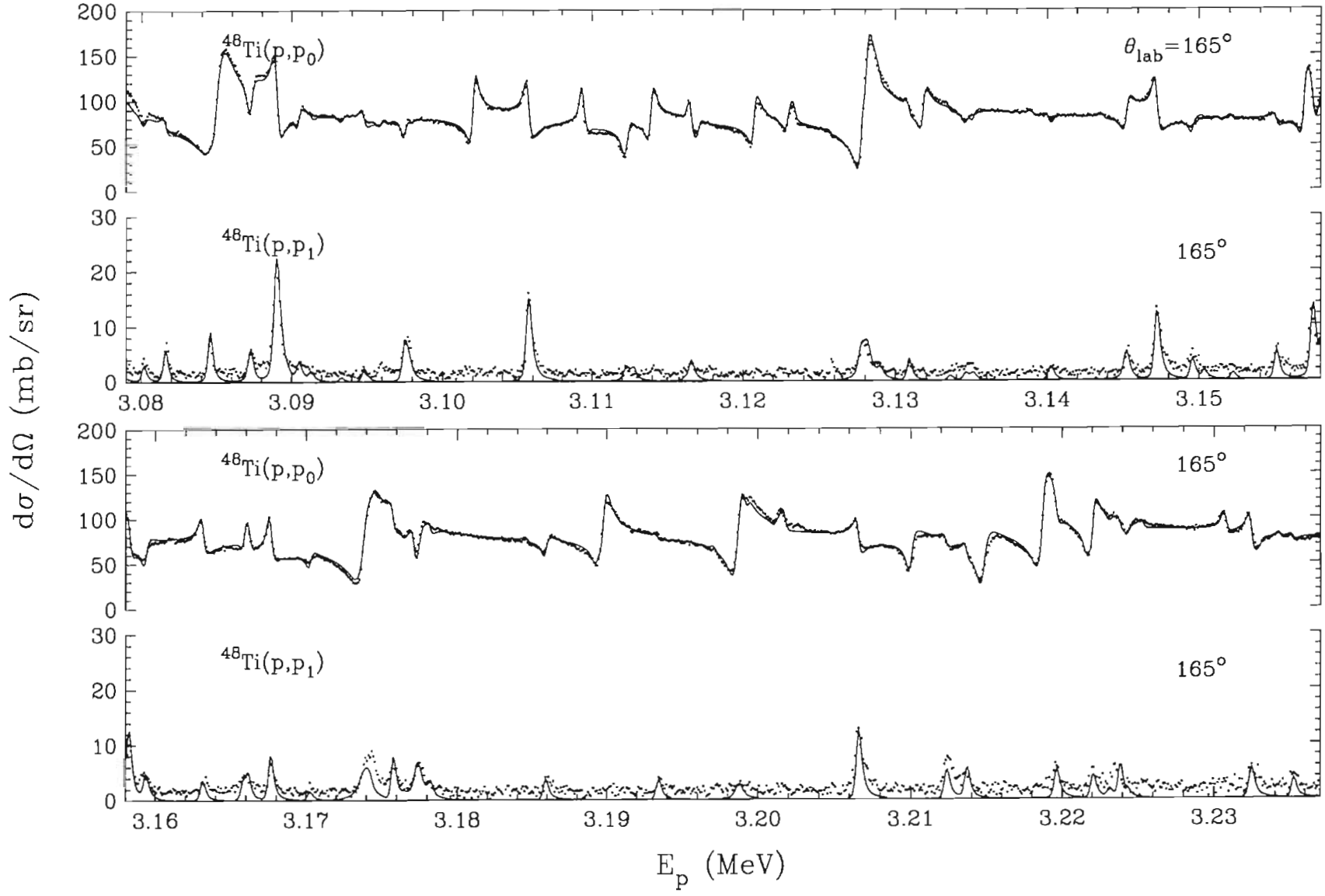
^{48}Ti(p,p$_0$)
θ_{lab}=165°
^{48}Ti(p,p$_1$)
165°
^{48}Ti(p,p$_0$)
165°
^{48}Ti(p,p$_1$)
165°
dσ/dΩ (mb/sr)
E$_p$ (MeV)

Figure 5.2 Data and fit for the Ti(p,p) and Ti(p,p') reactions at 165° for incident proton energies of 3.24 to 3.40 MeV.

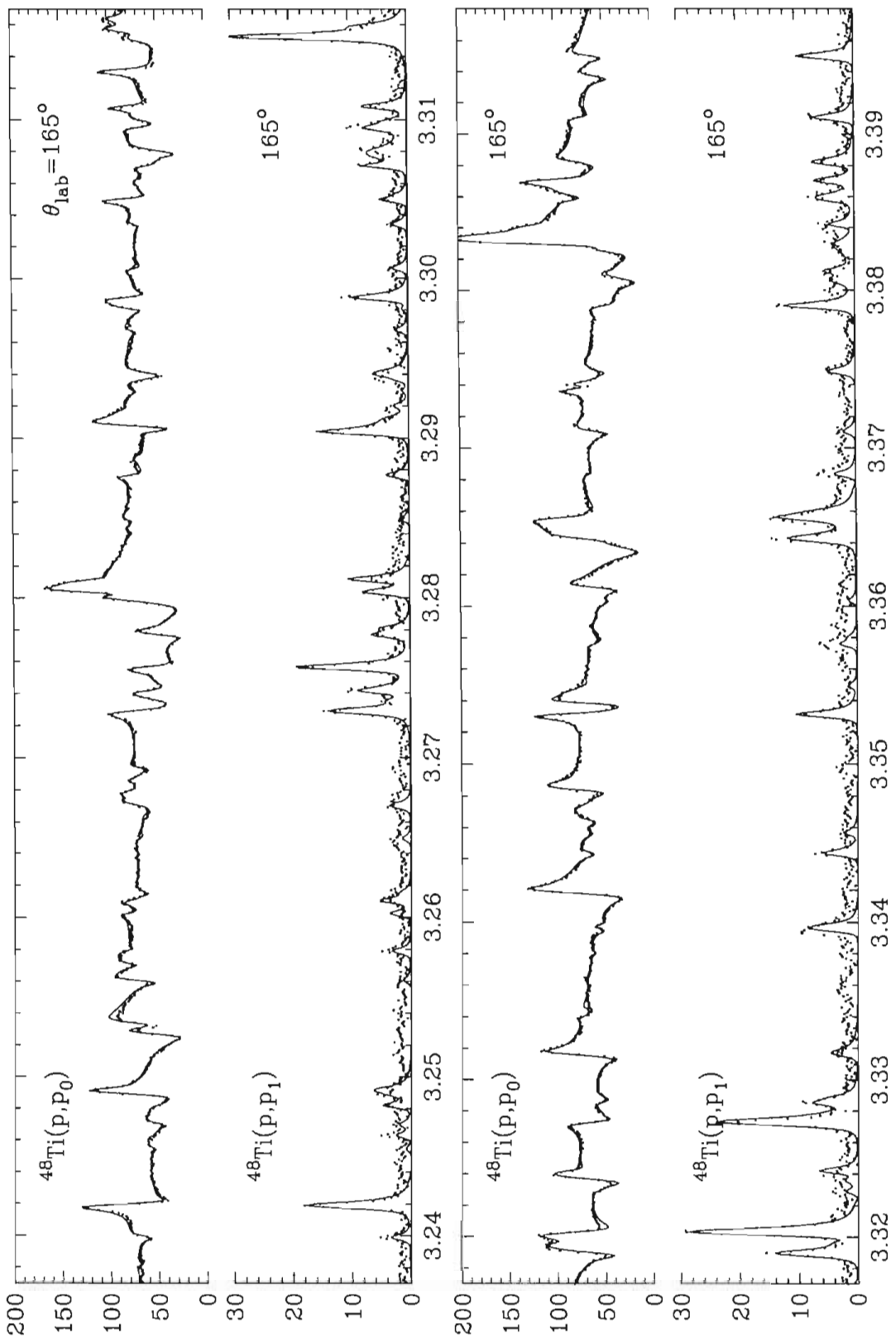
θ_{lab}=165°
^{48}Ti(p,p$_0$)
^{48}Ti(p,p$_1$)
165°
^{48}Ti(p,p$_0$)
^{48}Ti(p,p$_1$)
165°
165°
dσ/dΩ (mb/sr)
E$_p$ (MeV)

Figure 5.3 Data and fit for the Ti(p,p) and Ti(p,p') reactions at 165° for incident proton energies of 3.40 to 3.55 MeV.

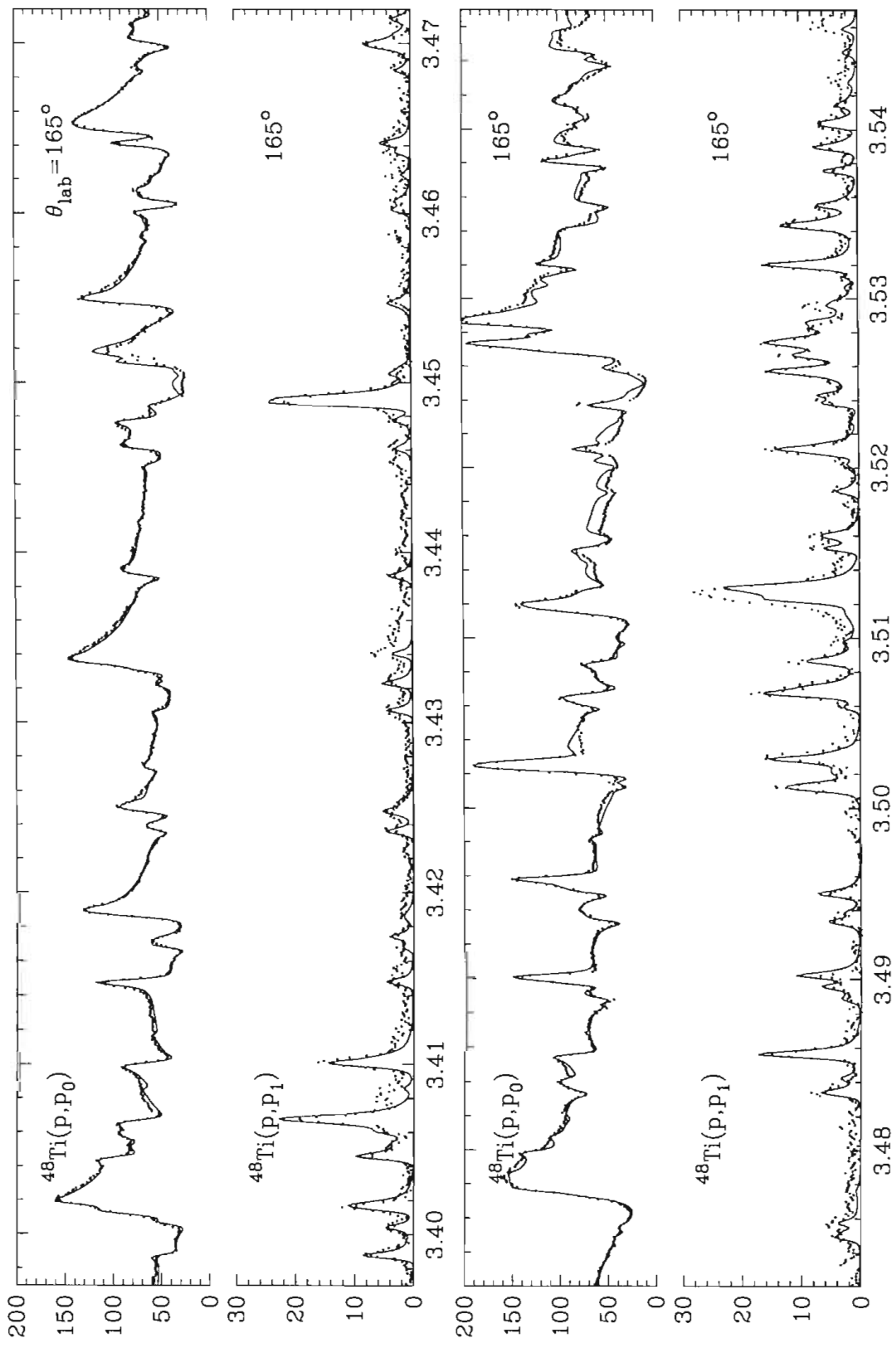
θ_{lab}=165°
^{48}Ti(p,p$_0$)
^{48}Ti(p,p$_1$)
^{48}Ti(p,p$_0$)
^{48}Ti(p,p$_1$)
165°
165°
165°
dσ/dΩ (mb/sr)
E$_p$ (MeV)

Figure 5.4 Data and fit for the Ti(p,p) and Ti(p,p') reactions at 165° for incident proton energies of 3.55 to 3.71 MeV.

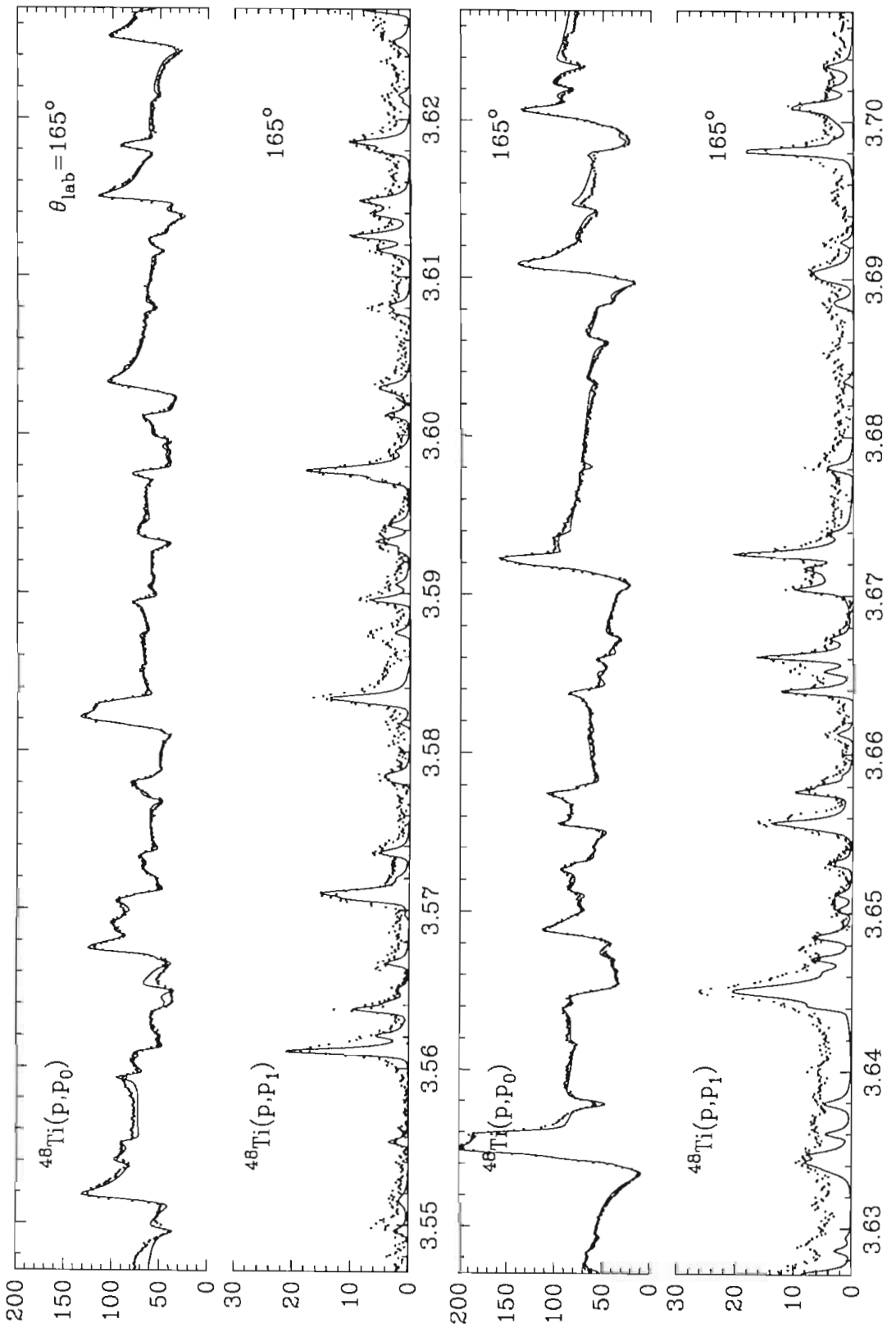
θ_{lab}=165°
^{48}Ti(p,p$_0$)
^{48}Ti(p,p$_1$)
^{48}Ti(p,p$_0$)
^{48}Ti(p,p$_1$)
165°
165°
165°
dσ/dΩ (mb/sr)
E$_p$ (MeV)

Figure 5.5 Data and fit for the Ti(p,p) and Ti(p,p') reactions at 165° for incident proton energies of 3.71 to 3.86 MeV.

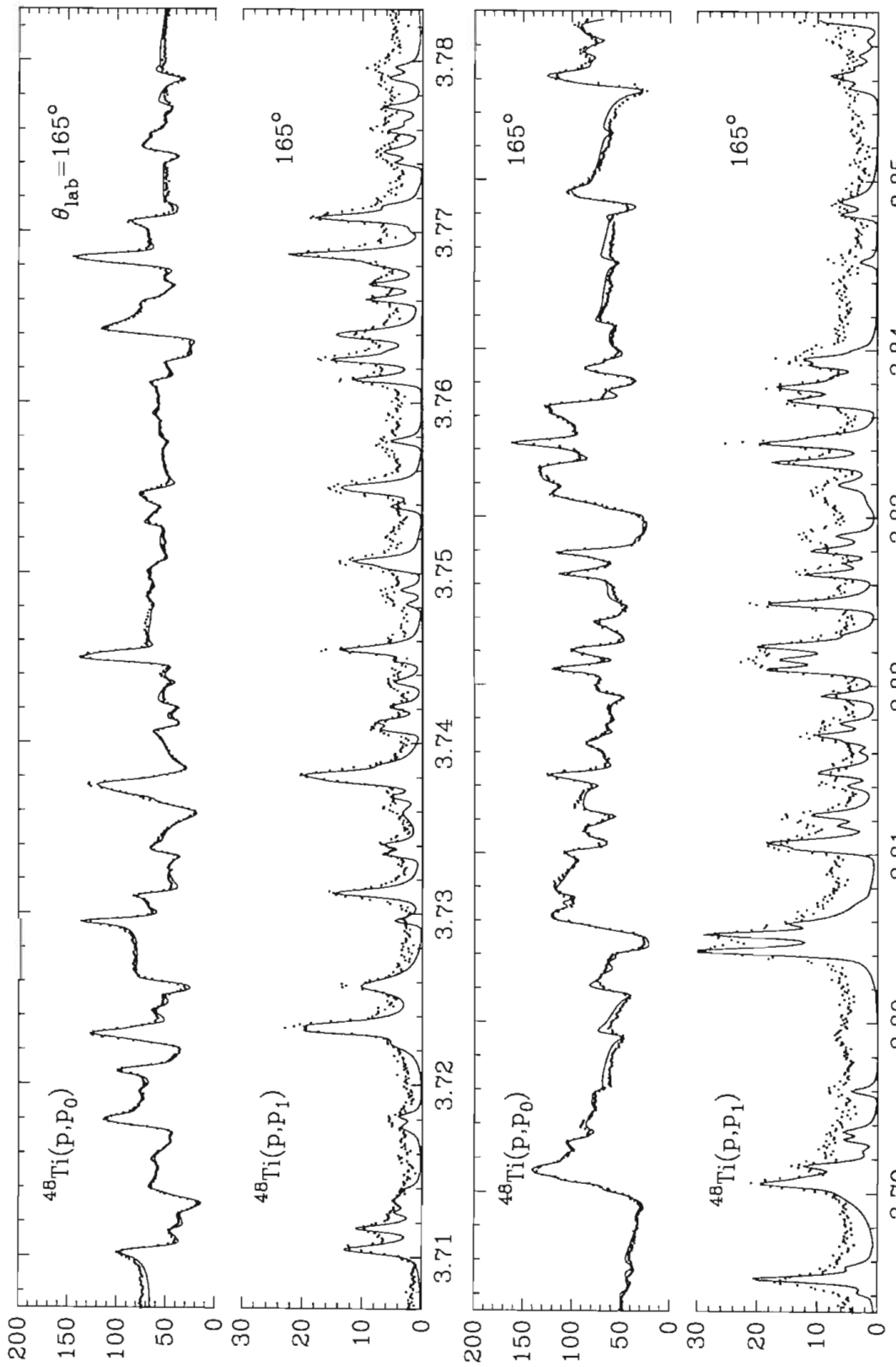
θ_{lab}=165°
^{48}Ti(p,p$_0$)
^{48}Ti(p,p$_1$)
165°
^{48}Ti(p,p$_0$)
^{48}Ti(p,p$_1$)
165°
dσ/dΩ (mb/sr)
E$_p$ (MeV)

centered at 10.212 MeV and was fragmented into at least six states.

The resonance parameters are listed in Appendix A. The level sequences are presented in Figure 5.6 to provide an overall view. Based on the number of levels present in each sequence, all five sequences seem to be good candidates for level density analysis. The reduced width sum and number plots are shown for each sequence in Figures 5.7 to 5.11. These plots show the strength distribution for each sequence. Since the analog states are usually observed as large anomalies (that is, resonances with large reduced widths) in the (p,p) data, plots of the reduced widths as a function of energy are helpful in the identification of analog states.

.

B. Analog States

In order to study the statistical properties of resonances, the analog state must be separated from the "background" states. From the known properties of low-lying states in ^{49}Ti, a number of analog states are expected in the energy range studied in this experiment. The three abnormally large increases in the reduced width sum plot in Figures 5.8 and 5.9 indicate the presence of analog states.

1. Energy Relation Between Analog State and Parent State

As shown in Figure 2.2, the energies of an analog state and parent state are related by

$$E_p^{cm} \equiv E_A = \Delta E_c - B_n + E_{exc}\,, \qquad (5.1)$$

where B_n is the binding energy of the last neutron in the parent system, which can be calculated from other nuclear data, and E_{exc} is the excitation energy of the parent state in the parent nucleus. ΔE_c is the Coulomb energy difference between the parent state and the analog state. E_p^{cm} is the energy of the incident proton in the center-of-mass system and

Figure 5.6 Summary of level sequences observed in ^{49}V for incident proton energy 3.08 to 3.86 MeV.

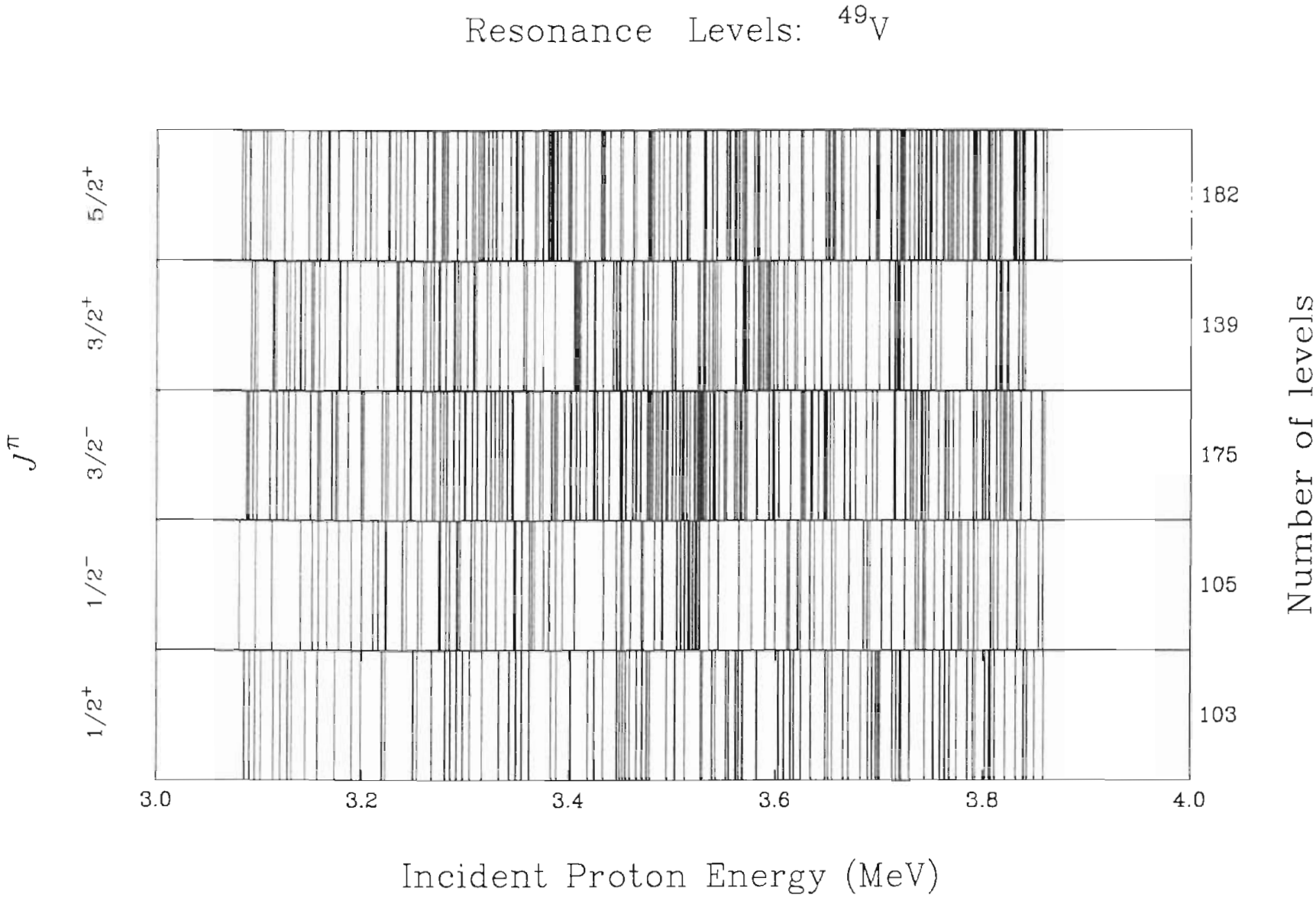
Resonance Levels: ^{49}V
J^π
$1/2^+$
$1/2^-$
$3/2^-$
$3/2^+$
$5/2^+$
182
139
175
105
103
Number of levels
3.0
3.2
3.4
3.6
3.8
4.0
Incident Proton Energy (MeV)

Figure 5.7 Sum of reduced widths plot and number plot for $1/2^+$ level sequence in ^{49}V.

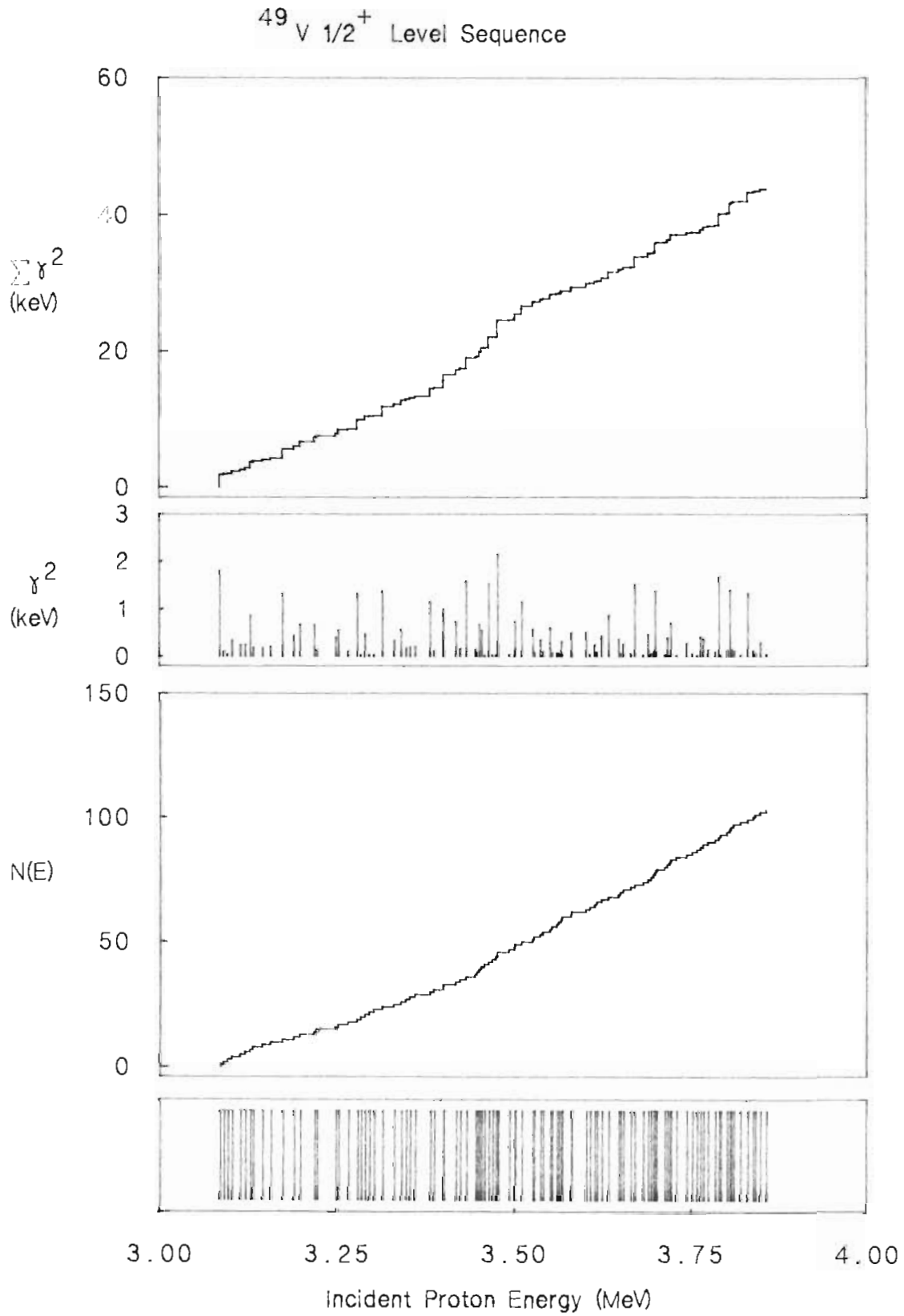
^{49}V 1/2^{+} Level Sequence
60
40
20
0
$\sum \gamma^2$
(keV)
3
2
1
0
γ^2
(keV)
150
100
50
0
N(E)
3.00
3.25
3.50
3.75
4.00
Incident Proton Energy (MeV)

Figure 5.8 Sum of reduced widths plot and number plot for $1/2^-$ level sequence in ^{49}V.

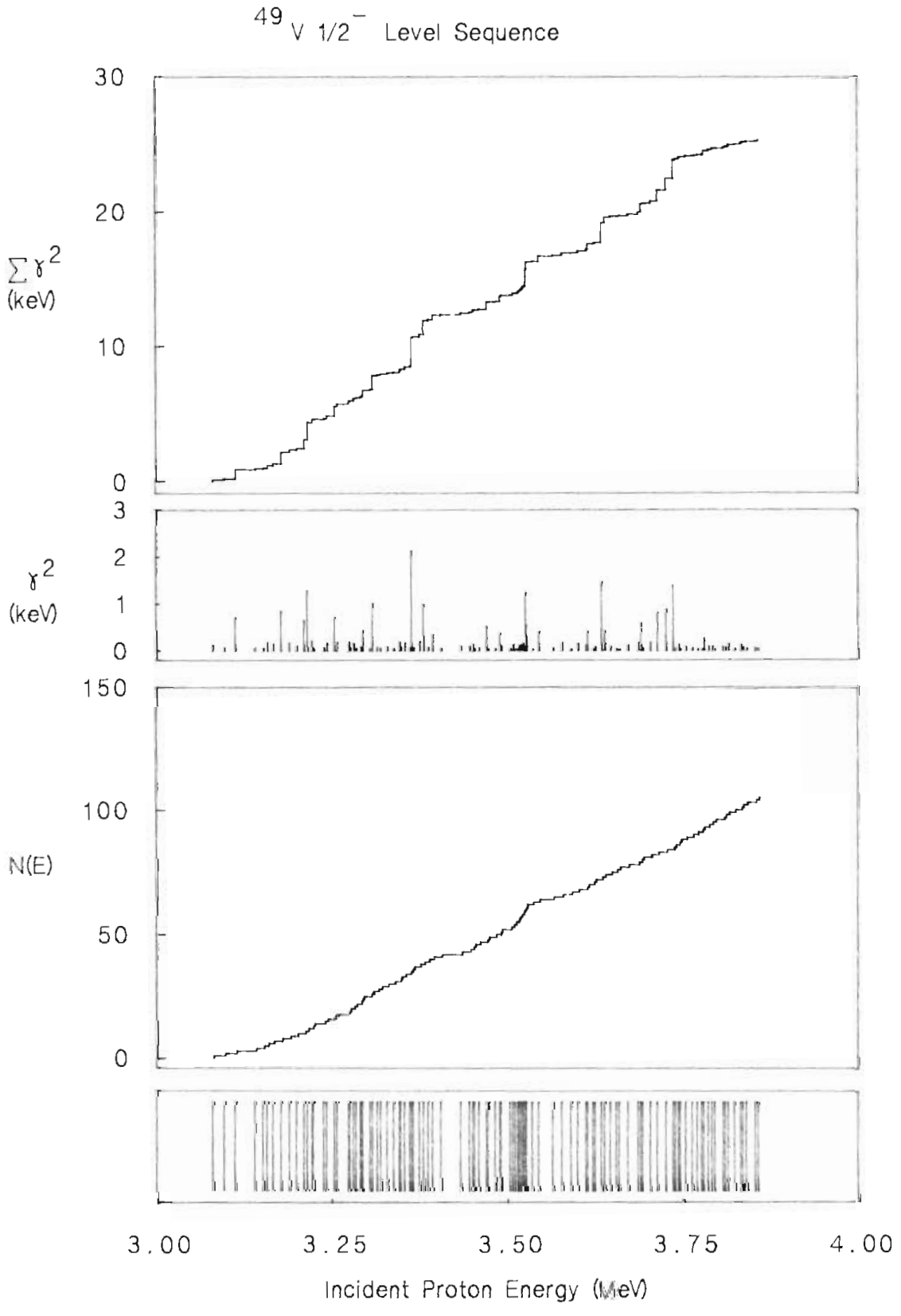
^{49}V 1/2$^-$ Level Sequence
30
20
10
0
$\sum\gamma^2$
(keV)
3
2
1
0
γ^2
(keV)
150
100
50
0
N(E)
3.00
3.25
3.50
3.75
4.00
Incident Proton Energy (MeV)

Figure 5.9 Sum of reduced widths plot and number plot for $3/2^-$ level sequence in ^{49}V.

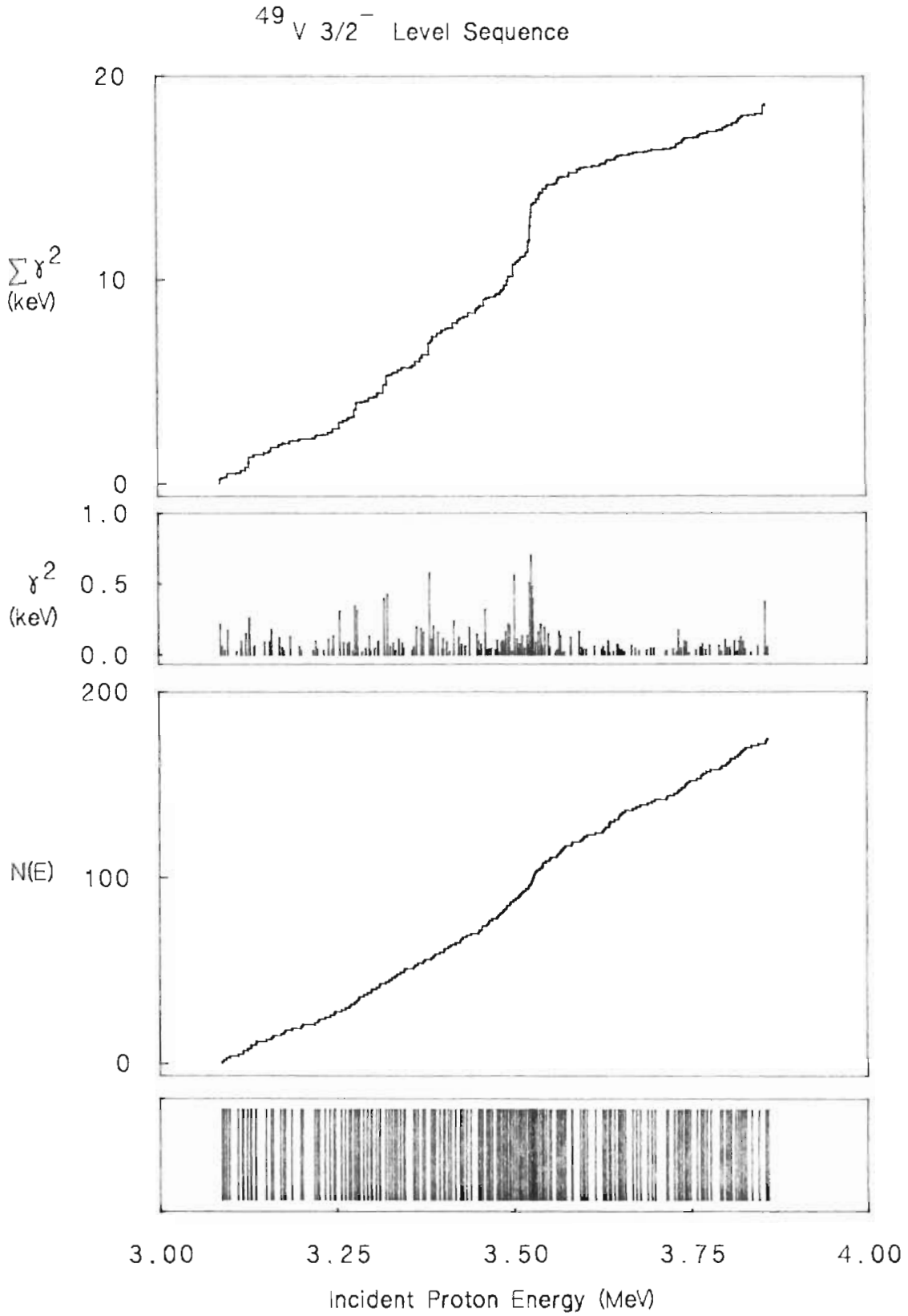
^{49}V 3/2$^-$ Level Sequence
20
10
0
$\sum\gamma^2$ (keV)
1.0
0.5
0.0
γ^2 (keV)
200
100
0
N(E)
3.00
3.25
3.50
3.75
4.00
Incident Proton Energy (MeV)

Figure 5.10 Sum of reduced widths plot and number plot for $3/2^+$ level sequence in ^{49}V.

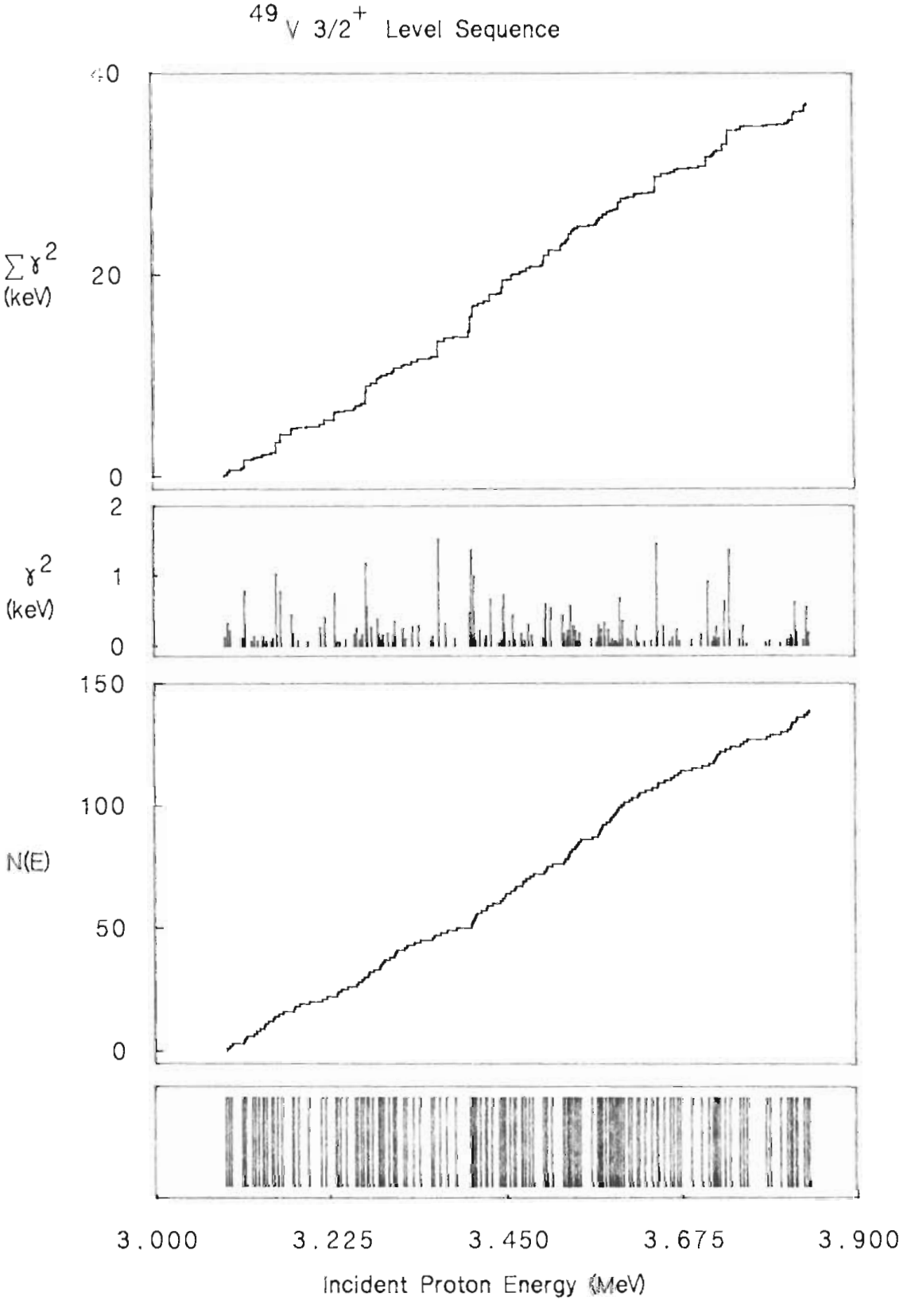
^{49}V 3/2^{+} Level Sequence
$\sum \gamma^2$ (keV)
40
20
0
γ^2 (keV)
2
1
0
N(E)
150
100
50
0
3.000
3.225
3.450
3.675
3.900
Incident Proton Energy (MeV)

Figure 5.11 Sum of reduced widths plot and number plot for $5/2^+$ level sequence in ^{49}V.

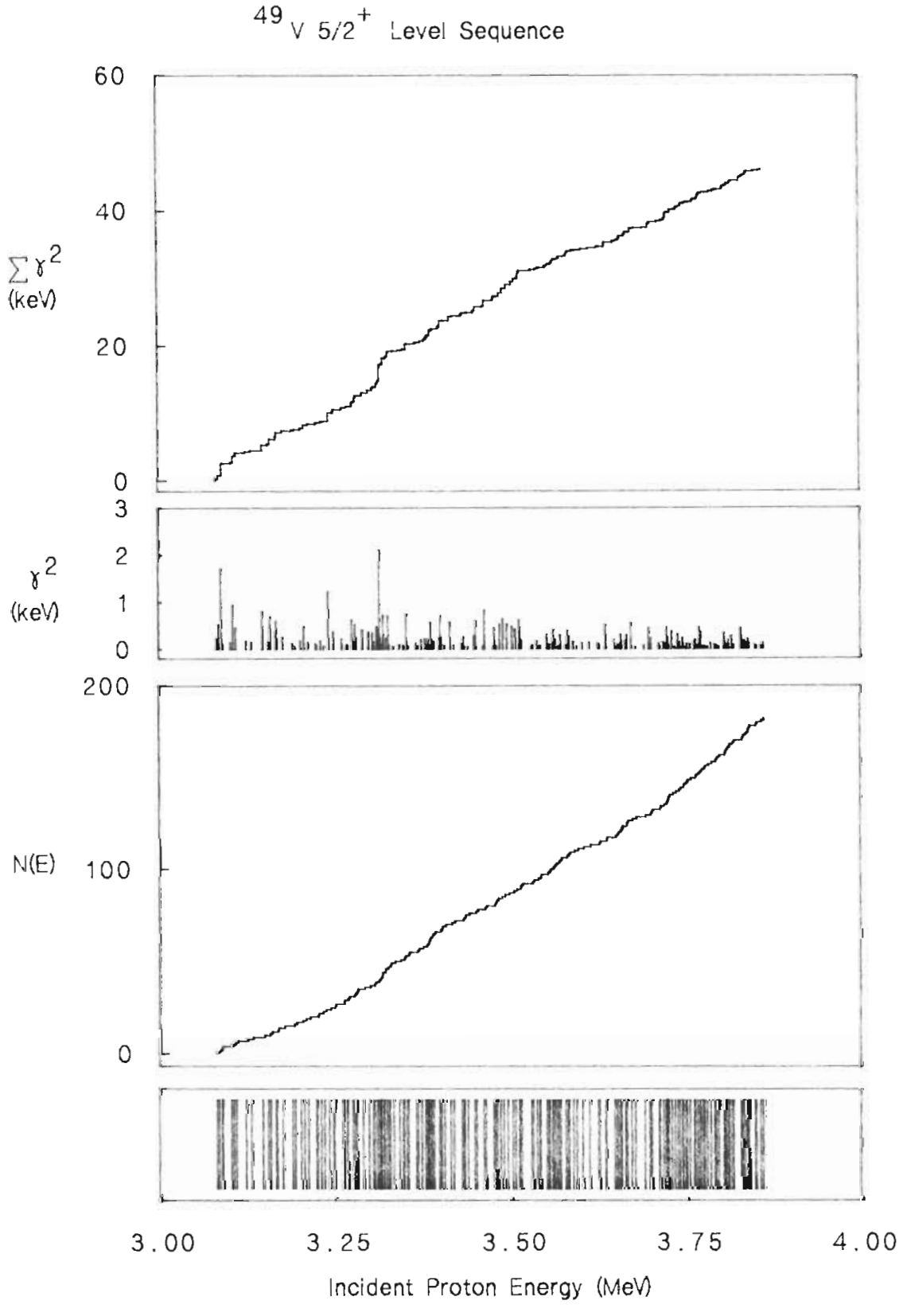
^{49}V 5/2^{+} Level Sequence
60
40
20
0
$\sum\gamma^2$ (keV)
3
2
1
0
γ^2 (keV)
200
100
0
N(E)
3.00
3.25
3.50
3.75
4.00
Incident Proton Energy (MeV)

$$E_p^{lab} \equiv [(M_1+M_2)/M_2]E_p^{cm} \quad . \tag{5.2}$$

Janecke (1969) summarized the experimental results on Coulomb energies and obtained a semi-empirical formula:

$$\Delta E_c^{cal} = [C_1 Z_< + C_2]/A^{\frac{1}{3}} \text{ keV} \tag{5.3}$$

where A is the mass of parent system, $Z_<$ is the proton number of the target and C_1 and C_2 are empirical constants. For Ti the values of the C's are C_1=1389 and C_2=-2041, which gives ΔE_c^{cal} = 7.793 MeV.

2. Spectroscopic Factors

As discussed in Chapter II, the parent state spectroscopic factors S_{dp} can be calculated from

$$S_{dp} = (2T_o+1)\Gamma_{Ap}/\Gamma_{s.p.} , \tag{5.4}$$

where T_o is the isospin of the target, and Γ_{Ap} is the laboratory width of the analog state. For fragmented analog states, this width is the sum of the widths of all components. S_{dp} can be obtained from the (d,p) reaction. $\Gamma_{s.p.}$ is the single particle width of the proton resonance and can be calculated using three different methods: the R-matrix method of Thompson, Adams and Robson (1968) (referred to as TAR); the shell model methods of Zaidi, Darmodjo and Harney (1967) (ZDH) and Mekjian and MacDonald (1968) (MM). These three methods are discussed in detail by Harney and Weidenmuller (1969) and incorporated into a computer code written by Harney (1969).

Proton optical model potential parameters are required in the calculation of the single particle width. A two step procedure is used to obtain these parameters. In the first step the input to the code includes the proton optical model parameters, the analog state parameters (E_λ, J^π) and the parent state parameters (B_n and the major shell number). The optical model parameters used were obtained from optical model analysis of proton elastic scattering on ^{48}Ti (Perey et al. 1968). In this first calculation the neutron optical

model parameters are obtained by varying the neutron real well depth until the parent state binding energy matches $B_{n.}$ A more accurate value of the proton real well depth is then obtained by adding to this neutron well depth the symmetry potential:

$$U_{sym} = [(2T_o+1)/2]\ 125/A\ \ MeV \qquad (5.5)$$

The resulting potential is used as input to Harney's program. The single particle widths calculated in this manner are listed in Table 5.1.

3. Experimental Results

Six analog states of ^{49}Ti were determined in this experiment. They are: $3/2^-$ at E_p= 3.13 MeV, $1/2^-$ at E_p= 3.18 MeV, $5/2^-$ at E_p= 3.32 MeV, $3/2^-$ at E_p= 3.52 MeV, $5/2^-$ at E_p= 3.53 MeV and $5/2^-$ at E_p= 3.83 MeV. All of the analog states are fragmented except the state at E_p= 3.32 MeV. The energy centroids for the five fragmented analog states were determined and the Coulomb energy differences calculated using Eq.(5.1). The average disagreement with Janecke's estimate is about 20 keV. The experimental Coulomb energy differences and spectroscopic factors are listed in Table 5.2.

The energy level $E_x(^{49}Ti)$ = 3.618 MeV was first found by Bjerregaard et al. (1964) in the (d,p) reaction and later by Barnes (1967). This level was so weakly populated that no *l*-value and spectroscopic factor were given. The J^π value was assigned $5/2^-$ by Ball et al. in a (t,p) reaction (1972) and the level was located at 3.618 MeV by Ruyl (1983), but there is still no spectroscopic factor available. In our experiment a $5/2^-$ resonance at E_p= 3.3153 MeV was observed with laboratory width Γ = 18 eV. The Coulomb energy difference of 7.771 MeV between the parent state and the tentative analog state is in good agreement with Janecke's estimate. This state at E_p = 3.3153 MeV is tentatively assigned as the analog of the $E_X(^{49}Ti)$ = 3.618, $5/2^-$ state and is listed in Table 5.2.

Table 5.1 Single Particle Widths

Parent	E_p^{lab} (MeV)	J^π	U_n (MeV)	U_p (MeV)	Single particle widths Γ'_{sp} (keV)[a] TAR	ZDH	MM
^{49}Ti	3.1249	$3/2^-$	-44.6	-51.1	39.9	45.5	45.9
	3.1861	$1/2^-$	-48.1	-54.6	41.5	48.0	48.3
	3.3153	$5/2^-$	-48.8	-55.3	1.18	1.35	1.37
	3.5160	$3/2^-$	-44.0	-50.4	66.9	75.1	75.5
	3.5260	$5/2^-$	-48.4	-55.0	1.78	2.07	2.08
	3.8310	$5/2^-$	-48.0	-54.5	3.06	3.54	3.56

(a) $\Gamma'_{sp} = \Gamma_{sp} / (2T_o+1)$

Table 5.2 Parameters of Analog States in ^{49}V

J^{π}	Number of fragments	E_p^{lab} (MeV)	$E_x^{parent(a)}$ (MeV)	$\Delta E_c^{(b)}$ (MeV)	$\Gamma_p^{(obs.)}$ (keV)	$S_p = (2T_o+1)\Gamma_p/\Gamma_{sp}$ (10^{-3}) TAR	ZDH	MM	$S'_{dp}{}^{(c)}$	S_p/S_{dp}
3/2⁻	9	3.1249	3.426	7.778	0.400	10.0	8.8	8.7	0.05	0.73
1/2⁻	4	3.1861	3.470	7.793	1.015	24.5	21.1	21.0	0.05	0.89
5/2⁻	1	3.3153	3.618	7.772	0.018	15.3	13.3	13.1	/	/
3/2⁻	13	3.5160	3.787	7.799	1.945	29.1	25.9	25.8	0.26	0.41
5/2⁻	6	3.5260	3.844	7.752	0.136	76.4	65.7	65.4	0.42	0.99
5/2⁻	5	3.8310	4.143	7.752	0.157	51.3	44.4	44.1	0.34	0.82

(a) E_x^{parent} values from Nuclear Data Sheets **48**, 611 (1986).

(b) The B_n value used in calculating ΔE_c is 8.142 MeV (Tuli. J. K. 1985).

(c) $S'_{dp} = (2J+1)S_{dp}$ with values from Nuclear Data Sheets **48**, 611 (1986).

C. Level Sequence Analysis in ^{49}V

After the identification of the analog states, it is possible to study the statistical properties of the level sequences. Because all of the $5/2^-$ states are fragments of analog states, only five sequences are suitable for this study. In this chapter these sequences are compared with the Wigner and Porter-Thomas distributions. The observed level densities are corrected using the iterative and bootstrap methods described in Chapter IV. Strength functions for all of the level sequences are obtained. The J-dependence of the level density is examined-- see discussion in Chapter II.

1. Statistical Tests of ^{49}V Level Sequences

The first test for the level sequences is the comparison of the observed level spacings with the Wigner distribution. The distribution of spacings is expected to be characterized by the Wigner distribution

$$P(x) = (\pi x/2) \exp(-\pi x^2/4).$$

In Figures 5.12 to 5.16 the observed spacings are plotted with a Wigner distribution superimposed; both binned and cumulative plots are presented. Overall agreement between the experimental distribution and the Wigner distribution is good. This agreement is particularly evident in the cumulative distribution comparison, in which the subjectivity in the data presentation has been removed. There are some discrepancies between the experimental and theoretical distributions. The excess of observed small spacings may be caused by misassignments, since the spacing distribution of all levels (different J^π) is a Poisson distribution. Misassignments lead to an excess of small spacings.

The other useful statistical test involves the Porter-Thomas distribution. In Figures 5.17 to 5.21 the observed level sequences for ^{49}V are presented in both binned and cumulative plots with an overlay of the PT distribution. The overall agreement be-

Figure 5.12 Wigner distribution overlay comparison for the $1/2^+$ level sequence in ^{49}V. Experimental level spacings are plotted (a) in 8 bins of equal probability and (b) as a cumulative distribution.

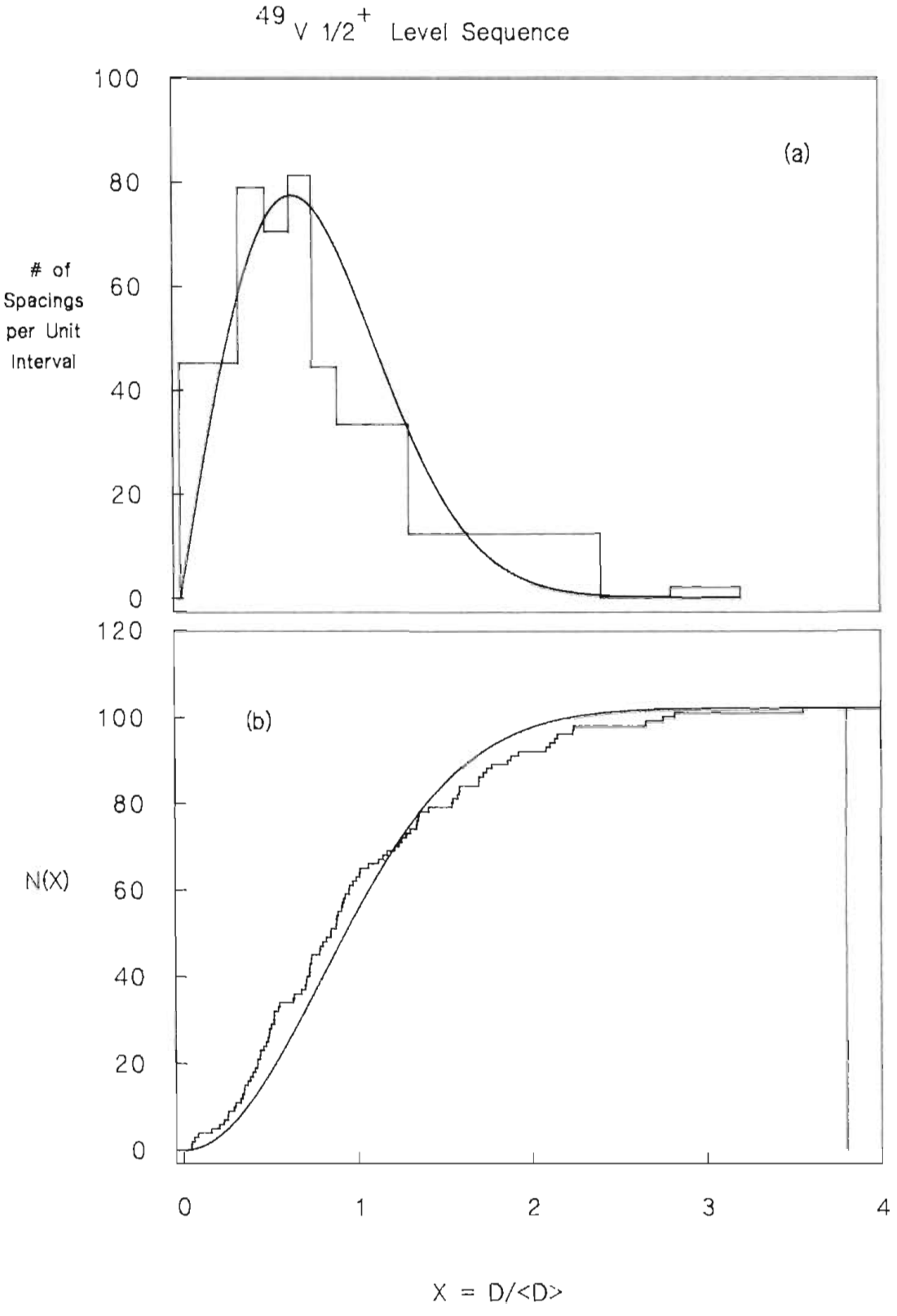
^{49}V 1/2^{+} Level Sequence
(a)
# of Spacings per Unit Interval
100
80
60
40
20
0
(b)
N(X)
120
100
80
60
40
20
0
0
1
2
3
4
X = D/<D>

Figure 5.13 Wigner distribution overlay comparison for the $1/2^-$ level sequence in ^{49}V. Experimental level spacings are plotted (a) in 6 bins of equal probability and (b) as a cumulative distribution.

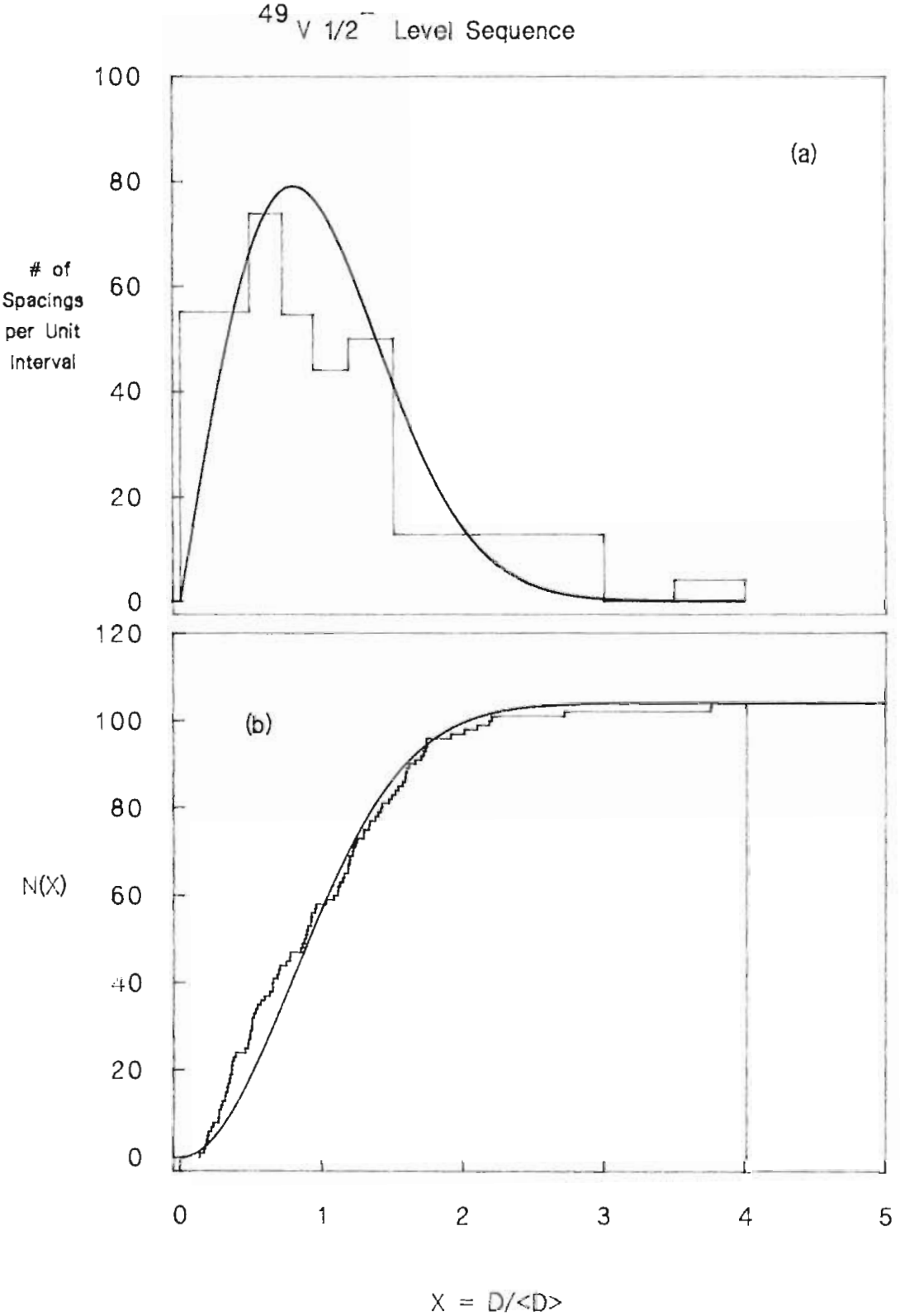
^{49}V 1/2$^-$ Level Sequence
(a)
# of Spacings per Unit Interval
100
80
60
40
20
0
(b)
N(X)
120
100
80
60
40
20
0
0
1
2
3
4
5
X = D/<D>

Figure 5.14 Wigner distribution overlay comparison for the $3/2^-$ level sequence in ^{49}V. Experimental level spacings are plotted (a) in 8 bins of equal probability and (b) as a cumulative distribution.

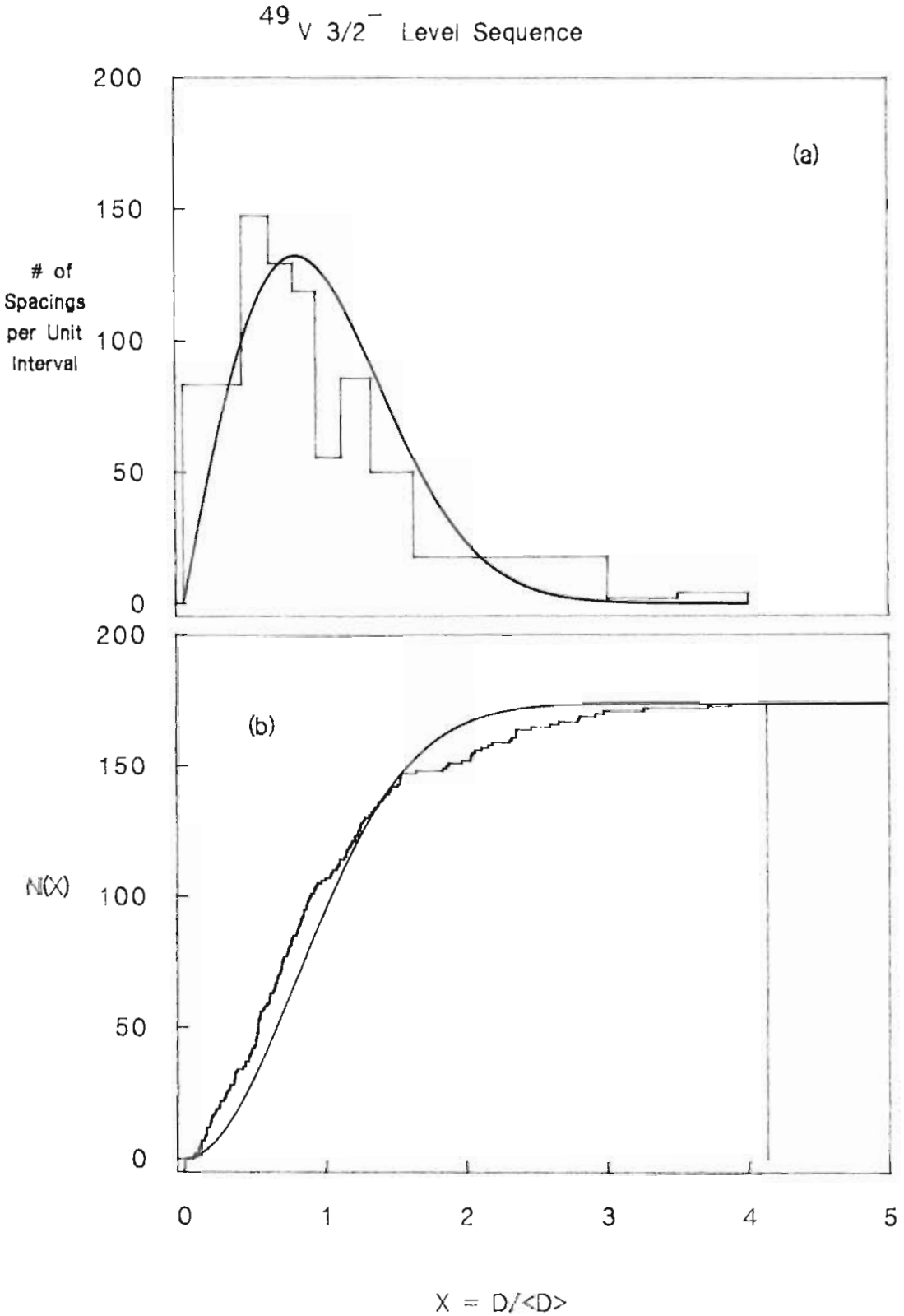
^{49}V 3/2$^-$ Level Sequence
(a)
(b)
# of Spacings per Unit Interval
N(X)
X = D/<D>
0
50
100
150
200
0
1
2
3
4
5

Figure 5.15 Wigner distribution overlay comparison for the $3/2^+$ level sequence in ^{49}V. Experimental level spacings are plotted (a) in 8 bins of equal probability and (b) as a cumulative distribution.

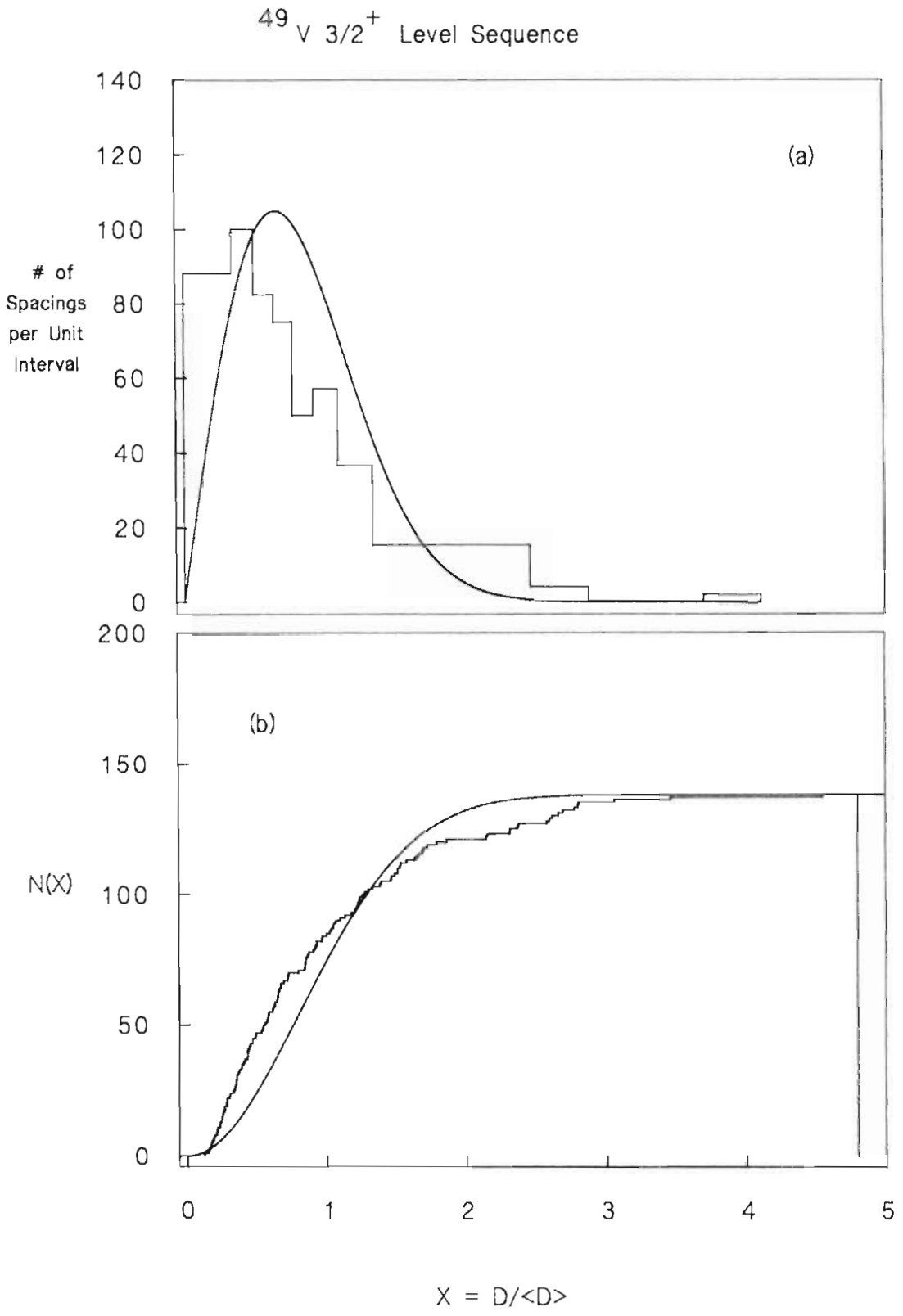
^{49}V 3/2^{+} Level Sequence
(a)
# of Spacings per Unit Interval
140
120
100
80
60
40
20
0
(b)
N(X)
200
150
100
50
0
0
1
2
3
4
5
X = D/<D>

Figure 5.16 Wigner distribution overlay comparison for the $5/2^+$ level sequence in ^{49}V. Experimental level spacings are plotted (a) in 9 bins of equal probability and (b) as a cumulative distribution.

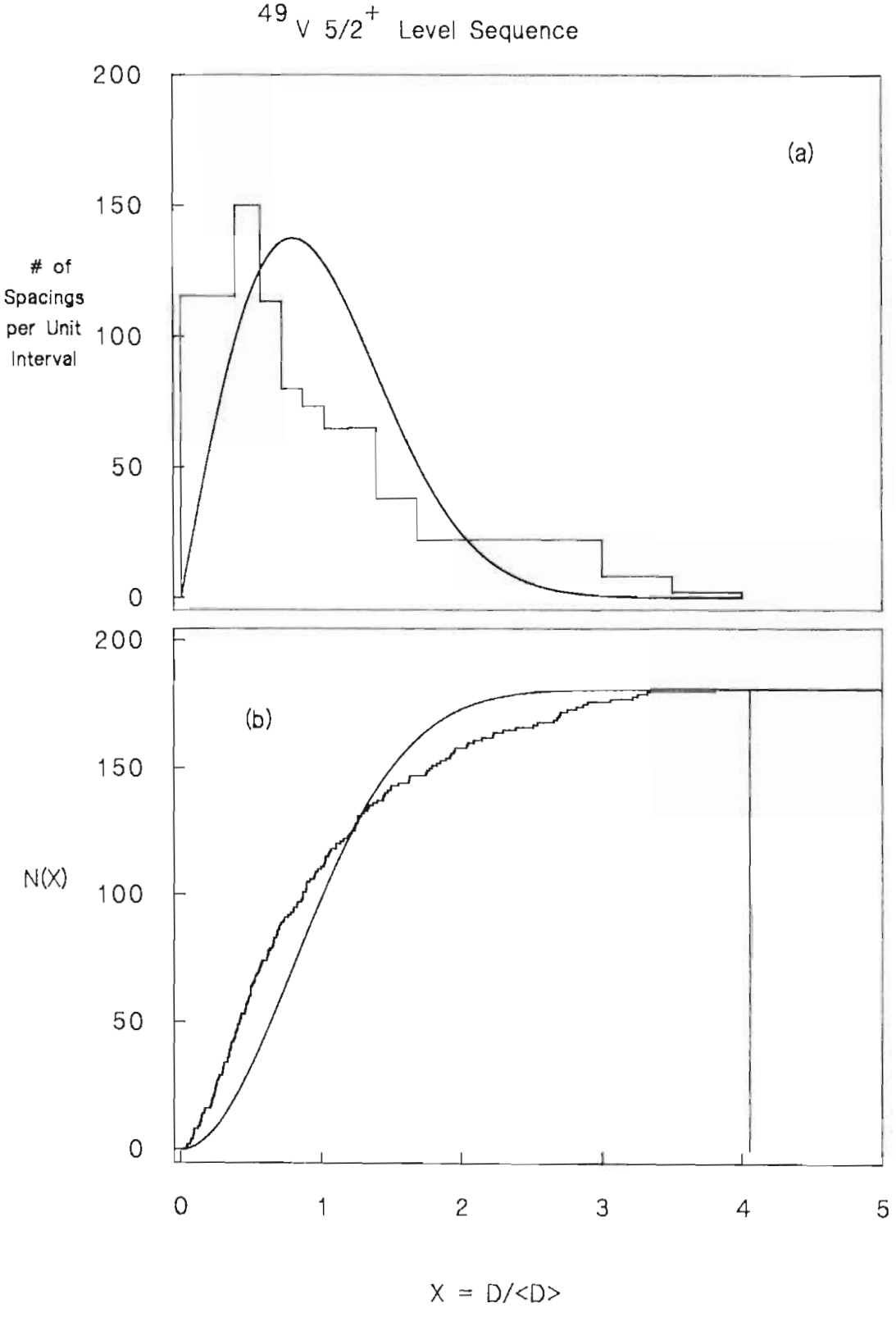
^{49}V 5/2^{+} Level Sequence
200
150
100
50
0
# of Spacings per Unit Interval
(a)
200
150
100
50
0
N(X)
(b)
0
1
2
3
4
5
X = D/<D>

Figure 5.17 Porter–Thomas distribution overlay comparison for the $1/2^+$ level sequence in ^{49}V. Experimental level widths are plotted (a) in 8 bins of equal probability and (b) as a cumulative distribution.

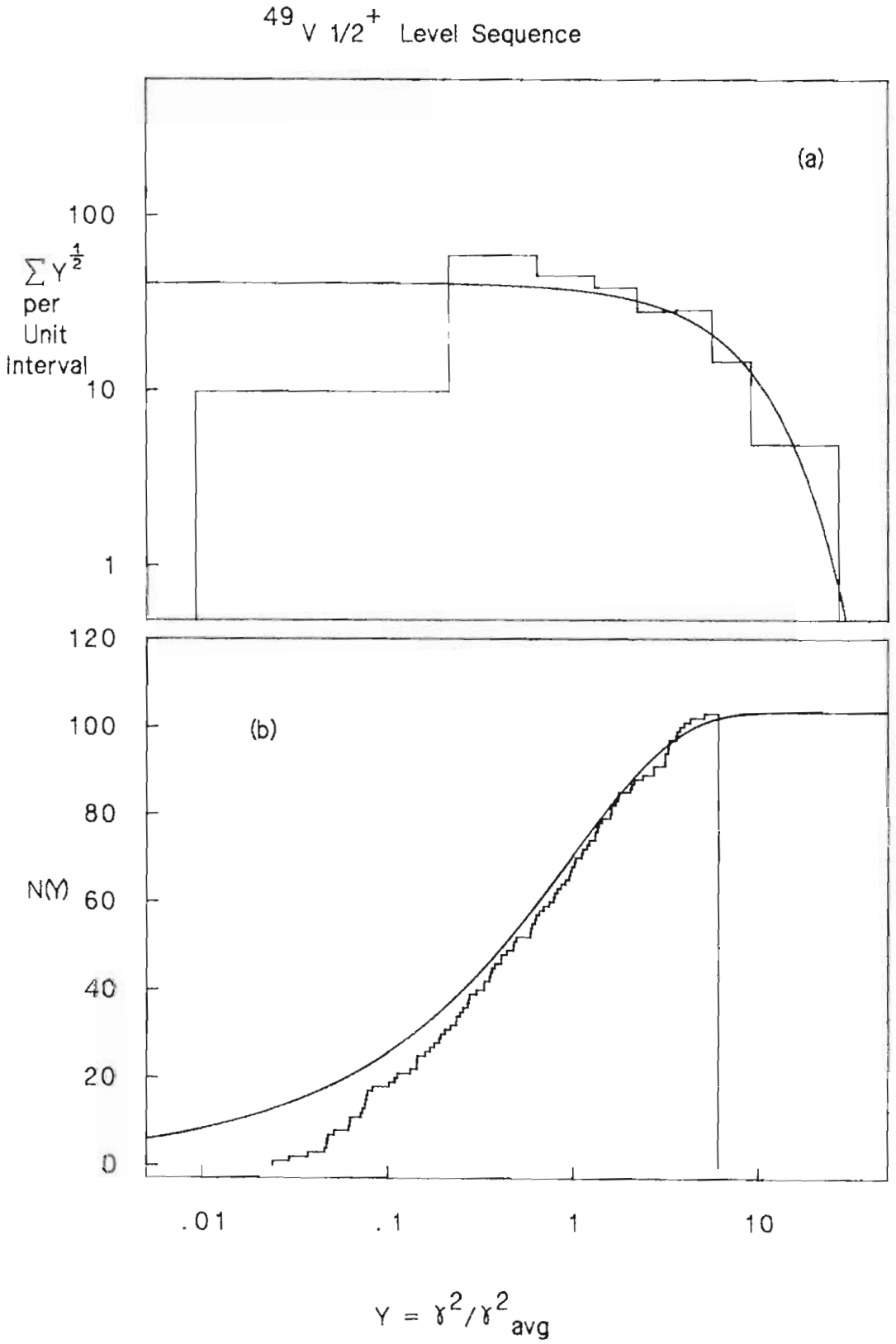
^{49}V 1/2^{+} Level Sequence
(a)
100
$\sum Y^{\frac{1}{2}}$ per Unit Interval
10
1
120
100
80
N(Y) 60
40
20
0
(b)
.01
.1
1
10
$Y = \gamma^2/\gamma^2_{avg}$

Figure 5.18 Porter–Thomas distribution overlay comparison for the $1/2^-$ level sequence in ^{49}V. Experimental level widths are plotted (a) in 8 bins of equal probability and (b) as a cumulative distribution.

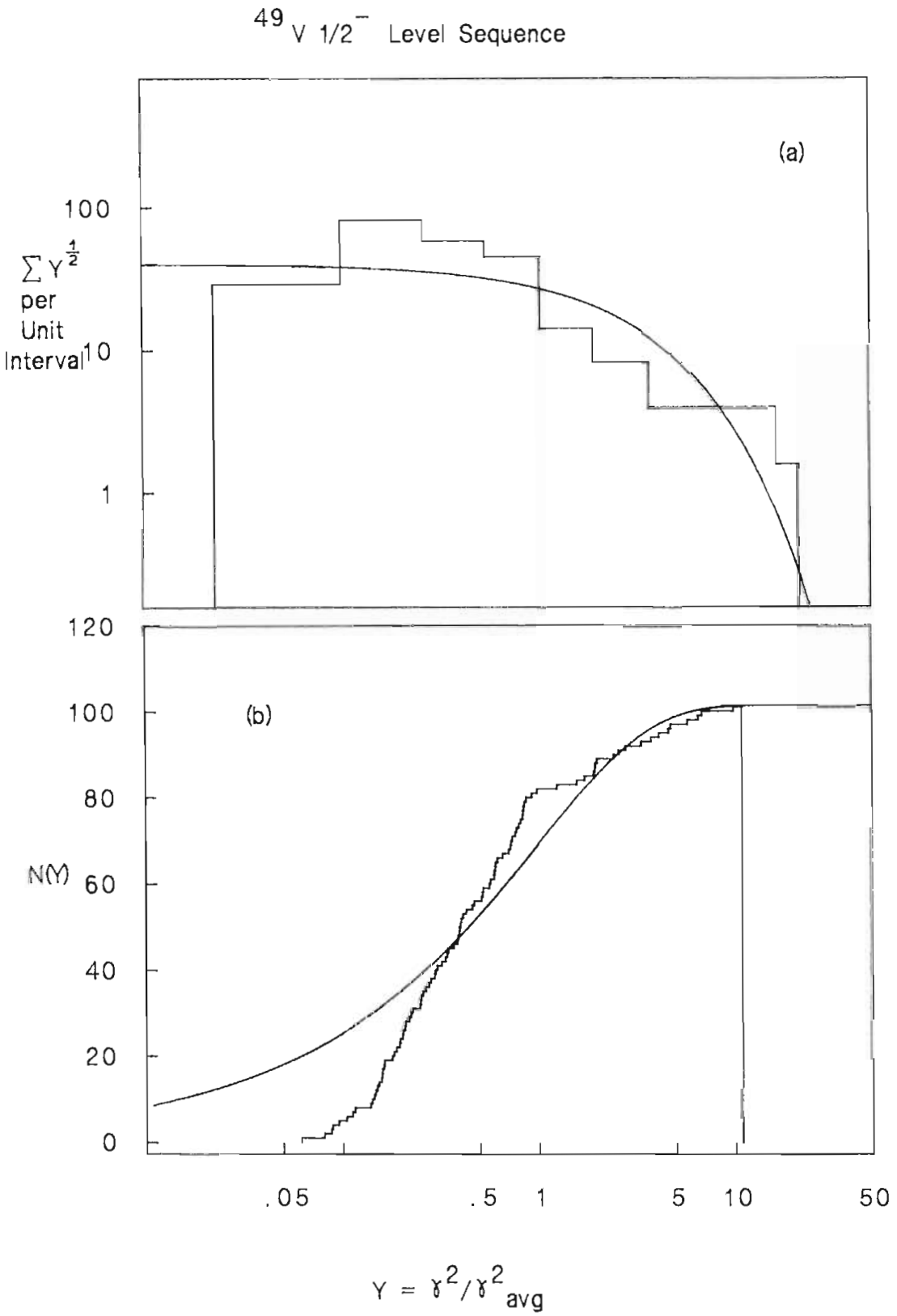
^{49}V 1/2$^-$ Level Sequence
(a)
100
$\sum Y^{\frac{1}{2}}$ per Unit Interval
10
1
120
100
(b)
80
N(Y)
60
40
20
0
.05
.5
1
5
10
50
$Y = \gamma^2/\gamma^2_{avg}$

Figure 5.19 Porter–Thomas distribution overlay comparison for the $3/2^-$ level sequence in ^{49}V. Experimental level widths are plotted (a) in 8 bins of equal probability and (b) as a cumulative distribution.

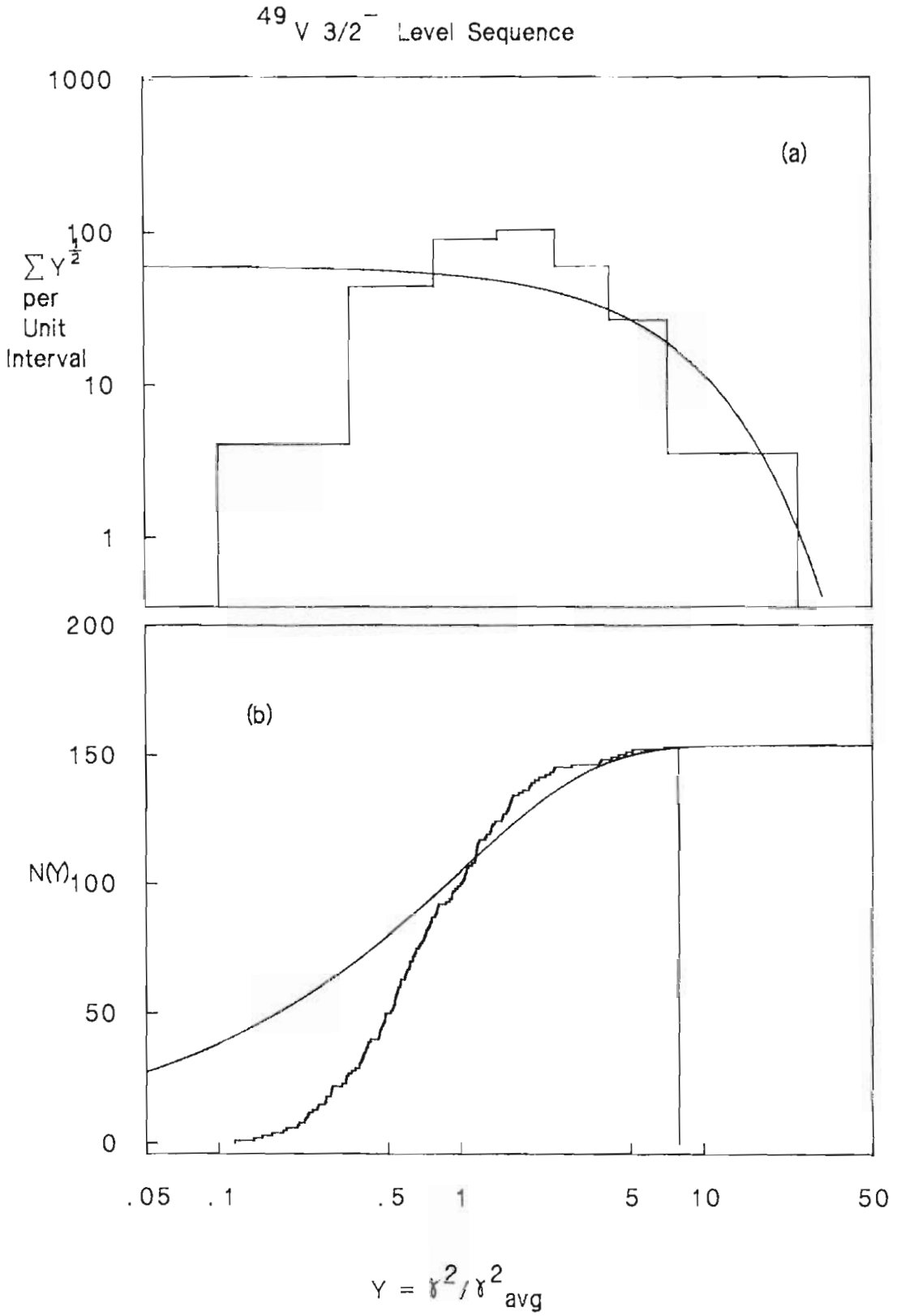
^{49}V 3/2$^-$ Level Sequence
1000
100
10
1
$\sum Y^{\frac{1}{2}}$ per Unit Interval
(a)
200
150
100
50
0
N(Y)
(b)
.05
.1
.5
1
5
10
50
$Y = \gamma^2 / \gamma^2_{avg}$

Figure 5.20 Porter–Thomas distribution overlay comparison for the $3/2^+$ level sequence in ^{49}V. Experimental level widths are plotted (a) in 8 bins of equal probability and (b) as a cumulative distribution.

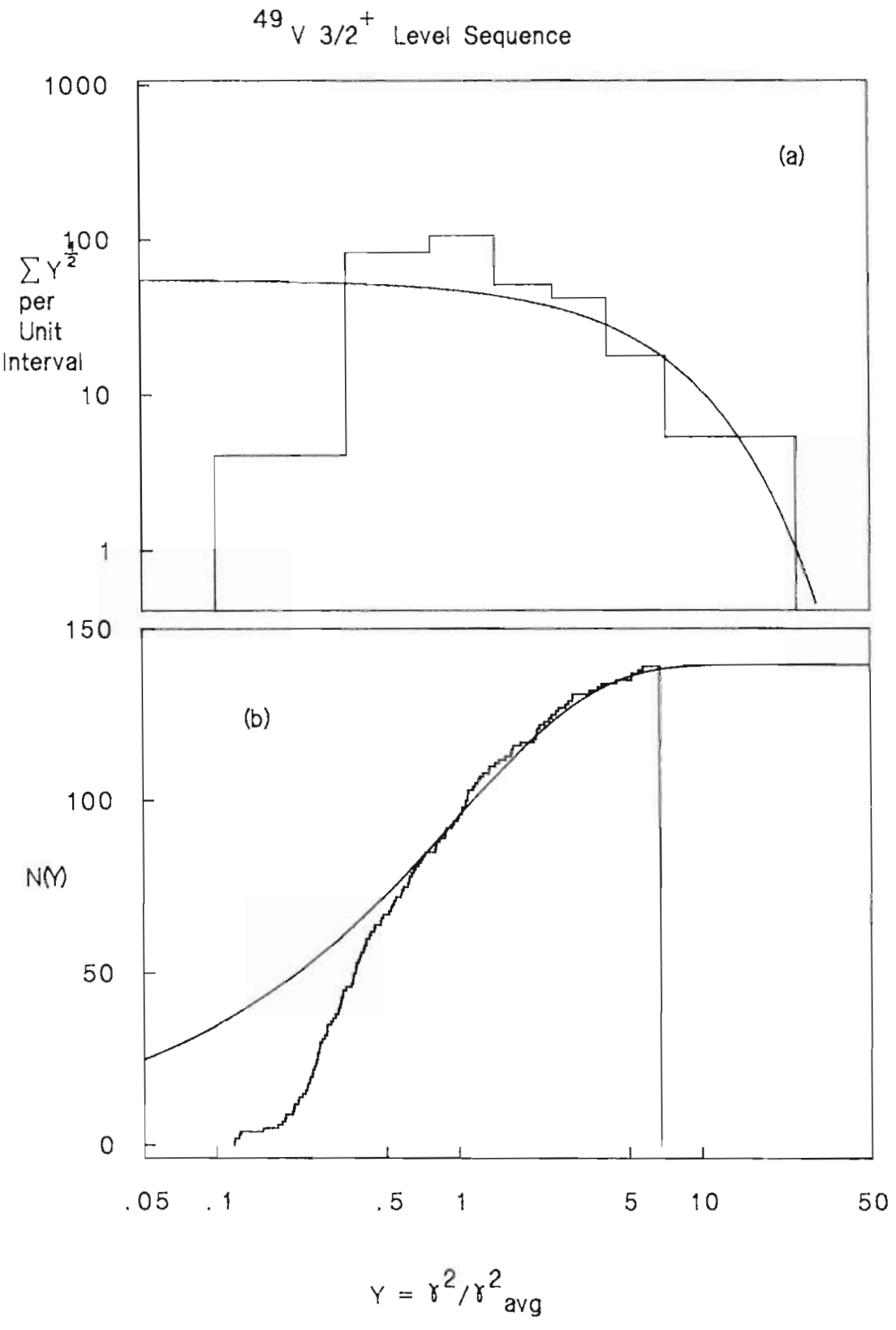
^{49}V 3/2^{+} Level Sequence
1000
100
10
1
$\sum Y^{\frac{1}{2}}$ per Unit Interval
(a)
150
100
50
0
N(Y)
(b)
.05
.1
.5
1
5
10
50
$Y = \gamma^2/\gamma^2_{avg}$

Figure 5.21 Porter–Thomas distribution overlay comparison for the $5/2^+$ level sequence in ^{49}V. Experimental level widths are plotted (a) in 8 bins of equal probability and (b) as a cumulative distribution.

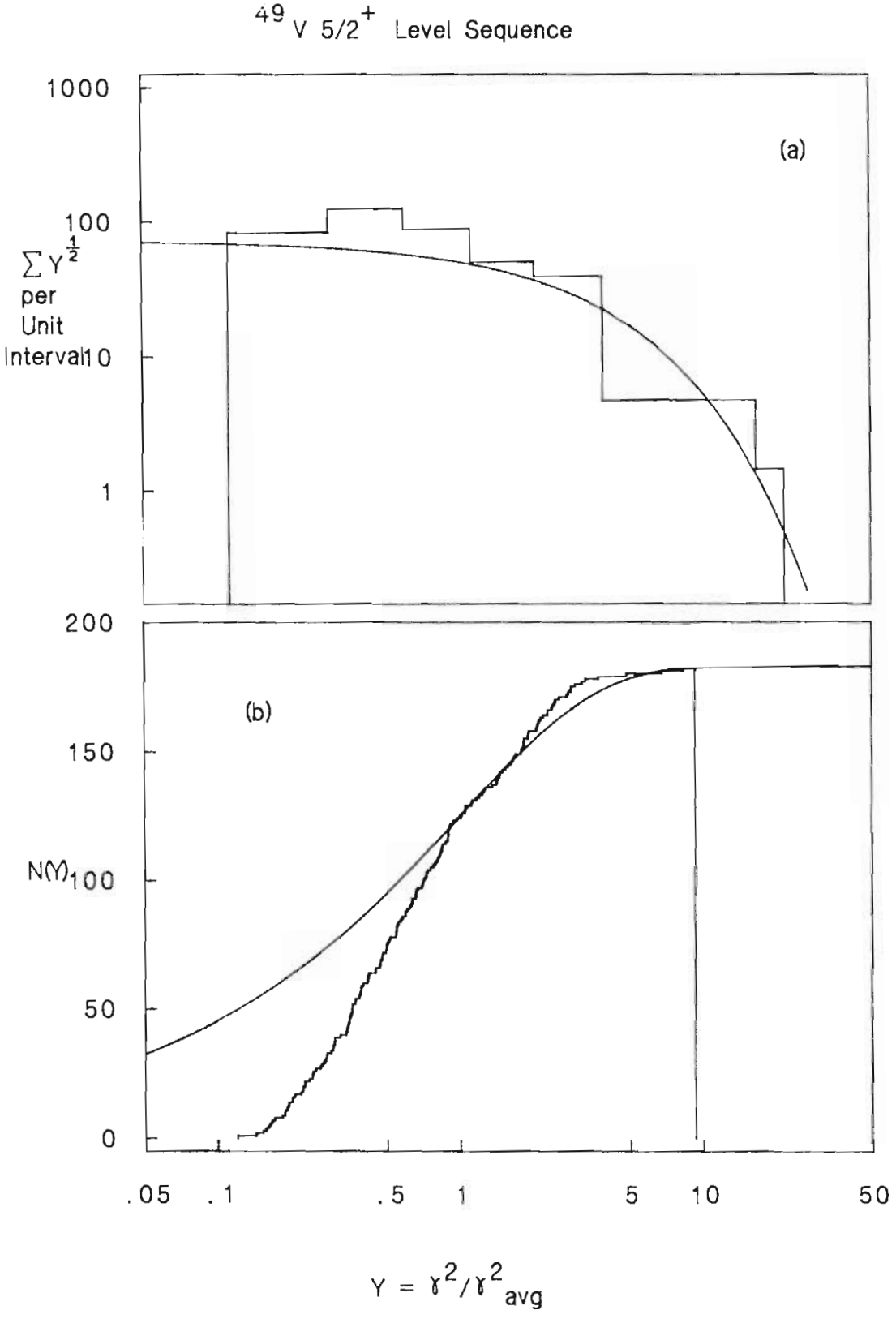
^{49}V 5/2^{+} Level Sequence
1000
100
10
1
$\sum Y^{\frac{1}{2}}$ per Unit Interval
(a)
200
150
100
50
0
N(Y)
(b)
.05
.1
.5
1
5
10
50
$Y = \gamma^2/\gamma^2_{avg}$

tween the experimental distributions and the PT distribution is good. However, it is clear from these comparisons that some weak levels (small reduced widths) have been missed. Corrections are needed to obtain the true level density.

2. Determination of Level Densities in ^{49}V

The observed level densities were corrected using the iterative and bootstrap methods discussed in Chapter IV. Missing fractions were obtained for the five level sequences in ^{49}V from both methods, and level densities were obtained using

$$N_{theoretical} = N_{observed} / (1 - M.F.),$$

where M.F. are the missing fractions. The results are summarized in Table 5.3.

3. Proton Strength Functions

The location (with respect to mass number or energy) of the proton single-particle giant resonances is important in nuclear structure theory. A measurement of the proton strength function as a function of mass number provides information on the location of the single-particle giant resonances. The proton strength function may be defined as

$$S.F. \equiv \langle \gamma_p^2 \rangle / \langle D \rangle,$$

where $\langle \gamma_p^2 \rangle$ is the observed average reduced width and $\langle D \rangle$ is the observed average level spacing. These results are listed in Table 5.3.

4. J^π- Dependence of Level Densities

As shown in chapter II, the J- dependence of the level density is

$$\rho(J) \propto \frac{2J+1}{\sigma^2} \exp\left[-\left(J+\frac{1}{2}\right)^2 / 2\sigma^2\right],$$

where σ is the spin cutoff parameter. Gilbert and Cameron (1965) gave a value of σ = 2.9 for ^{49}V. With this value for σ and the converted level densities of the $1/2^+$ and $1/2^-$ - level sequences, we determine the theoretical level densities for J = 3/2 and 5/2 states from this experiment for $\rho(J)$. These level densities are presented in Table 5.3.

Table 5.3 Summary of level sequence parameters for ^{49}V

Sequence[a] J^{π}	$N_{observed}$	$\langle\gamma^2\rangle_{observed}$[b] (eV)	ρ_o[c]	ρ_I[d]	ρ_B[e] (MeV^{-1})	ρ_C	Strength Function[h]
$1/2^+$	103	426.	133.	151.	154.	/	0.066
$1/2^-$	105	216.	135.	166.	169.	/	0.037
$3/2^-$	175	84.	227.	298.	302.	283.[f]	0.025
$3/2^+$	139	266.	186.	254.	255.	258.[g]	0.068
$5/2^+$	182	253.	234.	321.	326.	287.[g]	0.082

a All of the $5/2^-$ states are fragments of analog states, and are not included here.

b Analog states have been removed.

c Level density observed.

d Level density calculated using iterative method.

e Level density calculated using bootstrap method.

f Level density calculated using Bethe's formula and the level density calculated from bootstrap method for $1/2^-$ sequence.

g Level density calculated using Bethe's formula and the level density calculated from bootstrap method for $1/2^+$ sequence

h Strength function calculated using $\langle\gamma^2\rangle_{observed}$ and the level density determined from the bootstrap method.

Chapter VI Summary

Excitation functions for elastic and inelastic proton scattering from ^{48}Ti were measured in the energy range E_p = 3.08 to 3.86 MeV. The resonances observed in the excitation functions were analyzed in terms of parameters of the R-matrix theory. Resonance energies, spins, parities, total widths and partial widths were determined for a total of 716 resonances.

Six analog states were identified, five of which were found to be fragmented. Coulomb differences between analog states and parent states were extracted and showed a good agreement with Janecke's estimates. Spectroscopic factors were determined for all of the analog states identified, five of which were compared with the spectroscopic factors of the parent states. Reasonable agreement is found between the parent states and analog states spectroscopic factors.

Statistical properties of the resonances in ^{49}V were examined. The resonances observed were used to determined the level densities for the various level sequences. Two methods (iterative and bootstrap) were used to calculate the missing fractions. The values from the two methods are consistent. Level sequences were tested using the Wigner and Porter-Thomas distributions and reasonable agreement was found. The average values of the proton strength functions were also determined from the reduced widths of the $T_<$ levels. The level densities of the $1/2^+$ and $1/2^-$ states are approximately the same. Bethe's J-dependence level density formula was used to calculate the ratios of the level densities for $J > 1/2$ to the $J = 1/2$ density. After correcting for missing level, good agreement was found between the J dependence of theoretical and experimental level densities.

Appendix A

^{49}V Resonance Parameters

Resonance parameters for levels in the ^{49}V compound nucleus system observed in the ^{48}Ti(p,p) and ^{48}Ti(p,p') reactions. The incident proton energy range was 3.08 to 3.86 MeV.

All resonances were fit with the J^{π} that seemed to visually agree best with the data. Although in all cases the best fit was chosen, for some of the resonances there were ambiguities in the J assignment. This generally occurred for p-wave resonances with widths less than ~20 eV and for d-wave resonances with widths less than ~15 eV. These lower limits were larger when there was interference with neighboring levels.

The analysis for the inelastic widths is incomplete since there is only limited angular distribution information. In the analysis the lowest acceptable l' value was assigned and an $l'+2$ component was added only if necessary. The channel spin mixture was adjusted to give the best fit.

Absolute energy errors are ~ 3 keV. Errors for laboratory widths are ~ 10% increasing to 20% for very small resonances.

^{49}V Resonance Parameters

#	Energy (MeV)	J	π	l_p	Γ_p (KeV)	γ^2_p (KeV)	$s_{p'}$	$l_{p'}$	$\Gamma_{p'}$	$\gamma^2_{p'}$ (KeV)
1	3.0802	0.5	-1	1	0.030	0.121				
							1.5	1	0.025	0.987
2	3.0816	2.5	1	2	0.015	0.227				
							2.5	0	0.020	0.331
3	3.0846	2.5	1	2	0.035	0.528				
							2.5	0	0.025	0.410
4	3.0850	0.5	1	0	0.870	1.822				
5	3.0873	1.5	-1	1	0.055	0.219				
							1.5	1	0.025	0.965
							2.5	1	0.020	0.772
6	3.0890	2.5	1	2	0.115	1.719				
							2.5	0	0.100	1.617
7	3.0894	1.5	-1	1	0.015	0.060				
							1.5	1	0.005	0.192
8	3.0902	2.5	1	2	0.007	0.104				
9	3.0905	0.5	1	0	0.050	0.104				
							2.5	2	0.020	3.998
10	3.0913	1.5	1	2	0.008	0.119				
							1.5	0	0.010	0.161
							2.5	2	0.010	1.993
11	3.0933	1.5	-1	1	0.008	0.032				
							1.5	1	0.020	0.757
12	3.0949	1.5	1	2	0.022	0.325				
							1.5	0	0.005	0.079
							2.5	2	0.025	4.919
13	3.0960	0.5	1	0	0.015	0.031				
14	3.0965	0.5	-1	1	0.015	0.059				
15	3.0975	1.5	-1	1	0.045	0.176				
							1.5	1	0.030	1.120
							2.5	1	0.040	1.494
16	3.0978	1.5	1	2	0.015	0.221				
							1.5	0	0.050	0.788
							2.5	2	0.060	11.680
17	3.1020	0.5	1	0	0.165	0.338				
18	3.1023	2.5	1	2	0.010	0.146				
19	3.1057	2.5	1	2	0.065	0.942				
							2.5	0	0.055	0.846
20	3.1094	2.5	1	2	0.032	0.461				
21	3.1099	1.5	-1	1	0.006	0.023				
22	3.1123	0.5	-1	1	0.185	0.709				
							1.5	1	0.020	0.712
23	3.1128	1.5	1	2	0.008	0.114				
							1.5	0	0.010	0.151
							2.5	2	0.010	1.847
24	3.1140	0.5	1	0	0.125	0.252				

^{49}V Resonance Parameters

#	Energy (MeV)	J	π	l_p	Γ_p (KeV)	γ^2_p (KeV)	$S_{p'}$	$l_{p'}$	$\Gamma_{p'}$	$\gamma^2_{p'}$ (KeV)
25	3.1142	1.5	1	2	0.007	0.100				
26	3.1162	1.5	-1	1	0.010	0.038				
							1.5	1	0.020	0.703
27	3.1166	1.5	1	2	0.055	0.781				
							1.5	0	0.010	0.149
							2.5	2	0.010	1.823
28	3.1171	1.5	-1	1	0.025	0.095				
29	3.1208	0.5	1	0	0.125	0.250				
30	3.1230	1.5	-1	1	0.040	0.151				
31	3.1234	2.5	1	2	0.012	0.168				
32	3.1257	1.5	1	2	0.005	0.070				
33	3.1278	1.5	-1	1	0.065	0.243				
							1.5	1	0.030	1.017
34	3.1279	0.5	1	0	0.435	0.861				
							1.5	2	0.040	7.008
35	3.1281	1.5	-1	1	0.070	0.262				
							1.5	1	0.020	0.678
36	3.1290	1.5	1	2	0.010	0.139				
							1.5	0	0.005	0.072
							2.5	2	0.010	1.745
37	3.1309	2.5	1	2			0.012		0.166	
					2.5	0	0.012	0.171		
38	3.1319	0.5	1	0	0.095	0.187				
39	3.1336	1.5	1	2	0.005	0.069				
							1.5	0	0.005	0.071
							2.5	2	0.025	4.295
40	3.1346	1.5	-1	1	0.017	0.063				
							1.5	1	0.060	1.992
41	3.1351	1.5	-1	1	0.015	0.056				
							1.5	1	0.040	1.326
42	3.1390	1.5	1	2	0.005	0.068				
43	3.1401	1.5	1	2	0.010	0.136				
							1.5	0	0.005	0.070
							2.5	2	0.015	2.520
44	3.1403	0.5	-1	1	0.015	0.055				
							1.5	1	0.015	0.489
45	3.1438	1.5	1	2	0.005	0.068				
46	3.1453	0.5	1	0	0.090	0.174				
							2.5	2	0.050	8.253
47	3.1472	2.5	1	2	0.060	0.806				
							2.5	0	0.040	0.545
48	3.1496	1.5	-1	1	0.025	0.091				
							1.5	1	0.035	1.109
							2.5	1	0.020	0.634
49	3.1504	1.5	1	2	0.005	0.067				

^{49}V Resonance Parameters

#	Energy (MeV)	J	π	l_p	Γ_p (KeV)	γ^2_p (KeV)	$s_{p'}$	$l_{p'}$	$\Gamma_{p'}$	$\gamma^2_{p'}$ (KeV)
							1.5	0	0.010	0.135
50	3.1517	0.5	-1	1	0.012	0.043				
51	3.1523	1.5	1	2	0.008	0.106				
							1.5	0	0.005	0.067
							2.5	2	0.010	1.612
52	3.1551	2.5	1	2	0.012	0.159				
							2.5	0	0.035	0.466
53	3.1568	1.5	-1	1	0.025	0.090				
54	3.1569	0.5	1	0	0.110	0.210				
55	3.1575	1.5	1	2	0.078	1.028				
							1.5	0	0.040	0.529
							2.5	2	0.030	4.750
56	3.1575	0.5	-1	1	0.050	0.179				
							1.5	1	0.005	0.155
57	3.1582	2.5	1	2	0.053	0.698				
							2.5	0	0.030	0.396
58	3.1594	1.5	-1	1	0.050	0.178				
							1.5	1	0.030	0.923
							2.5	1	0.010	0.308
59	3.1631	1.5	1	2	0.060	0.783				
							1.5	0	0.010	0.130
							2.5	2	0.005	0.777
60	3.1658	0.5	-1	1	0.040	0.141				
							1.5	1	0.030	0.905
61	3.1662	2.5	1	2	0.030	0.389				
							2.5	0	0.008	0.103
62	3.1676	2.5	1	2	0.047	0.608				
							2.5	0	0.020	0.257
63	3.1703	1.5	-1	1	0.035	0.123				
							1.5	1	0.025	0.744
64	3.1739	0.5	1	0	0.710	1.325				
							2.5	2	0.110	16.480
65	3.1743	1.5	-1	1	0.015	0.052				
							1.5	1	0.070	2.057
							2.5	1	0.060	1.763
66	3.1758	2.5	1	2	0.020	0.255				
							2.5	0	0.030	0.377
67	3.1765	1.5	-1	1	0.008	0.028				
							1.5	1	0.010	0.292
68	3.1771	1.5	1	2	0.035	0.445				
69	3.1774	0.5	-1	1	0.245	0.851				
							1.5	1	0.070	2.038
70	3.1783	1.5	1	2	0.013	0.165				
							1.5	0	0.010	0.125
							2.5	2	0.020	2.953

^{49}V Resonance Parameters

#	Energy (MeV)	J	π	l_p	Γ_p (KeV)	γ^2_p (KeV)	$S_{p'}$	$l_{p'}$	$\Gamma_{p'}$	$\gamma^2_{p'}$ (KeV)
71	3.1846	1.5	1	2	0.006	0.075				
72	3.1859	1.5	-1	1	0.038	0.130				
							1.5	1	0.020	0.568
							2.5	1	0.010	0.284
73	3.1893	0.5	-1	1	0.050	0.171				
74	3.1896	2.5	1	2	0.010	0.124				
75	3.1898	0.5	1	0	0.235	0.430				
76	3.1934	2.5	1	2	0.005	0.062				
							2.5	0	0.020	0.239
							2.5	2	0.025	3.509
							1.5	2	0.005	0.702
77	3.1971	1.5	1	2	0.005	0.061				
78	3.1986	0.5	1	0	0.375	0.679				
							2.5	2	0.020	2.760
79	3.1988	1.5	-1	1	0.018	0.061				
							1.5	1	0.020	0.546
80	3.1993	0.5	-1	1	0.030	0.101				
81	3.2012	1.5	-1	1	0.010	0.034				
82	3.2017	2.5	1	2	0.015	0.183				
83	3.2066	2.5	1	2	0.040	0.483				
							2.5	0	0.060	0.692
84	3.2100	0.5	-1	1	0.195	0.646				
85	3.2123	2.5	1	2	0.012	0.144				
							2.5	0	0.070	0.795
86	3.2137	1.5	1	2	0.022	0.262				
							1.5	0	0.050	0.566
87	3.2148	0.5	-1	1	0.390	1.284				
88	3.2184	1.5	-1	1	0.010	0.033				
89	3.2187	0.5	1	0	0.380	0.671				
90	3.2196	1.5	1	2	0.035	0.413				
							1.5	0	0.040	0.445
							2.5	2	0.040	5.154
91	3.2217	0.5	-1	1	0.065	0.212				
92	3.2220	0.5	1	0	0.080	0.141				
							2.5	2	0.020	2.557
93	3.2221	1.5	-1	1	0.030	0.098				
							1.5	1	0.030	0.765
94	3.2232	0.5	-1	1	0.012	0.039				
							1.5	1	0.020	0.509
95	3.2239	2.5	1	2	0.010	0.117				
							2.5	0	0.010	0.110
							2.5	2	0.010	1.271
96	3.2244	1.5	-1	1	0.012	0.039				
							1.5	1	0.035	0.887
97	3.2253	2.5	1	2	0.006	0.070				

^{49}V Resonance Parameters

#	Energy (MeV)	J	π	l_p	Γ_p (KeV)	γ^2_p (KeV)	$s_{p'}$	$l_{p'}$	$\Gamma_{p'}$	$\gamma^2_{p'}$ (KeV)
98	3.2307	2.5	1	2	0.016	0.185				
99	3.2325	1.5	1	2	0.065	0.751				
							1.5	0	0.020	0.215
							2.5	2	0.020	2.472
100	3.2331	1.5	-1	1	0.010	0.032				
101	3.2343	1.5	1	2	0.005	0.058				
102	3.2352	2.5	1	2	0.005	0.057				
							2.5	0	0.010	0.107
							2.5	2	0.010	1.225
103	3.2380	1.5	1	2	0.005	0.057				
104	3.2382	0.5	-1	1	0.020	0.064				
105	3.2399	1.5	-1	1	0.035	0.111				
							1.5	1	0.020	0.485
							2.5	1	0.010	0.242
106	3.2419	2.5	1	2	0.108	1.227				
							2.5	0	0.065	0.682
107	3.2423	0.5	-1	1	0.050	0.158				
108	3.2455	1.5	-1	1	0.012	0.038				
							1.5	1	0.020	0.477
109	3.2463	1.5	1	2	0.008	0.090				
							1.5	0	0.030	0.311
110	3.2470	1.5	-1	1	0.043	0.135				
							1.5	1	0.030	0.712
111	3.2482	2.5	1	2	0.010	0.112				
							2.5	0	0.040	0.413
112	3.2490	0.5	1	0	0.240	0.409				
							1.5	2	0.040	4.691
113	3.2492	2.5	1	2	0.033	0.370				
							2.5	0	0.007	0.072
114	3.2527	0.5	1	0	0.330	0.559				
115	3.2533	0.5	-1	1	0.230	0.717				
116	3.2560	1.5	-1	1	0.100	0.311				
							1.5	1	0.015	0.347
117	3.2571	0.5	-1	1	0.060	0.186				
118	3.2579	1.5	1	2	0.015	0.166				
							1.5	0	0.025	0.252
							2.5	2	0.020	2.280
119	3.2603	1.5	1	2	0.023	0.253				
							1.5	0	0.015	0.150
120	3.2610	2.5	1	2	0.020	0.220				
							2.5	0	0.015	0.150
121	3.2613	2.5	1	2	0.008	0.088				
122	3.2615	1.5	-1	1	0.028	0.086				
							1.5	1	0.020	0.456
123	3.2650	1.5	1	2	0.008	0.087				

^{49}V Resonance Parameters

#	Energy (MeV)	J	π	l_p	Γ_p (KeV)	γ^2_p (KeV)	$s_{p'}$	$l_{p'}$	$\Gamma_{p'}$	$\gamma^2_{p'}$ (KeV)
							1.5	0	0.010	0.099
							2.5	2	0.030	3.345
124	3.2669	2.5	1	2	0.008	0.087				
125	3.2670	0.5	1	0	0.065	0.108				
							2.5	2	0.020	2.216
126	3.2671	1.5	-1	1	0.025	0.076				
							1.5	1	0.020	0.449
127	3.2679	1.5	1	2	0.015	0.163				
128	3.2687	2.5	1	2	0.007	0.076				
129	3.2694	1.5	-1	1	0.028	0.085				
130	3.2729	1.5	1	2	0.110	1.186				
							1.5	0	0.080	0.774
131	3.2736	0.5	-1	1	0.060	0.182				
							1.5	1	0.015	0.331
132	3.2741	1.5	1	2	0.052	0.559				
							1.5	0	0.045	0.434
							2.5	2	0.010	1.083
133	3.2746	1.5	-1	1	0.008	0.024				
							1.5	1	0.015	0.329
134	3.2752	0.5	-1	1	0.020	0.061				
135	3.2757	2.5	1	2	0.058	0.622				
							2.5	0	0.015	0.144
							1.5	2	0.015	1.618
							2.5	2	0.030	3.235
136	3.2777	1.5	-1	1	0.115	0.347				
							2.5	1	0.020	0.436
137	3.2781	2.5	1	2	0.015	0.160				
							2.5	0	0.010	0.095
138	3.2798	1.5	1	2	0.025	0.266				
139	3.2798	0.5	1	0	0.810	1.330				
140	3.2801	2.5	1	2	0.050	0.532				
141	3.2804	1.5	-1	1	0.105	0.315				
							1.5	1	0.025	0.540
							2.5	1	0.030	0.649
142	3.2804	0.5	-1	1	0.052	0.156				
							1.5	1	0.030	0.648
143	3.2812	2.5	1	2	0.025	0.266				
							2.5	0	0.005	0.047
							2.5	2	0.020	2.120
144	3.2812	1.5	-1	1	0.015	0.045				
							1.5	1	0.055	1.186
145	3.2840	0.5	-1	1	0.015	0.045				
146	3.2849	0.5	1	0	0.020	0.033				
							2.5	2	0.015	1.572
147	3.2877	1.5	1	2	0.037	0.389				

^{49}V Resonance Parameters

#	Energy (MeV)	J	π	l_p	Γ_p (KeV)	γ^2_p (KeV)	$s_{p'}$	$l_{p'}$	$\Gamma_{p'}$	$\gamma^2_{p'}$ (KeV)
							1.5	0	0.005	0.047
							2.5	2	0.015	1.558
148	3.2877	1.5	-1	1	0.006	0.018				
							1.5	1	0.015	0.318
149	3.2889	1.5	1	2	0.012	0.126				
150	3.2904	2.5	1	2	0.040	0.419				
							2.5	0	0.015	0.139
							2.5	2	0.015	1.545
							1.5	2	0.015	1.545
151	3.2908	0.5	-1	1	0.025	0.074				
152	3.2908	0.5	1	0	0.290	0.470				
							2.5	2	0.020	2.058
153	3.2912	1.5	1	2	0.008	0.084				
							1.5	0	0.008	0.074
154	3.2920	0.5	-1	1	0.018	0.053				
							1.5	1	0.020	0.419
155	3.2930	1.5	-1	1	0.015	0.044				
							1.5	1	0.015	0.313
156	3.2936	1.5	1	2	0.015	0.156				
							1.5	0	0.005	0.046
							2.5	2	0.020	2.040
157	3.2940	0.5	-1	1	0.145	0.428				
							1.5	1	0.060	1.249
158	3.2968	0.5	1	0	0.020	0.032				
							2.5	2	0.025	2.526
159	3.2981	1.5	-1	1	0.045	0.132				
							1.5	1	0.010	0.206
160	3.2988	2.5	1	2	0.035	0.361				
							2.5	0	0.035	0.317
161	3.2991	1.5	-1	1	0.010	0.029				
							1.5	1	0.010	0.205
162	3.3006	1.5	1	2	0.018	0.185				
							1.5	0	0.010	0.090
							2.5	2	0.025	2.496
163	3.3034	0.5	1	0	0.020	0.032				
							2.5	2	0.050	4.949
164	3.3045	0.5	-1	1	0.015	0.044				
165	3.3050	2.5	1	2	0.035	0.357				
							2.5	0	0.010	0.089
166	3.3053	1.5	-1	1	0.015	0.044				
							1.5	1	0.015	0.303
167	3.3062	1.5	1	2	0.005	0.051				
168	3.3071	2.5	1	2	0.015	0.153				
							2.5	0	0.012	0.106
							1.5	2	0.012	1.175

^{49}V Resonance Parameters

#	Energy (MeV)	J	π	l_p	Γ_p (KeV)	γ^2_p (KeV)	$s_{p'}$	$l_{p'}$	$\Gamma_{p'}$	$\gamma^2_{p'}$ (KeV)
							2.5	2	0.015	1.468
169	3.3077	1.5	1	2	0.015	0.153				
							1.5	0	0.005	0.044
							2.5	2	0.005	0.488
170	3.3080	0.5	-1	1	0.350	1.013				
							1.5	1	0.060	1.202
171	3.3095	1.5	1	2	0.035	0.355				
							1.5	0	0.080	0.706
							2.5	2	0.030	2.915
172	3.3099	1.5	-1	1	0.032	0.092				
							1.5	1	0.020	0.399
							2.5	1	0.005	0.100
173	3.3106	1.5	-1	1	0.033	0.095				
174	3.3108	2.5	1	2	0.048	0.486				
							2.5	0	0.020	0.176
175	3.3131	2.5	1	2	0.042	0.423				
176	3.3149	0.5	-1	1	0.025	0.072				
177	3.3152	2.5	1	2	0.210	2.109				
							2.5	0	0.030	0.261
							1.5	2	0.030	2.865
178	3.3153	2.5	-1	3	0.018	1.197				
							1.5	1	0.020	0.393
179	3.3154	0.5	1	0	0.880	1.387				
180	3.3159	2.5	1	2	0.023	0.231				
							2.5	0	0.015	0.130
181	3.3165	2.5	1	2	0.012	0.120				
182	3.3190	1.5	-1	1	0.140	0.399				
							2.5	1	0.080	1.556
183	3.3196	1.5	1	2	0.025	0.249				
							1.5	0	0.005	0.043
184	3.3197	0.5	-1	1	0.020	0.057				
185	3.3202	2.5	1	2	0.020	0.199				
							2.5	0	0.040	0.344
186	3.3204	2.5	1	2	0.073	0.727				
							2.5	0	0.040	0.343
							2.5	2	0.040	3.761
							1.5	2	0.035	3.291
187	3.3229	1.5	1	2	0.010	0.099				
							1.5	0	0.010	0.085
188	3.3236	1.5	-1	1	0.150	0.425				
							1.5	1	0.030	0.576
189	3.3242	2.5	1	2	0.024	0.237				
							2.5	0	0.020	0.170
190	3.3273	2.5	1	2	0.072	0.709				
							2.5	0	0.070	0.591

^{49}V Resonance Parameters

#	Energy (MeV)	J	π	l_p	Γ_p (KeV)	γ^2_p (KeV)	$s_{p'}$	$l_{p'}$	$\Gamma_{p'}$	$\gamma^2_{p'}$ (KeV)
							1.5	2	0.060	5.525
							2.5	2	0.060	5.525
191	3.3275	1.5	-1	1	0.020	0.056				
							1.5	1	0.020	0.380
192	3.3286	2.5	1	2	0.009	0.088				
							2.5	0	0.015	0.126
							2.5	2	0.010	0.917
193	3.3289	0.5	-1	1	0.030	0.084				
							1.5	1	0.060	1.137
194	3.3315	1.5	-1	1	0.030	0.084				
195	3.3317	0.5	1	0	0.215	0.333				
							2.5	2	0.040	3.635
196	3.3319	1.5	1	2	0.028	0.274				
197	3.3340	2.5	1	2	0.005	0.049				
198	3.3345	1.5	-1	1	0.010	0.028				
199	3.3381	0.5	-1	1	0.015	0.042				
200	3.3396	1.5	-1	1	0.040	0.111				
							1.5	1	0.015	0.276
							2.5	1	0.025	0.460
201	3.3398	1.5	1	2	0.030	0.289				
							1.5	0	0.005	0.041
							2.5	2	0.030	2.661
202	3.3419	0.5	1	0	0.375	0.574				
203	3.3422	2.5	1	2	0.010	0.096				
204	3.3444	1.5	-1	1	0.030	0.083				
							1.5	1	0.045	0.818
							2.5	1	0.060	1.091
205	3.3457	1.5	-1	1	0.017	0.047				
							1.5	1	0.050	0.906
							2.5	1	0.010	0.181
206	3.3465	0.5	-1	1	0.065	0.179				
207	3.3473	2.5	1	2	0.008	0.076				
208	3.3482	0.5	-1	1	0.025	0.069				
209	3.3484	0.5	1	0	0.115	0.175				
210	3.3489	2.5	1	2	0.007	0.067				
211	3.3531	2.5	1	2	0.080	0.755				
							2.5	0	0.030	0.238
212	3.3538	0.5	-1	1	0.060	0.163				
213	3.3539	0.5	1	0	0.135	0.204				
214	3.3545	2.5	1	2	0.006	0.056				
215	3.3549	1.5	1	2	0.008	0.075				
							1.5	0	0.010	0.079
					2.5	2	0.015	1.272		
216	3.3576	1.5	1	2	0.015	0.140				
							1.5	0	0.050	0.392

^{49}V Resonance Parameters

#	Energy (MeV)	J	π	l_p	Γ_p (KeV)	γ^2_p (KeV)	$s_{p'}$	$l_{p'}$	$\Gamma_{p'}$	$\gamma^2_{p'}$ (KeV)
							2.5	2	0.050	4.207
217	3.3580	1.5	-1	1	0.012	0.033				
							1.5	1	0.020	0.351
218	3.3603	1.5	-1	1	0.020	0.054				
							1.5	1	0.030	0.523
219	3.3610	0.5	-1	1	0.020	0.054				
220	3.3613	0.5	1	0	0.135	0.202				
221	3.3636	0.5	-1	1	0.790	2.125				
222	3.3643	1.5	-1	1	0.075	0.201				
							1.5	1	0.050	0.863
							2.5	1	0.120	2.071
223	3.3656	1.5	1	2	0.165	1.526				
							1.5	0	0.080	0.615
							2.5	2	0.020	1.644
224	3.3660	2.5	1	2	0.015	0.139				
225	3.3660	0.5	-1	1	0.020	0.054				
							1.5	1	0.020	0.344
226	3.3684	2.5	1	2	0.008	0.074				
							2.5	0	0.040	0.306
227	3.3710	1.5	-1	1	0.070	0.186				
							1.5	1	0.035	0.593
228	3.3737	2.5	1	2	0.023	0.210				
229	3.3740	1.5	-1	1	0.060	0.159				
230	3.3741	1.5	1	2	0.035	0.319				
231	3.3749	0.5	-1	1	0.075	0.199				
							1.5	1	0.050	0.839
232	3.3790	2.5	1	2	0.025	0.226				
							2.5	0	0.050	0.373
							2.5	2	0.040	3.162
							1.5	2	0.020	1.581
233	3.3807	0.5	-1	1	0.375	0.987				
							1.5	1	0.050	0.827
234	3.3812	2.5	1	2	0.010	0.090				
							2.5	0	0.015	0.111
235	3.3826	2.5	1	2	0.025	0.225				
236	3.3826	0.5	1	0	0.790	1.156				
							2.5	2	0.040	3.129
237	3.3830	1.5	-1	1	0.220	0.577				
							1.5	1	0.025	0.411
238	3.3836	2.5	1	2	0.020	0.180				
239	3.3842	2.5	1	2	0.010	0.090				
							2.5	0	0.020	0.147
240	3.3858	1.5	1	2	0.012	0.108				
							1.5	0	0.010	0.073
241	3.3860	1.5	-1	1	0.042	0.110				

^{49}V Resonance Parameters

#	Energy (MeV)	J	π	l_p	Γ_p (KeV)	γ^2_p (KeV)	$S_{p'}$	$l_{p'}$	$\Gamma_{p'}$	$\gamma^2_{p'}$ (KeV)
							1.5	1	0.120	1.958
							2.5	1	0.060	0.979
242	3.3870	2.5	1	2	0.065	0.581				
							2.5	0	0.015	0.110
243	3.3872	0.5	-1	1	0.025	0.065				
244	3.3881	2.5	1	2	0.024	0.214				
245	3.3882	0.5	1	0	0.080	0.116				
							2.5	2	0.040	3.079
246	3.3883	1.5	-1	1	0.078	0.203				
							1.5	1	0.060	0.973
247	3.3911	2.5	1	2	0.018	0.160				
							2.5	0	0.050	0.362
248	3.3937	0.5	-1	1	0.130	0.336				
249	3.3950	1.5	-1	1	0.062	0.160				
							2.5	1	0.040	0.638
250	3.3988	2.5	1	2	0.028	0.246				
							2.5	0	0.040	0.285
251	3.4004	1.5	-1	1	0.015	0.038				
							2.5	1	0.020	0.315
252	3.4007	2.5	1	2	0.020	0.175				
253	3.4012	0.5	1	0	0.700	1.004				
254	3.4016	2.5	1	2	0.083	0.725				
							2.5	0	0.005	0.035
255	3.4017	0.5	1	0	0.630	0.903				
							2.5	2	0.030	2.222
256	3.4018	1.5	-1	1	0.045	0.115				
							2.5	1	0.005	0.078
257	3.4046	1.5	1	2	0.055	0.478				
							1.5	0	0.030	0.211
							1.5	2	0.030	2.203
							2.5	2	0.040	2.938
258	3.4054	1.5	1	2	0.012	0.104				
							1.5	0	0.020	0.140
							2.5	2	0.020	1.465
259	3.4054	0.5	-1	1	0.015	0.038				
							1.5	1	0.020	0.311
260	3.4060	2.5	1	2	0.010	0.087				
							2.5	0	0.010	0.070
261	3.4067	1.5	1	2	0.158	1.369				
							1.5	0	0.055	0.384
							1.5	2	0.055	4.015
							2.5	2	0.070	5.110
262	3.4069	1.5	-1	1	0.035	0.089				
							1.5	1	0.030	0.464
263	3.4086	1.5	1	2	0.010	0.086				

^{49}V Resonance Parameters

#	Energy (MeV)	J	π	l_p	Γ_p (KeV)	γ^2_p (KeV)	$s_{p'}$	$l_{p'}$	$\Gamma_{p'}$	$\gamma^2_{p'}$ (KeV)
							1.5	0	0.005	0.035
							2.5	2	0.025	1.815
264	3.4100	1.5	1	2	0.115	0.991				
							1.5	0	0.120	0.832
265	3.4104	1.5	-1	1	0.008	0.020				
							1.5	1	0.020	0.307
266	3.4117	1.5	1	2	0.008	0.069				
267	3.4148	2.5	1	2	0.068	0.582				
							2.5	0	0.010	0.069
268	3.4168	1.5	-1	1	0.095	0.239				
							1.5	1	0.020	0.302
269	3.4174	1.5	1	2	0.025	0.213				
							1.5	0	0.015	0.102
270	3.4186	0.5	1	0	0.525	0.739				
							2.5	2	0.020	1.411
271	3.4191	2.5	1	2	0.010	0.085				
272	3.4236	1.5	-1	1	0.050	0.125				
							1.5	1	0.015	0.223
							2.5	1	0.015	0.223
273	3.4241	1.5	1	2	0.010	0.084				
274	3.4246	1.5	-1	1	0.020	0.050				
							1.5	1	0.020	0.296
275	3.4248	0.5	1	0	0.115	0.161				
							2.5	2	0.050	3.468
276	3.4254	1.5	1	2	0.017	0.143				
							1.5	0	0.005	0.033
							2.5	2	0.010	0.692
277	3.4272	1.5	-1	1	0.030	0.074				
278	3.4307	2.5	1	2	0.015	0.125				
							2.5	0	0.015	0.099
279	3.4323	1.5	1	2	0.080	0.666				
							1.5	0	0.020	0.132
280	3.4325	1.5	-1	1	0.025	0.062				
281	3.4331	2.5	1	2	0.032	0.266				
282	3.4333	0.5	1	0	1.150	1.594				
283	3.4335	0.5	-1	1	0.040	0.098				
284	3.4340	2.5	1	2	0.005	0.042				
							2.5	0	0.020	0.131
							2.5	2	0.010	0.676
285	3.4386	1.5	-1	1	0.080	0.196				
							1.5	1	0.020	0.286
							2.5	1	0.010	0.143
286	3.4392	2.5	1	2	0.006	0.049				
287	3.4420	1.5	1	2	0.005	0.041				
288	3.4451	1.5	1	2	0.010	0.082				

^{49}V Resonance Parameters

#	Energy (MeV)	J	π	l_p	Γ_p (KeV)	γ^2_p (KeV)	$s_{p'}$	$l_{p'}$	$\Gamma_{p'}$	$\gamma^2_{p'}$ (KeV)
289	3.4456	0.5	-1	1	0.035	0.085				
290	3.4461	0.5	1	0	0.110	0.150				
							2.5	2	0.025	1.634
291	3.4478	1.5	1	2	0.068	0.553				
							1.5	0	0.005	0.032
							2.5	2	0.020	1.301
292	3.4487	0.5	1	0	0.060	0.082				
							2.5	2	0.050	3.244
293	3.4488	2.5	1	2	0.035	0.284				
							2.5	0	0.016	0.102
							2.5	2	0.012	0.779
294	3.4490	1.5	-1	1	0.060	0.145				
							1.5	1	0.020	0.279
							2.5	1	0.035	0.488
295	3.4492	1.5	1	2	0.090	0.730				
							1.5	0	0.065	0.413
296	3.4505	0.5	-1	1	0.055	0.133				
							1.5	1	0.020	0.278
297	3.4510	1.5	-1	1	0.040	0.096				
							1.5	1	0.010	0.139
298	3.4512	2.5	1	2	0.075	0.606				
299	3.4516	0.5	1	0	0.500	0.680				
300	3.4526	0.5	-1	1	0.010	0.024				
301	3.4542	1.5	-1	1	0.010	0.024				
302	3.4546	0.5	1	0	0.410	0.556				
							1.5	2	0.020	1.277
303	3.4547	1.5	-1	1	0.030	0.072				
							1.5	1	0.020	0.275
304	3.4553	1.5	1	2	0.008	0.064				
305	3.4585	0.5	1	0	0.015	0.020				
306	3.4592	0.5	-1	1	0.020	0.048				
307	3.4602	1.5	1	2	0.055	0.438				
							1.5	0	0.005	0.031
							2.5	2	0.025	1.571
308	3.4607	1.5	-1	1	0.135	0.321				
							1.5	1	0.040	0.542
309	3.4615	2.5	1	2	0.008	0.064				
310	3.4623	1.5	1	2	0.010	0.079				
							1.5	0	0.005	0.031
							2.5	2	0.020	1.250
311	3.4636	1.5	-1	1	0.012	0.028				
							1.5	1	0.050	0.673
							2.5	1	0.030	0.404
312	3.4642	2.5	1	2	0.105	0.832				
							2.5	0	0.010	0.061

^{49}V Resonance Parameters

#	Energy (MeV)	J	π	l_p	Γ_p (KeV)	γ^2_p (KeV)	$s_{p'}$	$l_{p'}$	$\Gamma_{p'}$	$\gamma^2_{p'}$ (KeV)
313	3.4648	1.5	-1	1	0.017	0.040				
314	3.4649	0.5	1	0	1.150	1.543				
315	3.4684	1.5	-1	1	0.018	0.042				
							1.5	1	0.015	0.199
							2.5	1	0.010	0.133
316	3.4699	0.5	-1	1	0.220	0.518				
							1.5	1	0.095	1.259
317	3.4701	0.5	1	0	0.015	0.020				
							2.5	2	0.020	1.223
318	3.4705	1.5	1	2	0.008	0.063				
							1.5	0	0.005	0.030
							2.5	2	0.010	0.611
319	3.4715	1.5	1	2	0.022	0.172				
							1.5	0	0.010	0.060
							2.5	2	0.030	1.828
320	3.4719	0.5	-1	1	0.008	0.019				
321	3.4749	0.5	1	0	0.020	0.027				
							2.5	2	0.020	1.208
322	3.4750	1.5	1	2	0.010	0.078				
							1.5	0	0.010	0.060
							2.5	2	0.025	1.509
323	3.4753	1.5	-1	1	0.015	0.035				
							1.5	1	0.015	0.196
							2.5	1	0.010	0.131
324	3.4757	2.5	1	2	0.008	0.062				
							2.5	0	0.020	0.120
325	3.4774	2.5	1	2	0.060	0.466				
326	3.4774	0.5	1	0	1.630	2.159				
							2.5	2	0.020	1.199
327	3.4776	1.5	-1	1	0.045	0.105				
328	3.4778	0.5	1	0	0.200	0.265				
329	3.4787	2.5	1	2	0.005	0.039				
330	3.4799	1.5	1	2	0.040	0.310				
331	3.4800	1.5	-1	1	0.005	0.012				
332	3.4809	2.5	1	2	0.008	0.062				
333	3.4819	0.5	-1	1	0.015	0.035				
334	3.4834	1.5	-1	1	0.038	0.088				
							1.5	1	0.060	0.770
							2.5	1	0.060	0.770
335	3.4842	1.5	1	2	0.020	0.154				
							1.5	0	0.005	0.029
							2.5	2	0.025	1.472
336	3.4856	2.5	1	2	0.070	0.537				
							2.5	0	0.010	0.059
							1.5	2	0.030	1.760

^{49}V Resonance Parameters

#	Energy (MeV)	J	π	l_p	Γ_p (KeV)	γ^2_p (KeV)	$s_{p'}$	$l_{p'}$	$\Gamma_{p'}$	$\gamma^2_{p'}$ (KeV)
							2.5	2	0.030	1.760
337	3.4856	1.5	-1	1	0.043	0.099				
							1.5	1	0.015	0.191
338	3.4885	1.5	-1	1	0.035	0.081				
339	3.4889	0.5	-1	1	0.160	0.368				
							1.5	1	0.025	0.317
340	3.4896	1.5	-1	1	0.070	0.161				
							1.5	1	0.020	0.253
							2.5	1	0.025	0.316
341	3.4902	2.5	1	2	0.085	0.648				
							2.5	0	0.010	0.058
							2.5	2	0.010	0.579
342	3.4903	0.5	-1	1	0.040	0.092				
343	3.4934	1.5	-1	1	0.095	0.217				
							1.5	1	0.060	0.752
							2.5	1	0.015	0.188
344	3.4939	0.5	1	0	0.020	0.026				
							2.5	2	0.020	1.147
345	3.4950	1.5	-1	1	0.090	0.206				
							2.5	1	0.025	0.312
							1.5	1	0.020	0.250
346	3.4959	2.5	1	2	0.072	0.544				
347	3.4983	1.5	1	2	0.015	0.113				
348	3.4987	1.5	-1	1	0.010	0.023				
349	3.5012	1.5	1	2	0.050	0.375				
							1.5	0	0.030	0.170
							1.5	2	0.030	1.688
							2.5	2	0.020	1.125
350	3.5014	0.5	1	0	0.120	0.155				
							2.5	2	0.120	6.746
351	3.5015	2.5	-1	3	0.006	0.280				
352	3.5020	1.5	1	2	0.080	0.599				
							2.5	2	0.008	0.449
353	3.5020	0.5	1	0	0.575	0.743				
							2.5	2	0.020	1.123
354	3.5022	1.5	-1	1	0.250	0.566				
							1.5	1	0.005	0.061
355	3.5029	2.5	1	2	0.065	0.486				
							2.5	0	0.065	0.367
356	3.5034	0.5	-1	1	0.015	0.034				
							1.5	1	0.030	0.367
357	3.5059	1.5	-1	1	0.050	0.113				
							1.5	1	0.050	0.609
358	3.5067	2.5	1	2	0.058	0.431				
							2.5	0	0.100	0.561

^{49}V Resonance Parameters

#	Energy (MeV)	J	π	l_p	Γ_p (KeV)	γ^2_p (KeV)	$s_{p'}$	$l_{p'}$	$\Gamma_{p'}$	$\gamma^2_{p'}$ (KeV)
359	3.5072	0.5	-1	1	0.057	0.128				
							1.5	1	0.070	0.849
360	3.5082	1.5	-1	1	0.018	0.040				
361	3.5086	1.5	1	2	0.073	0.541				
							1.5	0	0.060	0.335
							2.5	2	0.060	3.308
362	3.5098	1.5	-1	1	0.035	0.079				
							1.5	1	0.050	0.603
363	3.5108	0.5	-1	1	0.010	0.022				
364	3.5115	0.5	1	0	0.900	1.152				
							2.5	2	0.020	1.095
365	3.5122	2.5	1	2	0.050	0.368				
							2.5	0	0.070	0.388
							2.5	2	0.070	3.823
							1.5	2	0.020	1.092
366	3.5128	1.5	-1	1	0.060	0.134				
							2.5	1	0.140	1.677
367	3.5130	2.5	1	2	0.085	0.626				
							2.5	0	0.035	0.194
							2.5	2	0.035	1.908
							1.5	2	0.010	0.545
368	3.5145	0.5	-1	1	0.020	0.045				
369	3.5153	2.5	1	2	0.025	0.183				
							2.5	0	0.020	0.110
370	3.5159	0.5	-1	1	0.050	0.111				
							1.5	1	0.040	0.476
371	3.5161	1.5	-1	1	0.020	0.045				
							2.5	1	0.025	0.297
							1.5	1	0.025	0.297
372	3.5186	0.5	-1	1	0.055	0.122				
							1.5	1	0.045	0.532
373	3.5202	1.5	-1	1	0.060	0.133				
							1.5	1	0.020	0.235
374	3.5208	1.5	-1	1	0.030	0.066				
							2.5	1	0.025	0.294
375	3.5211	2.5	-1	3	0.020	0.901				
							1.5	1	0.030	0.352
376	3.5214	0.5	-1	1	0.070	0.155				
							1.5	1	0.010	0.117
377	3.5228	0.5	-1	1	0.040	0.088				
							1.5	1	0.006	0.070
378	3.5235	1.5	-1	1	0.230	0.508				
379	3.5238	1.5	1	2	0.060	0.435				
							1.5	0	0.015	0.081
							2.5	2	0.015	0.794

^{49}V Resonance Parameters

#	Energy (MeV)	J	π	l_p	Γ_p (KeV)	γ^2_p (KeV)	$S_{p'}$	$l_{p'}$	$\Gamma_{p'}$	$\gamma^2_{p'}$ (KeV)
380	3.5243	1.5	-1	1	0.020	0.044				
							2.5	1	0.020	0.233
381	3.5252	0.5	-1	1	0.560	1.234				
382	3.5257	2.5	-1	3	0.030	1.340				
							2.5	1	0.040	0.465
383	3.5257	1.5	1	2	0.025	0.181				
							1.5	0	0.005	0.027
							1.5	2	0.010	0.527
384	3.5258	1.5	-1	1	0.320	0.705				
							2.5	1	0.055	0.639
							1.5	1	0.025	0.290
385	3.5262	0.5	-1	1	0.250	0.550				
386	3.5267	1.5	-1	1	0.220	0.484				
							1.5	1	0.100	1.160
							2.5	1	0.050	0.580
387	3.5273	0.5	1	0	0.460	0.580				
							2.5	2	0.100	5.249
388	3.5274	2.5	-1	3	0.025	1.114				
							2.5	1	0.100	1.158
							1.5	1	0.040	0.463
389	3.5278	1.5	-1	1	0.090	0.198				
							1.5	1	0.040	0.463
390	3.5282	1.5	-1	1	0.180	0.395				
							1.5	1	0.040	0.462
							2.5	1	0.010	0.116
391	3.5287	2.5	-1	3	0.035	1.556				
							2.5	1	0.010	0.116
							1.5	1	0.005	0.058
392	3.5288	0.5	1	0	0.060	0.076				
393	3.5292	1.5	1	2	0.010	0.072				
							1.5	0	0.020	0.107
							2.5	2	0.030	1.567
394	3.5296	2.5	1	2	0.008	0.057				
							2.5	0	0.015	0.080
							2.5	2	0.015	0.783
							1.5	2	0.015	0.783
395	3.5298	1.5	-1	1	0.007	0.015				
							2.5	1	0.010	0.115
							1.5	1	0.025	0.288
396	3.5307	1.5	1	2	0.018	0.129				
							1.5	0	0.005	0.027
							2.5	2	0.015	0.780
397	3.5313	1.5	1	2	0.030	0.215				
					1.5	0	0.005	0.027		
					2.5	2	0.010	0.519		

^{49}V Resonance Parameters

#	Energy (MeV)	J	π	l_p	Γ_p (KeV)	γ^2_p (KeV)	$s_{p'}$	$l_{p'}$	$\Gamma_{p'}$	$\gamma^2_{p'}$ (KeV)
398	3.5315	2.5	1	2	0.012	0.086				
399	3.5319	1.5	-1	1	0.040	0.087				
							1.5	1	0.055	0.630
							2.5	1	0.030	0.344
400	3.5320	2.5	-1	3	0.020	0.883				
							1.5	1	0.025	0.286
401	3.5343	1.5	1	2	0.080	0.571				
							1.5	0	0.060	0.318
							1.5	2	0.060	3.092
							2.5	2	0.060	3.092
402	3.5349	0.5	-1	1	0.015	0.033				
							1.5	1	0.030	0.341
403	3.5355	1.5	-1	1	0.075	0.163				
							1.5	1	0.055	0.625
							2.5	1	0.025	0.284
404	3.5375	2.5	1	2	0.025	0.177				
							2.5	2	0.020	1.022
405	3.5380	0.5	1	0	0.280	0.349				
406	3.5382	1.5	1	2	0.040	0.284				
407	3.5389	1.5	-1	1	0.100	0.217				
							1.5	1	0.030	0.338
							2.5	1	0.025	0.282
408	3.5402	1.5	-1	1	0.030	0.065				
							1.5	1	0.025	0.281
							2.5	1	0.015	0.169
409	3.5405	1.5	1	2	0.030	0.212				
							1.5	0	0.010	0.052
							2.5	2	0.030	1.521
410	3.5409	1.5	-1	1	0.020	0.043				
411	3.5414	2.5	1	2	0.010	0.071				
412	3.5414	0.5	1	0	0.080	0.099				
							2.5	2	0.030	1.518
413	3.5419	2.5	1	2	0.008	0.056				
414	3.5428	1.5	1	2	0.010	0.070				
							1.5	0	0.005	0.026
							2.5	2	0.015	0.756
415	3.5439	0.5	-1	1	0.190	0.410				
416	3.5445	1.5	-1	1	0.090	0.194				
							1.5	1	0.040	0.445
417	3.5459	1.5	1	2	0.025	0.175				
							2.5	2	0.040	2.000
418	3.5496	1.5	-1	1	0.070	0.150				
							1.5	1	0.050	0.550
419	3.5515	2.5	1	2	0.045	0.313				
420	3.5515	0.5	1	0	0.490	0.603				

^{49}V Resonance Parameters

#	Energy (MeV)	J	π	l_p	Γ_p (KeV)	γ^2_p (KeV)	$S_{p'}$	$l_{p'}$	$\Gamma_{p'}$	$\gamma^2_{p'}$ (KeV)
							2.5	2	0.020	0.985
421	3.5517	1.5	-1	1	0.025	0.053				
422	3.5540	2.5	1	2	0.013	0.090				
423	3.5540	0.5	1	0	0.055	0.068				
424	3.5553	2.5	1	2	0.015	0.104				
							2.5	0	0.010	0.051
425	3.5594	2.5	1	2	0.020	0.138				
426	3.5598	1.5	-1	1	0.010	0.021				
427	3.5605	1.5	1	2	0.015	0.103				
428	3.5610	0.5	1	0	0.050	0.061				
							2.5	2	0.060	2.885
429	3.5611	2.5	1	2	0.060	0.412				
							2.5	0	0.025	0.125
							1.5	2	0.020	0.961
							2.5	2	0.025	1.202
430	3.5621	1.5	-1	1	0.015	0.032				
							2.5	1	0.030	0.321
431	3.5637	0.5	1	0	0.050	0.061				
432	3.5637	2.5	1	2	0.030	0.205				
							2.5	0	0.060	0.299
433	3.5642	0.5	-1	1	0.020	0.042				
							1.5	1	0.030	0.320
434	3.5650	1.5	-1	1	0.080	0.168				
							1.5	1	0.030	0.319
435	3.5666	1.5	-1	1	0.065	0.137				
							1.5	1	0.030	0.318
							2.5	1	0.010	0.106
436	3.5671	2.5	1	2	0.007	0.048				
437	3.5673	0.5	1	0	0.260	0.315				
438	3.5679	1.5	1	2	0.008	0.054				
439	3.5685	0.5	1	0	0.025	0.030				
440	3.5692	2.5	1	2	0.010	0.068				
441	3.5697	1.5	1	2	0.015	0.102				
442	3.5697	1.5	-1	1	0.006	0.013				
							1.5	1	0.020	0.210
443	3.5707	1.5	1	2	0.045	0.304				
							1.5	0	0.040	0.197
							1.5	2	0.020	0.938
444	3.5711	2.5	1	2	0.045	0.304				
							2.5	0	0.030	0.147
							1.5	2	0.030	1.406
							2.5	2	0.010	0.469
445	3.5720	1.5	-1	1	0.009	0.019				
							1.5	1	0.020	0.209
							2.5	1	0.010	0.105

^{49}V Resonance Parameters

#	Energy (MeV)	J	π	l_p	Γ_p (KeV)	γ^2_p (KeV)	$S_{p'}$	$l_{p'}$	$\Gamma_{p'}$	$\gamma^2_{p'}$ (KeV)
446	3.5727	1.5	1	2	0.007	0.047				
447	3.5736	1.5	1	2	0.035	0.236				
							2.5	2	0.040	1.862
							1.5	0	0.040	0.196
448	3.5769	0.5	-1	1	0.080	0.166				
449	3.5782	1.5	1	2	0.050	0.335				
							2.5	2	0.030	1.380
							1.5	2	0.010	0.460
450	3.5786	2.5	1	2	0.012	0.080				
							2.5	2	0.010	0.460
451	3.5811	1.5	-1	1	0.030	0.062				
452	3.5816	2.5	1	2	0.060	0.400				
453	3.5817	0.5	1	0	0.420	0.502				
454	3.5818	1.5	-1	1	0.060	0.124				
							1.5	1	0.030	0.307
455	3.5820	0.5	1	0	0.060	0.072				
456	3.5831	1.5	1	2	0.035	0.233				
							1.5	0	0.040	0.192
457	3.5834	2.5	1	2	0.040	0.266				
							2.5	0	0.065	0.312
458	3.5851	1.5	1	2	0.005	0.033				
459	3.5875	1.5	1	2	0.015	0.099				
							1.5	2	0.020	0.899
							2.5	2	0.020	0.899
460	3.5896	2.5	1	2	0.025	0.165				
							2.5	0	0.030	0.142
461	3.5900	0.5	-1	1	0.010	0.020				
462	3.5906	1.5	1	2	0.010	0.066				
							1.5	0	0.010	0.047
463	3.5927	1.5	1	2	0.010	0.066				
							1.5	0	0.005	0.024
							2.5	2	0.015	0.665
464	3.5933	1.5	-1	1	0.080	0.163				
							1.5	1	0.010	0.100
							2.5	1	0.020	0.200
465	3.5943	2.5	1	2	0.008	0.052				
							2.5	0	0.005	0.023
							2.5	2	0.005	0.221
466	3.5946	1.5	1	2	0.005	0.033				
							2.5	2	0.010	0.441
467	3.5972	1.5	-1	1	0.025	0.051				
							2.5	1	0.025	0.248
468	3.5977	1.5	1	2	0.105	0.683				
							1.5	0	0.100	0.466
							1.5	2	0.030	1.314

^{49}V Resonance Parameters

#	Energy (MeV)	J	π	l_p	Γ_p (KeV)	γ^2_p (KeV)	$s_{p'}$	$l_{p'}$	$\Gamma_{p'}$	$\gamma^2_{p'}$ (KeV)
469	3.5990	1.5	-1	1	0.015	0.030				
							1.5	1	0.010	0.099
							2.5	1	0.005	0.049
470	3.5997	0.5	-1	1	0.075	0.152				
471	3.6013	1.5	1	2	0.055	0.356				
							1.5	0	0.010	0.046
							2.5	2	0.020	0.868
472	3.6027	2.5	1	2	0.020	0.129				
473	3.6028	0.5	1	0	0.440	0.516				
							2.5	2	0.070	3.027
474	3.6031	1.5	-1	1	0.020	0.040				
							1.5	1	0.010	0.098
							2.5	1	0.020	0.196
475	3.6077	1.5	1	2	0.015	0.096				
							1.5	0	0.020	0.091
476	3.6082	0.5	1	0	0.030	0.035				
							2.5	2	0.050	2.133
477	3.6114	1.5	1	2	0.010	0.064				
							2.5	2	0.020	0.846
478	3.6116	0.5	-1	1	0.055	0.110				
							1.5	1	0.075	0.720
479	3.6126	2.5	1	2	0.022	0.140				
							2.5	0	0.035	0.158
							1.5	2	0.025	1.055
							2.5	2	0.035	1.477
480	3.6139	0.5	-1	1	0.210	0.418				
							1.5	1	0.060	0.573
481	3.6148	0.5	1	0	0.220	0.255				
							1.5	2	0.040	1.679
482	3.6149	1.5	-1	1	0.030	0.060				
							1.5	1	0.020	0.191
483	3.6180	0.5	1	0	0.080	0.092				
							2.5	2	0.080	3.331
484	3.6186	1.5	1	2	0.046	0.291				
							1.5	0	0.035	0.157
							2.5	2	0.010	0.416
							1.5	2	0.010	0.416
485	3.6211	1.5	1	2	0.005	0.031				
							1.5	0	0.010	0.045
486	3.6216	0.5	-1	1	0.015	0.030				
							1.5	1	0.030	0.282
487	3.6243	0.5	-1	1	0.040	0.079				
488	3.6249	2.5	1	2	0.020	0.125				
489	3.6249	0.5	1	0	0.380	0.437				
							1.5	2	0.040	1.637

^{49}V Resonance Parameters

#	Energy (MeV)	J	π	l_p	Γ_p (KeV)	γ^2_p (KeV)	$s_{p'}$	$l_{p'}$	$\Gamma_{p'}$	$\gamma^2_{p'}$ (KeV)
490	3.6251	1.5	-1	1	0.020	0.039				
							1.5	1	0.020	0.186
491	3.6269	2.5	1	2	0.012	0.075				
							2.5	0	0.020	0.088
							2.5	2	0.020	0.815
492	3.6271	1.5	-1	1	0.030	0.059				
							2.5	1	0.080	0.743
493	3.6286	1.5	1	2	0.010	0.062				
							1.5	0	0.050	0.219
494	3.6294	1.5	-1	1	0.010	0.020				
							1.5	1	0.040	0.370
495	3.6337	0.5	-1	1	0.750	1.461				
							1.5	1	0.070	0.641
496	3.6343	1.5	-1	1	0.030	0.058				
							1.5	1	0.010	0.091
							2.5	1	0.005	0.046
497	3.6345	0.5	1	0	0.770	0.877				
							1.5	2	0.080	3.198
498	3.6347	1.5	-1	1	0.050	0.097				
							2.5	1	0.010	0.091
499	3.6356	2.5	1	2	0.015	0.093				
500	3.6360	2.5	1	2	0.085	0.524				
							2.5	0	0.010	0.043
501	3.6361	1.5	-1	1	0.005	0.010				
502	3.6375	1.5	1	2	0.012	0.074				
503	3.6379	0.5	-1	1	0.215	0.417				
							1.5	1	0.050	0.454
504	3.6418	1.5	-1	1	0.010	0.019				
505	3.6440	1.5	1	2	0.018	0.110				
							1.5	0	0.025	0.106
506	3.6450	1.5	1	2	0.240	1.461				
							1.5	2	0.160	6.234
							1.5	0	0.160	0.680
							2.5	2	0.140	5.454
507	3.6464	0.5	-1	1	0.045	0.086				
							1.5	1	0.070	0.624
508	3.6471	1.5	-1	1	0.040	0.077				
							2.5	1	0.030	0.267
509	3.6483	1.5	-1	1	0.030	0.058				
510	3.6485	2.5	1	2	0.035	0.212				
							2.5	0	0.010	0.042
511	3.6486	0.5	1	0	0.325	0.365				
							2.5	2	0.020	0.772
512	3.6502	1.5	-1	1	0.020	0.038				
							1.5	1	0.020	0.177

^{49}V Resonance Parameters

#	Energy (MeV)	J	π	l_p	Γ_p (KeV)	γ^2_p (KeV)	$s_{p'}$	$l_{p'}$	$\Gamma_{p'}$	$\gamma^2_{p'}$ (KeV)
							2.5	1	0.010	0.088
513	3.6512	2.5	1	2	0.006	0.036				
							2.5	2	0.020	0.767
514	3.6512	0.5	1	0	0.050	0.056				
515	3.6527	2.5	1	2	0.015	0.090				
516	3.6531	1.5	1	2	0.047	0.283				
							2.5	2	0.010	0.382
							1.5	2	0.020	0.764
517	3.6532	1.5	-1	1	0.018	0.034				
518	3.6549	0.5	-1	1	0.010	0.019				
519	3.6554	0.5	1	0	0.240	0.268				
							1.5	2	0.120	4.558
520	3.6557	2.5	1	2	0.020	0.120				
							2.5	0	0.025	0.104
							2.5	2	0.010	0.380
521	3.6569	1.5	-1	1	0.010	0.019				
522	3.6577	2.5	1	2	0.053	0.317				
							2.5	0	0.035	0.145
523	3.6580	2.5	1	2	0.025	0.149				
							2.5	0	0.010	0.041
524	3.6587	0.5	-1	1	0.007	0.013				
							1.5	1	0.020	0.174
525	3.6613	1.5	1	2	0.010	0.060				
							1.5	0	0.040	0.165
526	3.6639	2.5	1	2	0.030	0.178				
							2.5	0	0.020	0.082
							2.5	2	0.020	0.744
527	3.6641	2.5	1	2	0.023	0.136				
							2.5	0	0.010	0.041
528	3.6652	1.5	1	2	0.020	0.118				
							1.5	2	0.050	1.855
529	3.6660	0.5	1	0	0.055	0.061				
							2.5	2	0.050	1.851
530	3.6661	2.5	1	2	0.050	0.296				
							2.5	0	0.025	0.102
							1.5	2	0.025	0.925
							2.5	2	0.020	0.740
531	3.6673	1.5	-1	1	0.035	0.066				
							1.5	1	0.050	0.426
							2.5	1	0.020	0.171
532	3.6704	1.5	1	2	0.040	0.235				
							1.5	0	0.070	0.284
533	3.6715	0.5	1	0	1.380	1.520				
							2.5	2	0.200	7.308
534	3.6717	0.5	-1	1	0.060	0.112				

^{49}V Resonance Parameters

#	Energy (MeV)	J	π	l_p	Γ_p (KeV)	γ^2_p (KeV)	$s_{p'}$	$l_{p'}$	$\Gamma_{p'}$	$\gamma^2_{p'}$ (KeV)
							1.5	1	0.040	0.338
535	3.6725	2.5	1	2	0.095	0.557				
							2.5	0	0.020	0.081
							1.5	2	0.020	0.729
							2.5	2	0.010	0.364
536	3.6727	1.5	-1	1	0.025	0.047				
							1.5	1	0.020	0.169
537	3.6739	1.5	1	2	0.012	0.070				
							1.5	2	0.020	0.727
538	3.6779	2.5	1	2	0.007	0.041				
							2.5	0	0.020	0.080
539	3.6782	1.5	-1	1	0.015	0.028				
							2.5	1	0.020	0.167
							1.5	1	0.010	0.083
540	3.6835	0.5	1	0	0.020	0.022				
							2.5	2	0.020	0.710
541	3.6860	0.5	-1	1	0.095	0.175				
542	3.6883	1.5	1	2	0.015	0.086				
							2.5	2	0.015	0.526
							1.5	0	0.015	0.059
543	3.6886	1.5	-1	1	0.018	0.033				
							1.5	1	0.020	0.163
							2.5	1	0.010	0.082
544	3.6899	0.5	-1	1	0.325	0.596				
							1.5	1	0.050	0.407
545	3.6905	0.5	1	0	0.440	0.477				
							1.5	2	0.080	2.794
546	3.6911	2.5	1	2	0.015	0.086				
547	3.6923	0.5	-1	1	0.022	0.040				
							1.5	1	0.030	0.243
548	3.6944	0.5	1	0	0.040	0.043				
549	3.6946	1.5	-1	1	0.025	0.046				
550	3.6981	0.5	1	0	0.080	0.086				
							2.5	2	0.050	1.715
551	3.6981	2.5	1	2	0.080	0.453				
							2.5	0	0.005	0.019
							2.5	2	0.010	0.343
							1.5	2	0.035	1.200
552	3.6988	1.5	-1	1	0.025	0.045				
							1.5	1	0.030	0.240
553	3.6998	2.5	1	2	0.020	0.113				
554	3.7002	0.5	1	0	1.280	1.375				
							2.5	2	0.100	3.413
555	3.7009	2.5	1	2	0.040	0.226				
							2.5	0	0.040	0.153

^{49}V Resonance Parameters

#	Energy (MeV)	J	π	l_p	Γ_p (KeV)	γ^2_p (KeV)	$s_{p'}$	$l_{p'}$	$\Gamma_{p'}$	$\gamma^2_{p'}$ (KeV)
556	3.7011	1.5	1	2	0.030	0.169				
							1.5	2	0.030	1.022
557	3.7022	0.5	1	0	0.075	0.080				
							1.5	2	0.040	1.359
558	3.7036	0.5	-1	1	0.100	0.181				
							1.5	1	0.050	0.396
559	3.7104	1.5	1	2	0.165	0.918				
							1.5	0	0.025	0.094
							1.5	2	0.020	0.666
							2.5	2	0.080	2.665
560	3.7117	2.5	1	2	0.023	0.128				
							2.5	0	0.040	0.150
							2.5	2	0.040	1.329
							1.5	2	0.030	0.997
561	3.7126	2.5	1	2	0.010	0.056				
							2.5	0	0.020	0.075
562	3.7133	0.5	-1	1	0.450	0.805				
							1.5	1	0.060	0.466
563	3.7139	0.5	1	0	0.025	0.027				
							2.5	2	0.020	0.661
564	3.7153	1.5	-1	1	0.012	0.021				
565	3.7160	1.5	1	2	0.010	0.055				
566	3.7169	1.5	-1	1	0.015	0.027				
567	3.7176	2.5	1	2	0.025	0.138				
568	3.7176	0.5	1	0	0.380	0.402				
							2.5	2	0.040	1.311
569	3.7182	1.5	1	2	0.023	0.127				
							1.5	0	0.015	0.056
570	3.7197	1.5	1	2	0.010	0.055				
571	3.7207	2.5	1	2	0.022	0.121				
572	3.7208	0.5	1	0	0.015	0.016				
573	3.7210	1.5	1	2	0.050	0.274				
574	3.7225	2.5	1	2	0.037	0.203				
575	3.7225	0.5	1	0	0.680	0.716				
							2.5	2	0.060	1.943
576	3.7231	2.5	1	2	0.085	0.465				
							2.5	0	0.075	0.276
577	3.7234	2.5	1	2	0.047	0.257				
							2.5	0	0.055	0.203
578	3.7244	1.5	1	2	0.020	0.109				
579	3.7252	2.5	1	2	0.014	0.076				
580	3.7257	0.5	-1	1	0.500	0.883				
							1.5	1	0.260	1.969
581	3.7260	1.5	-1	1	0.025	0.044				
582	3.7296	2.5	1	2	0.070	0.380				

^{49}V Resonance Parameters

#	Energy (MeV)	J	π	l_p	Γ_p (KeV)	γ^2_p (KeV)	$S_{p'}$	$l_{p'}$	$\Gamma_{p'}$	$\gamma^2_{p'}$ (KeV)
							2.5	0	0.010	0.036
583	3.7302	0.5	1	0	0.012	0.013				
584	3.7309	1.5	-1	1	0.010	0.018				
							1.5	1	0.020	0.150
585	3.7312	1.5	1	2	0.118	0.639				
							1.5	0	0.040	0.145
							1.5	2	0.040	1.270
							2.5	2	0.020	0.635
586	3.7335	1.5	-1	1	0.100	0.175				
							2.5	1	0.020	0.149
587	3.7341	2.5	1	2	0.008	0.043				
							2.5	0	0.010	0.036
							2.5	2	0.010	0.315
588	3.7360	0.5	-1	1	0.800	1.398				
							1.5	1	0.100	0.742
589	3.7369	1.5	-1	1	0.030	0.052				
							2.5	1	0.020	0.148
590	3.7378	1.5	1	2	0.255	1.368				
							1.5	0	0.060	0.215
							1.5	2	0.050	1.563
							2.5	2	0.020	0.625
591	3.7382	2.5	1	2	0.060	0.322				
							2.5	0	0.060	0.215
592	3.7387	0.5	-1	1	0.020	0.035				
							1.5	1	0.020	0.148
593	3.7408	2.5	1	2	0.028	0.150				
							2.5	0	0.028	0.100
594	3.7413	1.5	-1	1	0.028	0.049				
							2.5	1	0.030	0.220
595	3.7422	1.5	-1	1	0.055	0.095				
							1.5	1	0.045	0.330
							2.5	1	0.020	0.147
596	3.7436	0.5	-1	1	0.075	0.130				
							1.5	1	0.060	0.439
597	3.7448	2.5	1	2	0.043	0.229				
598	3.7448	0.5	1	0	0.270	0.279				
599	3.7448	1.5	-1	1	0.050	0.087				
							2.5	1	0.010	0.073
600	3.7455	2.5	1	2	0.040	0.213				
							2.5	0	0.030	0.106
							2.5	2	0.030	0.922
							1.5	2	0.040	1.229
601	3.7457	0.5	-1	1	0.010	0.017				
							1.5	1	0.015	0.109
602	3.7482	1.5	-1	1	0.008	0.014				

^{49}V Resonance Parameters

#	Energy (MeV)	J	π	l_p	Γ_p (KeV)	γ^2_p (KeV)	$s_{p'}$	$l_{p'}$	$\Gamma_{p'}$	$\gamma^2_{p'}$ (KeV)
							2.5	1	0.030	0.217
603	3.7490	2.5	1	2	0.008	0.042				
							2.5	0	0.030	0.106
604	3.7503	1.5	1	2	0.018	0.095				
							1.5	0	0.035	0.123
							1.5	2	0.035	1.063
605	3.7507	2.5	1	2	0.020	0.105				
							2.5	0	0.045	0.158
							2.5	2	0.045	1.366
606	3.7528	0.5	1	0	0.045	0.046				
607	3.7539	0.5	-1	1	0.050	0.086				
							1.5	1	0.050	0.358
608	3.7548	1.5	1	2	0.055	0.289				
							1.5	0	0.035	0.122
							1.5	2	0.035	1.052
							2.5	2	0.030	0.902
609	3.7551	2.5	1	2	0.020	0.105				
							2.5	0	0.025	0.087
							2.5	2	0.025	0.751
							1.5	2	0.020	0.601
610	3.7578	1.5	-1	1	0.020	0.034				
							2.5	1	0.040	0.284
611	3.7592	0.5	1	0	0.010	0.010				
612	3.7595	1.5	1	2	0.006	0.031				
613	3.7614	2.5	1	2	0.030	0.156				
							2.5	0	0.020	0.069
							2.5	2	0.020	0.592
							1.5	2	0.020	0.592
614	3.7625	2.5	1	2	0.040	0.208				
							2.5	0	0.050	0.172
							2.5	2	0.050	1.477
615	3.7630	0.5	-1	1	0.020	0.034				
							1.5	1	0.040	0.282
616	3.7639	1.5	-1	1	0.030	0.051				
							2.5	1	0.030	0.211
617	3.7640	0.5	1	0	0.410	0.417				
							1.5	2	0.080	2.356
618	3.7641	1.5	-1	1	0.030	0.051				
							2.5	1	0.020	0.140
619	3.7661	2.5	1	2	0.017	0.088				
							2.5	0	0.015	0.051
							2.5	2	0.015	0.440
620	3.7670	1.5	-1	1	0.045	0.076				
							2.5	1	0.035	0.244
621	3.7681	0.5	1	0	0.380	0.385				

^{49}V Resonance Parameters

#	Energy (MeV)	J	π	l_p	Γ_p (KeV)	γ^2_p (KeV)	$s_{p'}$	$l_{p'}$	$\Gamma_{p'}$	$\gamma^2_{p'}$ (KeV)
							2.5	2	0.070	2.043
622	3.7687	2.5	1	2	0.090	0.464				
							2.5	0	0.030	0.102
							2.5	2	0.020	0.583
							1.5	2	0.020	0.583
623	3.7701	0.5	-1	1	0.020	0.034				
							1.5	1	0.015	0.104
624	3.7708	2.5	1	2	0.070	0.360				
							2.5	0	0.045	0.153
							2.5	2	0.045	1.305
							1.5	2	0.040	1.160
625	3.7716	1.5	-1	1	0.020	0.034				
							2.5	1	0.040	0.277
626	3.7741	2.5	1	2	0.010	0.051				
							2.5	0	0.010	0.034
							2.5	2	0.005	0.144
627	3.7747	0.5	1	0	0.140	0.141				
							1.5	2	0.090	2.587
628	3.7759	2.5	1	2	0.010	0.051				
							2.5	0	0.025	0.084
							2.5	2	0.025	0.717
629	3.7765	0.5	-1	1	0.018	0.030				
							1.5	1	0.020	0.137
630	3.7774	1.5	-1	1	0.040	0.067				
							2.5	1	0.030	0.205
631	3.7791	0.5	-1	1	0.160	0.268				
							1.5	1	0.070	0.478
632	3.7796	2.5	1	2	0.006	0.030				
							2.5	0	0.015	0.050
							2.5	2	0.015	0.426
633	3.7841	1.5	1	2	0.010	0.050				
							1.5	0	0.010	0.033
634	3.7849	0.5	1	0	0.100	0.100				
							2.5	2	0.100	2.809
635	3.7850	2.5	1	2	0.025	0.126				
							2.5	0	0.015	0.050
							2.5	2	0.015	0.421
							1.5	2	0.015	0.421
636	3.7857	0.5	-1	1	0.050	0.083				
							1.5	1	0.050	0.337
637	3.7887	1.5	1	2	0.015	0.075				
638	3.7902	2.5	1	2	0.020	0.100				
639	3.7902	0.5	1	0	1.690	1.682				
							2.5	2	0.250	6.941
640	3.7905	1.5	-1	1	0.040	0.066				

^{49}V Resonance Parameters

#	Energy (MeV)	J	π	l_p	Γ_p (KeV)	γ^2_p (KeV)	$s_{p'}$	$l_{p'}$	$\Gamma_{p'}$	$\gamma^2_{p'}$ (KeV)
							2.5	1	0.050	0.334
							1.5	1	0.020	0.133
641	3.7909	0.5	-1	1	0.050	0.083				
							1.5	1	0.050	0.333
642	3.7917	2.5	1	2	0.015	0.075				
							2.5	0	0.040	0.131
							2.5	2	0.040	1.107
643	3.7925	0.5	1	0	0.020	0.020				
							2.5	2	0.030	0.829
644	3.7931	2.5	1	2	0.012	0.060				
							2.5	0	0.010	0.033
							2.5	2	0.010	0.276
645	3.7936	1.5	-1	1	0.014	0.023				
							2.5	1	0.045	0.299
646	3.7949	0.5	-1	1	0.015	0.025				
647	3.7960	2.5	1	2	0.008	0.040				
							2.5	0	0.020	0.065
							2.5	2	0.020	0.548
648	3.7993	1.5	-1	1	0.065	0.106				
649	3.8019	0.5	1	0	0.130	0.128				
650	3.8021	1.5	-1	1	0.030	0.049				
651	3.8029	1.5	1	2	0.010	0.049				
652	3.8036	2.5	1	2	0.010	0.049				
653	3.8042	2.5	1	2	0.070	0.344				
							2.5	0	0.045	0.144
							2.5	2	0.045	1.211
							1.5	2	0.010	0.269
654	3.8052	1.5	-1	1	0.030	0.049				
							2.5	1	0.040	0.260
655	3.8053	2.5	1	2	0.020	0.098				
							2.5	0	0.025	0.080
							2.5	2	0.025	0.671
656	3.8056	0.5	1	0	1.420	1.395				
							2.5	2	0.300	8.050
657	3.8059	1.5	-1	1	0.015	0.024				
							2.5	1	0.015	0.097
658	3.8069	0.5	-1	1	0.045	0.073				
659	3.8075	2.5	1	2	0.020	0.098				
660	3.8075	0.5	1	0	0.155	0.152				
661	3.8096	0.5	-1	1	0.030	0.049				
662	3.8103	2.5	1	2	0.040	0.195				
							2.5	0	0.035	0.111
							2.5	2	0.035	0.929
							1.5	2	0.030	0.797
663	3.8107	2.5	1	2	0.020	0.098				

^{49}V Resonance Parameters

#	Energy (MeV)	J	π	l_p	Γ_p (KeV)	γ^2_p (KeV)	$s_{p'}$	$l_{p'}$	$\Gamma_{p'}$	$\gamma^2_{p'}$ (KeV)
							2.5	0	0.005	0.016
							2.5	2	0.005	0.133
							1.5	2	0.005	0.133
664	3.8108	0.5	1	0	0.120	0.117				
							2.5	2	0.080	2.122
665	3.8117	1.5	1	2	0.018	0.088				
							1.5	0	0.020	0.063
							1.5	2	0.020	0.529
666	3.8123	1.5	-1	1	0.060	0.097				
							2.5	1	0.070	0.449
							1.5	1	0.030	0.192
667	3.8141	0.5	-1	1	0.080	0.129				
							1.5	1	0.100	0.638
668	3.8148	2.5	1	2	0.058	0.282				
							2.5	0	0.030	0.095
669	3.8151	1.5	1	2	0.020	0.097				
							1.5	0	0.020	0.063
670	3.8161	1.5	-1	1	0.015	0.024				
							2.5	1	0.010	0.064
671	3.8167	1.5	1	2	0.030	0.145				
							1.5	0	0.030	0.094
672	3.8171	2.5	1	2	0.020	0.097				
							2.5	0	0.020	0.063
							2.5	2	0.020	0.523
673	3.8178	1.5	1	2	0.020	0.097				
							1.5	0	0.020	0.063
							1.5	2	0.020	0.522
674	3.8194	1.5	-1	1	0.060	0.096				
							2.5	1	0.050	0.316
675	3.8207	0.5	1	0	0.020	0.019				
							2.5	2	0.020	0.519
676	3.8210	2.5	-1	3	0.035	0.949				
							1.5	1	0.050	0.315
677	3.8215	1.5	-1	1	0.080	0.128				
							2.5	1	0.160	1.008
678	3.8223	1.5	1	2	0.130	0.625				
							1.5	0	0.050	0.156
							1.5	2	0.050	1.293
679	3.8231	0.5	-1	1	0.020	0.032				
							1.5	1	0.020	0.126
680	3.8239	1.5	1	2	0.040	0.192				
681	3.8248	1.5	-1	1	0.060	0.096				
							2.5	1	0.140	0.876
682	3.8249	2.5	-1	3	0.012	0.323				
							1.5	1	0.050	0.313

^{49}V Resonance Parameters

#	Energy (MeV)	J	π	l_p	Γ_p (KeV)	γ^2_p (KeV)	$s_{p'}$	$l_{p'}$	$\Gamma_{p'}$	$\gamma^2_{p'}$ (KeV)
683	3.8266	2.5	-1	3	0.035	0.941				
							1.5	1	0.025	0.156
							2.5	3	0.010	2.002
684	3.8273	1.5	-1	1	0.025	0.040				
							2.5	1	0.025	0.156
685	3.8280	2.5	1	2	0.095	0.453				
							2.5	0	0.015	0.046
							2.5	2	0.010	0.255
686	3.8289	2.5	1	2	0.010	0.048				
							2.5	0	0.045	0.139
							2.5	2	0.045	1.147
687	3.8305	2.5	1	2	0.040	0.190				
688	3.8308	0.5	1	0	1.380	1.328				
							2.5	2	0.050	1.269
689	3.8319	0.5	-1	1	0.080	0.127				
							1.5	1	0.160	0.988
690	3.8331	1.5	1	2	0.018	0.085				
							1.5	0	0.010	0.031
							1.5	2	0.010	0.253
691	3.8333	2.5	1	2	0.035	0.166				
							2.5	0	0.030	0.092
							2.5	2	0.030	0.757
692	3.8344	2.5	-1	3	0.065	1.726				
							1.5	1	0.080	0.492
							2.5	1	0.040	0.246
693	3.8349	0.5	-1	1	0.040	0.063				
							1.5	1	0.040	0.246
694	3.8356	1.5	-1	1	0.010	0.016				
695	3.8363	2.5	1	2	0.015	0.071				
696	3.8367	2.5	1	2	0.025	0.118				
							2.5	0	0.020	0.061
697	3.8370	1.5	1	2	0.118	0.557				
							1.5	0	0.040	0.122
							1.5	2	0.040	1.002
							2.5	2	0.030	0.752
698	3.8378	2.5	1	2	0.048	0.226				
							2.5	0	0.045	0.137
							2.5	2	0.045	1.125
							1.5	2	0.040	1.000
699	3.8385	0.5	1	0	0.120	0.115				
							2.5	2	0.060	1.498
700	3.8391	2.5	1	2	0.025	0.118				
							2.5	0	0.020	0.061
							2.5	2	0.010	0.249
701	3.8395	1.5	1	2	0.040	0.188				

^{49}V Resonance Parameters

#	Energy (MeV)	J	π	l_p	Γ_p (KeV)	γ^2_p (KeV)	$s_{p'}$	$l_{p'}$	$\Gamma_{p'}$	$\gamma^2_{p'}$ (KeV)
							1.5	0	0.035	0.106
							1.5	2	0.035	0.872
702	3.8400	0.5	-1	1	0.020	0.031				
							1.5	1	0.030	0.183
703	3.8416	0.5	1	0	0.050	0.048				
704	3.8452	1.5	-1	1	0.040	0.063				
							2.5	1	0.010	0.060
							1.5	1	0.020	0.120
705	3.8480	2.5	1	2	0.020	0.093				
							2.5	2	0.020	0.489
706	3.8488	0.5	1	0	0.310	0.294				
							2.5	2	0.080	1.954
707	3.8496	2.5	1	2	0.010	0.046				
708	3.8529	0.5	-1	1	0.030	0.047				
709	3.8556	1.5	-1	1	0.240	0.372				
							1.5	1	0.020	0.118
							2.5	1	0.020	0.118
710	3.8560	2.5	1	2	0.015	0.069				
							2.5	0	0.010	0.029
711	3.8563	2.5	-1	3	0.015	0.385				
							1.5	1	0.010	0.059
712	3.8560	1.5	-1	1	0.030	0.047				
713	3.8568	0.5	-1	1	0.020	0.031				
							1.5	1	0.040	0.236
714	3.8574	0.5	1	0	0.035	0.033				
							2.5	2	0.035	0.839
715	3.8584	1.5	-1	1	0.035	0.054				
							1.5	1	0.050	0.294
716	3.8595	2.5	1	2	0.030	0.138				
							2.5	0	0.030	0.088
							1.5	2	0.030	0.716
							2.5	2	0.030	0.716

Bibliography

Amaldi, E., D'AGostino, O., Fermi, E., Pontecorvo, B., Rasetti, F. and Segre, E., Proc. R. Soc. **A149**, 522 (1935).

Anderson, J. D. and Wong, C., Phys. Rev. Letters **7**, 250 (1961).

Ball, A. E., Brown, G., Denning, A. and Glover, R. N., Nucl. Phys. **A183**, 472 (1972).

Barens, P. D., Comfort, J. R. and Bockelman, C. K., Nucl. Phys. **51**, 641 (1967).

Bethe, H.A., Phys. Rev. **47**, 747 (1935).

Bethe, H.A., Phys. Rev. **50,** 332 (1936).

Bethe, H.A., Rev. Mod. Phys. **9**, 79 (1937).

Bjerregaard, J. H., Dahl, P. F., Hansen, O. and Sidenius, G. Phys. Rev. **159**, 920 (1964).

Bloch,I., Hull, M. H., Broyles, A. A., Bouricius, W. G., Freeman, B. E., and Breit, G., Phys. Rev. **80,** 553 (1950); Rev. Mod. Phys. **23,** 147 (1951).

Bohr, N., Nature (London) **137**, 344 (1936).

Breit, G., and Wigner, E. P., Phys. Rev. **49**, 519 (1936); **49**, 642 (1936).

Breit, G., Phys. Rev. **58**, 1068 (1940).

Bull, J. S., "Entrance Channel Correlations in ^{40}Ca." Ph.D. dissertation, Duke University, 1989.

Feld, B. T., Feshbach, H., Goldberger, M. L., Goldstein, H. and Weisskopf, V. F., Final Report of the Fast Neutron Data Project, A. E. C. report No. NYO-636 (1951).

Fox, J. D., Moore, C. F. and Robson, D., Phys. Rev. Letters **12**, 198 (1964).

Gales, S., Fortier, S., Laurent, H., Maison, J. M. and Schapira, J. P., Nucl. Phys. **A259**, 189 (1976)

Gilbert, A. and Cameron, A. G. W., Can. J. Phys. **V43**, 1446 (1965).

Harney, H. L. and Weidenmuller, H., Nucl.Phys. **A139**, 241 (1969).

Ignatyuk, A. V. and Stavinskii, V. S., Sov. J. Nucl. Phys. **11**, 674 (1970).

Ignatyuk, A. V., Smirenkin, G. N. and Tishin, A. S., Sov. J. Nucl. Phys. **21**, 255 (1975).

Janecke, J., Isospin in Nuclear Physics, ed. Wilkinson, D. H. (North-Holland, Amsterdam, 1969).

Kapur, P. L. and Peierls, R. E., Proc. Roy. Soc. (London) **A166**, 277 (1938).

Kataria, S. K., Ramamurthy, V. S. and Kapoor, S. S., Phys. Rev. **C18**, 549 (1978).

Keyworth, G. A., Kyker, G. C. Jr., Bilpuch, E. G. and Newson, H. W., Nucl. Phys. **89,** 590 (1966).

Keyworth, G. A., Wilhjelm, P., Kyker, G. C. Jr., Newson, H. W. and Bilpuch, E. G., Phys. Rev. **176**, 1302 (1968).

King, S. E., Lau, Y. C. and Gould C.R., IEEE Trans. Nucl. Sci. **NS-28**, 3822 (1981).

Lane, A. M. and Thomas, R. G., Wigner, E. P., Phys. Rev. **98**, 693 (1955).

Lane, A. M. and Thomas, R. G., Rev. Mod. Phys. **30**, 257 (1958).

Lane, A. M. and Soper, J. M., Phys. Rev. Letters **7**, 420 (1961); Nucl. Phys. **37**, 663 (1962).

Mekjian, A. and MacDonald, W. M., Nucl. Phys. **A121**, 385 (1968).

Mello, P. A., Lectures on Reaction Theory and Isosbaric Analogue Resonances. (unpublished).

Mitchell, G. E., Bilpuch, E. G., Shriner, J. F. Jr. and Lane, A. M., Phys. Reports **117**, 1 (1985).

Moon, P. B. and Tillman, R., Proc. R. Soc. **153**, 421 (1936).

Nelson, R. O., "Proton Resonance Spectroscopy in ^{28}Si and ^{30}P." Ph.D. dissertation, Duke University, 1983.

Newton, T. D., Can. J. Phys. **V34**, 804 (1956).

Parks, P. B., Newson, H. W. and Williamson, R. M., Rev. Sci. Instrum. **29**, 834 (1958).

Perey, C. M., Perey, F. G., Dickens, J. K. and Silva, R. J., Phys. Rev. **175**, B1460 (1968).

Porter, C. E. and Thomas, R. G., Phys. Rev. **104**, 384 (1956).

Porter, C. E. and Rosenzweig, N., Ann. Acad. Sci. Fennicae AVI No. **44** (1960).

Porter, C. E., Statistical Theories of Spectra: Fluctuations. (Academic, New York, 1965).

Prochnow, N. H., "A High Resolution Study of Proton Resonances in ^{47}V, ^{49}V and ^{51}V." Ph.D. dissertation, Duke University, 1971.

Rasetti, F., Segre, E., Fink, G., Dunning, J. R. and Pegram, G. B., Phys. Rev. **49**, 104 (1936).

Richard, P., Moore, C. F., Robson, D. and Fox, J. D., Phys. Rev. Letters **13**, 343a (1964).

Roberson, N. R. and Gould, C. R., IEEE Trans. Nucl. Sci. **NS-32,** 1447 (1985).

Robson, D., Phys. Rev. **137**, B535 (1965).

Ruyl, J. F. A. G. and Endt, P.M., Nucl. Phys. **A407**, 60 (1983).

Sellin, D. L., "Excited Statess in ^{19}F." Ph.D. dissertation, Duke University, 1969.

Shiff, L. I., Quantum Mechanics (McGraw-Hill Book Company, Inc., New York, 1949).

Shriner, J. F. Jr., Mitchell, G.E. and Bilpuch, E. G., Nucl. Instrum. Methods. **A254**, 139 (1987).

Thompson, W. J., Adams, J. L. and Robson, D., Phys. Rev. **173**, 975 (9168).

Tuli, J. K., Nuclear Wallet Card. (New York, 1985).

Vogt, E., Rev. Mod. Phys. **34**, 723 (1962).

Vonach, H., Uhl, M., Strohmaier, B., Smith, B. W., Bilpuch, E. G. and Mitchell, G. E., Phys. Rev. **C38,** 2541(1988).

Westerfeldt, C. R., Nelson, R. O., Bilpuch, E. G. and Mitchell, G. E., Nucl. Instrum. Methods **A270**, 467 (1988).

Wigner, E. G. and Eisenbud, E., Phys. Rev. **72**, 29 (1947)

Wilkinson, D. H. Isospin in Nuclear Physics, ed. Wilkinson, D. H. (North-Holland, Amsterdam, 1969).

Zaidi, S. A. S. and Darmodjo, S., Phys. Rev. Letters **19**, 1446 (1967).

Biography

Jianying Li

Personal: Born May 18, 1963, Jiangsu, P.R. China
Married to Yan Chen, July 18, 1988.

Education: B.S. in Physics, Fudan University, Shanghai, P.R.China, 1984
M.S. in Physics, Fudan University, Shanghai, P.R.China, 1987

Positions: Teaching Assistant, Fudan University, February, 1986 - July, 1986
Research Assistant, Fudan University, 1985 - 1987
Research Assistant, TUNL, Duke University, 1988 - present

Abstracts: "High Resolution Proton Resonance Spectroscopy of ^{49}V," J. Li, E. G. Bilpuch, C. R. Westerfeldt and G. E. Mitchell, Bull. Am. Phys. Soc. **34**, 23 (1989).

"Impact Parameter Dependence of K-Shell Ionization Probability by Protons," J. LI, H. J. Xu, C. G. Ren, F. Q. Lu, F. J. Yang, First National Atomic and Molecular Meeting of the Chinese Physical Society, Qinhuang Dao, Hebei, 1987.

"The Absolute Efficiency Calibration of Si(Li) Detector," H. J. Xu, J. Li, C. G. Ren, Third National Conference on Nuclear Instruments and Detectors," Anhui, 1986.

Papers: "The Measurement of Impact Parameter Dependence of K-Shell Ionization Probability by Protons," J. Li, H. J. Xu, C. G. Ren, F. Q. Lu, Nucl. Instrum. Method **B30**, 16 (1988).